Time Dependent Nonlinear Optics using a Phase Conjugated Laser

by

Patrick Klövekorn

Thesis submitted for the degree of

Doctor of Philosophy

in

The University of Adelaide

Department of Physics and Mathematical Physics

December, 1997

Contents

List of Figures

List of Tables

This work contains no material which has been accepted for the award of any other degree or diploma in any university or other tertiary institution and, to the best of my knowledge and belief, contains no material previously published or written by another person, except where due reference has been made in the text.

I give consent to this copy of my thesis, when deposited in the University Library, being available for loan and photocopying.

SIGNED:
DATE: 23/6/1998

Supervisor: Prof. J. Munch

Acknowledgments

There are a lot of people who have influenced this Ph.D. and they all deserve thanks. Firstly I want to thank my wife, Lisa and my parents, Henning and Irena. Their constant support, belief, patience and the occasional whipping motivation has made this work possible. Without them, there would be no thesis. Then I'd like to thank Omi und Opi, Horst, Bill and Kathy, Michael, Tim and Rom for their support and belief in me. My thanks to Henning, my brother, for keeping me sane and alert (of the red kind).

My gratitude also goes toward DSTO, the ARC, Jesper Munch, Anne-Marie Grisogono and the University of Adelaide for much needed financial support. Outside the Optics Group I have had valuable discussions with the following people, Tim McKay, Julianne Davy, Tim Bubner, Jacky Craig, Jeremy Bolger and Marek Samoc.

I'd like to thank Blair, David, Damien, Kerry, Peter Foster, Petar, Thu-Lan, Geoff, Sharaam, Igor, Laurence Alex(Bill?), Peter Veitch, Rob, and Murray for invaluable lengthy discussions and help. I think I thank the MOB, Dave, Damien, Peter, Geoff and Ben for all the outings that I thought I wouldn't wake up from.

Special thanks also goes to Blair for his help in building, maintaining and repairing of equipment. I think that shaved at least six months off my Ph.D.. Thanks also to other people in the Department, Carmel, Tanja, Arlene, Albert, Janet, Margaret, Bob Hurn, Bob Nation, Mike Shorthose, Mark Ferraretto and Don McCoy for their help in the course of my work.

Finally my gratitude goes to my supervisor, Professor Jesper Munch for training me as a physicist. It wasn't easy, but now I am ready to 'Comb my hair with a cactus and have horse shoes for breakfast!'

Abstract

In the present work we demonstrate the combined use of stimulated Brillouin scattering (SBS) for aberration correction, auto alignment and pulse compression as an ideal technology for studies of nonlinear optical processes, in particular nonlinear optical scattering (NLS).

We built a master oscillator/power amplifier laser using SBS phase conjugation and pulse compression which provided single longitudinal mode optical pulses that were continuously variable between 0.65 and 9.5 ns at 1064 nm. We utilize a variable pulse length laser (VPLL) to examine the transient nonlinear scattering properties of an optical power limiter, platinum ethynyl, using degenerate four-wave mixing (DFWM). Intensity, polarization and pulse length control allow us to measure acoustic scattering and decay parameters, $\chi^{(3)}$ magnitudes and the transient, laser-induced grating behaviour. Phase conjugation lead to excellent laser beam quality and auto-alignment. Both are necessary in DFWM which has very stringent alignment criteria and requires precise knowledge of the electric field distribution inside the material.

The strong electric field of the laser excites both intrinsic and opto-mechanical nonlinearites which can be excited selectively by setting the pulse length to 0.65 ns and 9.5 ns, respectively. We observe the transient nonlinear scattering behaviour using nanosecond pulses and determine the underlying physical mechanisms using sub-nanosecond pulses. In addition, using the continous variability of the pulse lengths between the indicated values we observe the response in the transitional regime where intrinsic polarizabilities compete with opto-mechanical nonlinearities. To our knowledge this was the first time this had been done in the time regime of Q-switched lasers. As a benchmark, we compare the nonlinear optical response of the power limiter to that of carbon disulphide.

Abbreviations

FWM	four-wave mixing
DFWM	degenerate four-wave mixing
SBS	stimulated Brillouin scattering
STBS	stimulated thermal Brillouin scattering
SRLS	stimulated Rayleigh scattering
STRS	stimulated thermal Rayleigh scattering
SRS	stimulated Raman scattering
LIDG	laser induced dynamic grating
TRTH	transient real-time holography
NLS	nonlinear scattering
ESA	excited state absorption
RSA	reverse saturable absorption
OL	optical limiting
PE	platinum ethynyl
CS_2	carbon disulfide

Chapter 1

Introduction

The motivation for this thesis resulted from the need of the Defence Science and Technology Organization of South Australia (DSTO) for an optical power limiter to prevent sensitive optical detectors from laser damage. Their [1], as well as another group's studies [2] showed the organometallic molecule platinum ethynyl (PE) to be a good optical limiter in the visible wavelength region via excited state absorption (ESA). Early experiments [3] had also shown nonlinear scattering (NLS) to take place in PE, however this has not been investigated in detail. ESA and NLS are very important optical limiting mechanisms [4] and as such there was an urgent need to investigate further the NLS properties of PE. To avoid RSA we characterized PE at 1064 nm using degenerate four-wave mixing (DFWM). This approach complemented experiments done in the resonant regime and allowed us to investigate NLS mechanisms in PE.

DFWM probes the third-order nonlinearity of a material, which consists of opto-mechanical nonlinearities and intrinsic nonlinearites, and is directly related to the intensity dependent refractive index. It is thus a direct probe of the behaviour of a material subject to intense laser radiation. We used DFWM to force nonlinear scattering processes in the material and observe their dynamic evolution. This enabled us to measure the associated scattering parameters and determine their dominant time regimes. DFWM is especially useful due to the great amount of experimental control which can be exercised, with selective access to various physical mechanisms

which may contribute to the nonlinear interaction. This can be achieved by careful selection of the laser[5, 2, 6], geometry[7, 8, 9], intensity[10] and polarization[11, 12]. In the present work we add continuous pulse length control in the subnanosecond to nanosecond time regime to this list of variable parameters.

In the course of our experiments we found our commercial laser system to be limited in its utility for nonlinear optical experiments. The beam quality was not Gaussian and hence the electric field was not well defined in the interaction region. In addition, to determine the mechanisms giving rise to the nonlinearities, we needed pulse lengths much shorter than the 30 ns provided by the laser. As a result we developed a laser system capable of providing pulse durations continuously variable from 0.65 ns to 9.5 ns, while maintaining perfectly the alignment of the laser beam. At the same time the beam quality of the laser was improved to provide a Gaussian transverse profile.

This thesis is organized into two theory and review chapters, Ch.2 and 3, and three experimental chapters, Ch.4, 5 and 6. Chapter 2 contains an in-depth description of laser-induced gratings, the contributing mechanisms, important references and the relevant mathematical theory. Chapter 3 provides the background for SBS pulse compression and SBS phase conjugation which are used as a basis for the laser system. In Ch.4 I describe a preliminary DFWM experiment which established the operating parameters as well as practical requirements of DFWM. I then proceed to the versatile, complex DFWM experiment using 8 ns laser pulses. The results of this chapter outline the need for shorter laser pulse lengths, and hence Ch. 5 describes the setup of a variable pulse length laser (VPLL). Ch. 6 contains the results of applying the VPLL to the DFWM experiment. Included in the appendices are five publications which represent the results of this thesis.

As I will show, the VPLL provides ideal technology to study nonlinear optical processes, in particular nonlinear scattering. Control of laser pulse duration extends significantly the range of experiments and measurements which can be done with a single laser system.

Chapter 2

Degenerate Four-Wave Mixing

2.1 Introduction

It is convenient to start an introduction to four-wave mixing with the question, 'What is nonlinear optics?'. As it turns out this is not easily answered. One could say, 'Nonlinear optics refers to optical effects that take place in the presence of strong light sources', but that doesn't say anything about what actually occurs and is open to the question, 'How strong is strong?'. Another explanation might say, 'Nonlinear optics occurs when light itself changes a material's optical properties, such as refraction', and then proceed to give the example of self-focussing. This works well because people are familiar with lenses and their focusing properties. However, this explanation only applies in some cases, since some nonlinear effects change a material's optical properties, such as the optical Kerr effect, while others do not change them, such as third-harmonic generation. In the latter case it is the high intensity of a laser beam which enables us to see the nonlinear effect due to the material's properties.

In a more detailed description one might declare that the electric field of a laser beam inside a material produces a polarization field, which is given by the nonlinear susceptibility of the material. This polarization in turn couples with the existing electric field to produce higher order polarization terms, thus giving rise to nonlinear optical effects. This is a *wave mixing* process. The material's susceptibility, the input

field configuration and phase matching conditions all lead to specific effects such as DFWM and SHG. The nonlinear susceptibility is a tensor which contains all the necessary information such as the material's history of electromagnetic interaction, its temporal response and re-distribution of vectorial components. It is subject to resonant enhancement due to absorption into any energy levels of the material and thus provides a quantum mechanical link to an otherwise classical picture.

Historically, nonlinear optics is a very broad and still young field. The invention of the laser [13, 14] in 1960 was followed very quickly by the first experimental discovery of a nonlinear effect by Franken et al [15] in the form of second harmonic generation. In fact, the most fundamental discoveries and investigations in nonlinear optics took place immediately after this, for example sum-frequency generation [16], stimulated Raman scattering [17] and self-focusing [18]. The advent of the mode-locked laser in 1965 allowed further resolution of nonlinear mechanisms and increased the power density while lowering the amount of energy transferred into the material.

Pertinent to this thesis are the experimental demonstrations of stimulated Brillouin scattering in 1964 by Chiao et al [19] and light-by-light scattering by Carman et al in 1966 [20]. SBS distinguishes itself from Brillouin scattering in its stimulated nature, in analogy with stimulated emission. The most startling effect of SBS is of course phase conjugation [21, 22]. In SBS the scattering centers are stimulated phonons, which are seeded by spontaneous phonons already present before the optical interaction. In Carman's light-by-light scattering experiments [20] the physical mechanism was the optical Kerr effect and thus it can be regarded as self-diffraction off a laser-induced dynamic grating (LIDG). An important application of this is the optical switch.

DFWM was first proposed theoretically in 1977 by Hellwarth [23]. In his paper Hellwarth described a method for generating dynamically a phase conjugate wave pattern in a nonlinear medium. He also suggested an experimental setup to demonstrate this effect. The first experimental demonstration of DFWM was published by Bloom and Bjorklund in 1977 [24]. They used a Q-switched, frequency-doubled Nd:YAG laser as a source. Counter-propagation of the pumps was achieved with

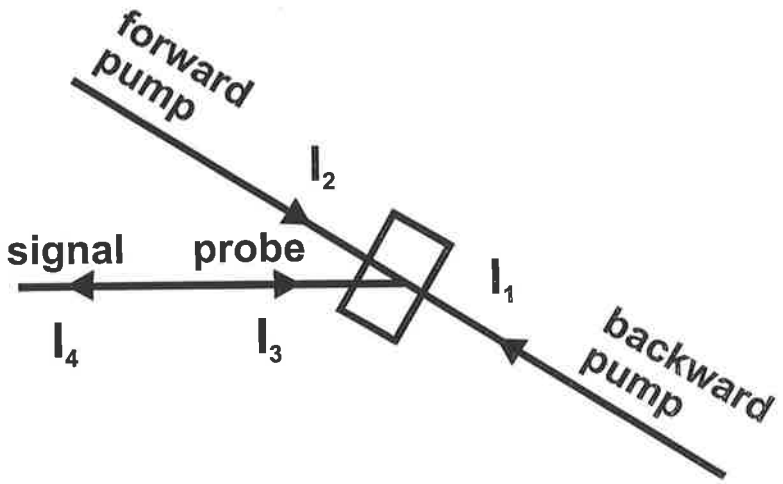

Figure 2.1: Simple DFWM setup

a retro-reflecting mirror and the probe beam was focussed into the sample. Carbon disulfide was used as a nonlinear material and phase conjugation of an Airforce resolution chart and aberration correction were used as verification of the method.

To continue the historical overview, a brief description of the DFWM process and its consequences is necessary. DFWM describes the coupling of three laser beams within an optically nonlinear material leading to the generation of a fourth beam. It is the special configuration as shown in Fig. 2.1 and the frequency degeneracy which distinguishes it from other four-wave mixing processes, such as third harmonic generation [25]. The nomenclature of DFWM is easily confused with that used for LIDG. In DFWM the two powerful, colinear and antiparallel laser beams are referred to as the *pump* beams. A weaker third beam, intersecting the pumps at an angle θ is called the *probe* and leads to generation of the fourth beam which is called the *return* or *signal* beam. The pump beam which makes the smaller angle with the probe beam is called the *forward* pump and the other is called the *backward* pump. The pump beams and the probe interact in the presence of the nonlinear material and produce the signal [26]. *It is important to note that the process is entirely light induced.* In the LIDG picture the forward pump and the probe are often called the *write* beams and the backward pump the *probe* or *read* beam. To avoid any

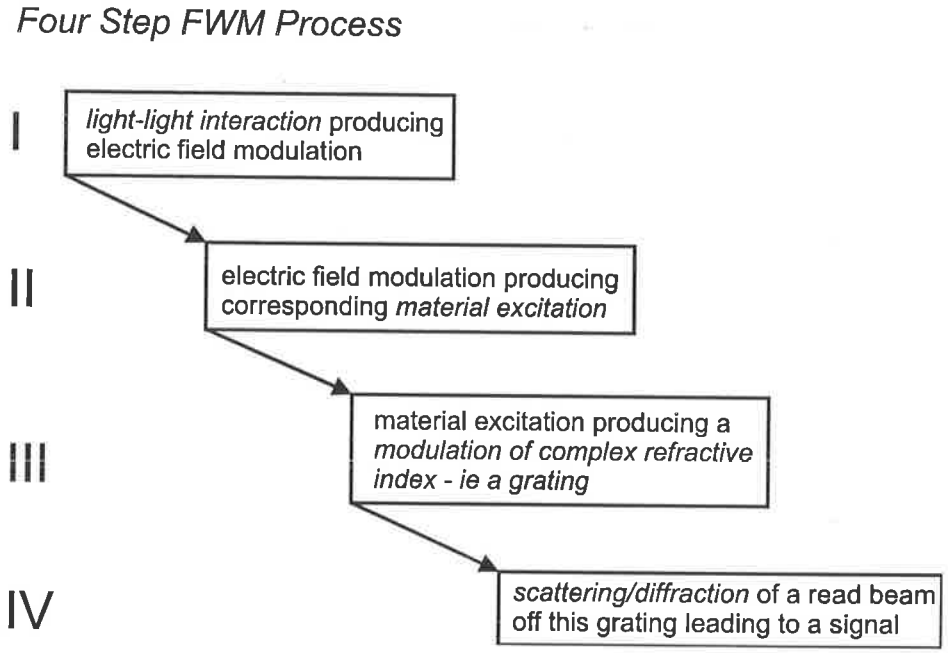

Figure 2.2: FWM divided into four logical steps

confusion, I will use the DFWM convention of *back*-and *forward pumps* and the *probe*, or where appropriate also call the forward pump and the probe 'write' beams and the backward pump the 'read' beam. I will not however, call the backward pump the 'probe'.

DFWM can generally be viewed as a four step process, as shown in Fig. 2.2. These events can occur simultaneously and as in the case of virtual electronic excitations should not be separated, because of cross-coupling. However, it is conceptually useful to separate them logically and for some mechanisms this indeed presents no problems at all.

In the overlap volume of two or more coherent beams an *interference modulation* of the electric field results. If the beams have the same optical frequency, then this modulation of the electric field remains stationary in space for the duration of the overlap of the beams. The resultant direction and magnitude of this modulation can be determined completely and easily although it is complicated by the possibility of interference of non parallel and circular polarizations.

In the presence of a material, this stationary (and dynamically evolving) *inter-*

ference pattern induces a polarization which is dependent on the nonlinear optical properties of the material. Examples of this are electronic cloud distortions or electrostrictively induced changes in the local density of the material. This is called a *material excitation.* This material excitation leads to a change in the light transmitting properties of the material, ie. localized changes in the complex refractive index. Hence the interaction of the pumps and the probe establishes a dynamic grating inside the material, called a *material grating.* Although trivial, it is important to distinguish between the interference modulation and the material grating which is an actual physical structure which requires the presence of a material.

Scattering or diffraction off one of the pumps by the material grating leads to the signal. In DFWM we probe the first order diffracted beam *which is phase conjugate to the probe.* Diffraction efficiency will determine the size of the signal and the dominant physical mechanisms will *determine the dynamics of the temporal shape.* The latter is given by the convolution of the input pulse intensity with the temporal response function of the material and its dominant mechanisms. This also implies that if the temporal response is comparable to the length of the input pulse, and if there are competing mechanisms, the signal will exhibit a more complex structure than the input pulse.

To summarize, DFWM has a number of very useful properties, the most important of which are susceptibility dependence, which allows for resonant enhancement of the nonlinearity, phase conjugation, and being an entirely light induced process. Each of these has been studied and modelled in a large number of publications, and this continues to be the case.

The feasibility of amplified reflection was first shown in 1977 by Yariv and Pepper [27]. It was made possible experimentally using resonant enhancement by Bloom et al [28] and analyzed as a two-level system by Abrams and Lind [29] in 1978 and a three-level system by Agrawal [30] in 1981. The first CW demonstration of DFWM was in Ruby by Liao and Bloom [31]. Resonant enhancement has lead to a number of important applications for DFWM, such as Doppler-free spectroscopy [32] and remote sensing of trace particles [33].

Phase conjugation in DFWM implies a very close association to holography and it is often referred to as transient real-time holography (TRTH) [26]. This property has provided a huge number of applications in the fields of image processing [34, 35, 36] and aberration correction [37].

The frequency degeneracy and photon momentum conservation has enabled the use of DFWM for frequency stabilization of lasers [38] and narrow band optical filters [39, 40, 41].

Because the process is entirely light induced, it presents the possibility of using it as an optical switch [42] and also as a temporal auto-correlation device [43] to measure the duration of ultra-short pulses.

The diversity of these startlingly useful applications of DFWM is the most important stimulus for the research explosion we see today. However, the most common use of DFWM is as a method for material analysis of nonlinear optical properties over all time scales. Section 2.4 will describe this in more detail. We now turn to a detailed description of DFWM, starting with the laser input beams and the multitude of interference patterns they can produce.

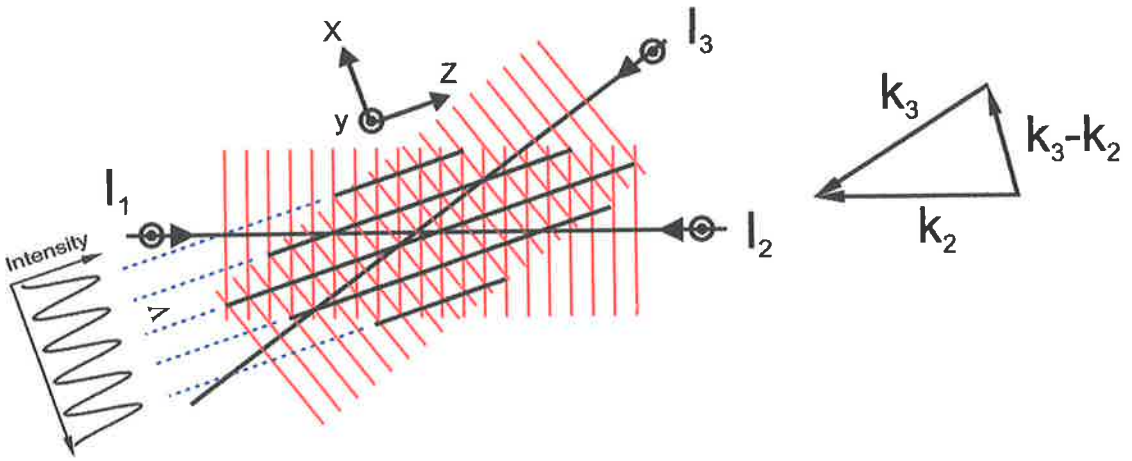

Figure 2.3: First order interference grating produced between two beams k_2 and k_3. The resultant grating is given by $k = k_2 - k_1$

2.2 Interference Patterns

Fig. 2.3 shows the resulting interference pattern that is produced between two coherent beams including its direction as well as its spacing. If the momentum vectors are given by $\mathbf{k}_2$ and $\mathbf{k}_3$ the resultant grating is given by $\mathbf{k} = \mathbf{k}_3 - \mathbf{k}_2$. Two S-polarized beams of intensity I_1 and I_2 produce a modulated intensity pattern as shown and given by

$$I = I_1 + \sqrt{I_1 I_2}\cos\Phi + I_2$$

where Φ is the phase difference at any point in the overlap region. The spacing of the grating is given by

$$\Lambda = \frac{n\lambda}{2\sin\frac{\theta_n}{2}} \tag{2.1}$$

where n is the refractive index of the medium, λ is the wavelength of the laser in air, and θ_n is the angle between the two beams inside the medium. Hence choice of laser and geometry allows spacings between a few hundred nanometers and infinity. This is however only the simplest case of interference and is subject to treatment in many undergraduate texts. Additional types of interference patterns, which are more complex and somewhat counter-intuitive, can be established by various polarization combinations.

The treatment which follows is based on an excellent description in Eichler's book for the geometry and intensity modulation of interference [8] and Jones' matrices treatment for polarization addition [44].

Fig. 2.3 shows the coordinate system used in this treatment. The z axis is along the bisector of the direction of propagation of the two intersecting beams. The x axis is along $\mathbf{k}_4 = \mathbf{k}_3$ - $\mathbf{k}_2$ and the y axis points up, out of the page defining a right handed system. Hence the phase difference between the two beams at any point along the x axis will vary by

$$\Phi(x) = |\mathrm{k}_4|\, x \tag{2.2}$$

where

$$|\mathrm{k}_4| = \frac{4\pi}{\lambda} \sin\frac{\theta}{2} \tag{2.3}$$

For any polarization combination there are three things to consider:

- the form of the intensity modulation, $\triangle$I
- the type of the resultant polarization
- the resultant plane of the polarization

The intensity modulation is given by the dot product of the electric field vectors, $\mathbf{E}_1 \cdot \mathbf{E}_2$, i.e.

$$\triangle I = \sum_{i=x,y,z} E_{1i} E_{2i}$$

This shows that it is possible for the intensity modulation to be zero if $\mathbf{E}_1 \perp \mathbf{E}_2$.

In order to model the resultant polarization it must first be noted that the addition of two beams with linear polarization vectors $\mathbf{p}_1$ and $\mathbf{p}_2$ leads to a resultant polarization confined to the plane defined by $\mathbf{p}_1$ and $\mathbf{p}_2$. For the polarization treatment, we will change to the coordinate system defined by these two vectors, ie. the new x axis will be in the direction of $\mathbf{p}_1$ and the new y axis will be in the *plane* of $\mathbf{p}_2$. The latter is necessary if $\mathbf{p}_1$ and $\mathbf{p}_2$ are not orthogonal. Now we can easily find the resultant polarization in that plane by the use of Jones matrices.

A laser beam can be described using

$$\begin{aligned}\mathbf{E}_1 &= [\mathbf{i}E_{1x}e^{i\phi_x} + \mathbf{j}E_{1y}e^{i\phi_y}]e^{i(kz-\omega t)} \\ &= \tilde{\mathbf{E}}_1 e^{i(kz-\omega t)}\end{aligned}$$

where $\mathbf{i}$ and $\mathbf{j}$ are unit vectors in the complex plane. ϕ_x and ϕ_y are the phases of each component of the electric field in the $\mathbf{i}$ and $\mathbf{j}$ directions.

$$\tilde{\mathbf{E}}_1 = \mathbf{i}E_{1x}e^{i\phi_x} + \mathbf{j}E_{1y}e^{i\phi_y}$$

is the complex amplitude of the polarized wave which is a vector and can be written in Jones matrix form:

$$\tilde{\mathbf{E}}_1 = \begin{bmatrix} E_{1x}e^{i\phi_x} \\ E_{1y}e^{i\phi_y} \end{bmatrix}$$

Thus a beam linearly polarized in the y direction would have the following Jones matrix.

$$\tilde{\mathbf{E}}_1 = \begin{bmatrix} 0 \\ 1 \end{bmatrix}$$

where $E_{1x} = 0$ and the vector has been normalized. If $\tilde{\mathbf{E}}_1$ contains components that are real, as well as components that are imaginary, then $\tilde{\mathbf{E}}_1$ describes elliptically polarized light. Otherwise $\tilde{\mathbf{E}}_1$ is linearly polarized.

In the case of interference between two beams, the resultant electric field is given by their superposition

$$\begin{aligned}\tilde{\mathbf{E}}_r &= \tilde{\mathbf{E}}_1 + \tilde{\mathbf{E}}_2 \\ &= \begin{bmatrix} E_{1x}e^{i\phi_{1x}} + E_{2x}e^{i\phi_{2x}} \\ E_{1y}e^{i\phi_{1y}} + E_{2y}e^{i\phi_{2y}} \end{bmatrix}\end{aligned}$$

In our case, for any point across the grating, the phase difference between $\tilde{\mathbf{E}}_1$ and

$\tilde{\mathbf{E}}_2$ is given by Φ in Equation 2.2, i.e.

$$\begin{aligned}\Phi &= \phi_{2x} - \phi_{1x} \\ &= \phi_{2y} - \phi_{1y}\end{aligned}$$

Note that for linearly polarized light $\phi_{ix} = \phi_{iy}$. This will be the case for all input beams used in this work. Since we are dealing only with relative phases, we can set $\phi_{1x} = \phi_{1y} = 0$. Hence

$$\tilde{\mathbf{E}}_r = \begin{bmatrix} E_{1x} + E_{2x}e^{i\Phi} \\ E_{1y} + E_{2y}e^{i\Phi} \end{bmatrix}$$

We will now use this result to deduce the resultant electric field produced by the most commonly used and indeed most useful interference gratings, depicted in Fig. 2.4.Case a) This case was already described above, however I will include it here as a simple example of the method.

The electric field vectors are given by

$$\hat{\mathbf{E}}_1 = \begin{bmatrix} 0 \\ 1 \end{bmatrix} \text{ and } \hat{\mathbf{E}}_2 = \begin{bmatrix} 0 \\ 1 \end{bmatrix} e^{i\Phi}$$

and hence the normalized Jones vector is just[1]

$$\hat{\mathbf{E}}_r = \begin{bmatrix} 0 \\ 1 \end{bmatrix}$$

Thus the resultant field is, as expected, out of the page and linear. The intensity modulation is given by

$$\triangle I = \sum_{i=x,y,z} E_{1i}E_{2i} = E_1E_2$$

Case b) Note that in this case the resultant polarization will be in the plane of the

[1]Any factors, real or complex, of the Jones matrix can be ignored if one is interested only in the polarization vector.

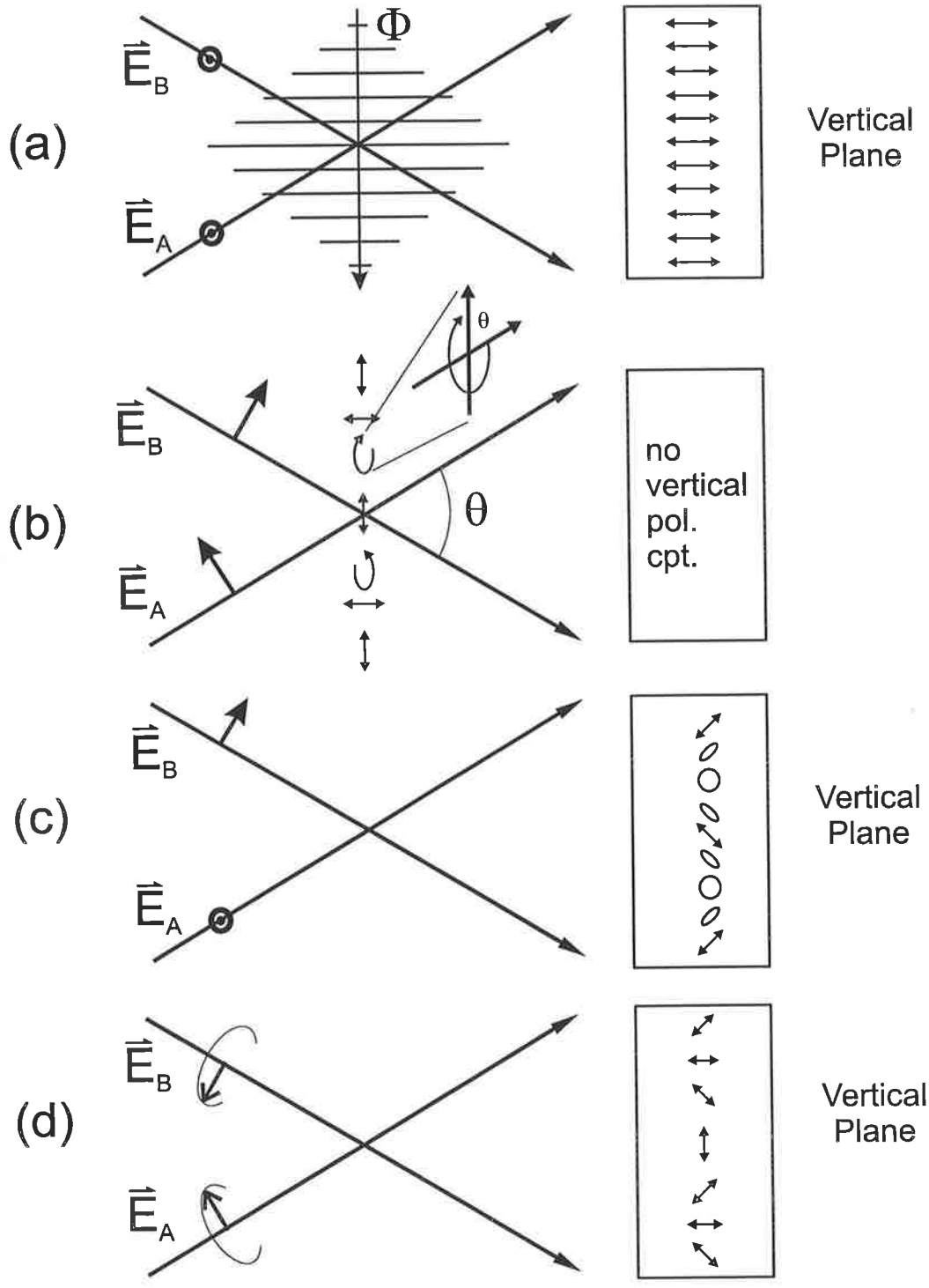

Figure 2.4: Four grating types that can be written with two laser beams. The resultant polarization directions are shown in the box labelled 'Vertical Plane', which represents the plane defined by the grating vector and the normal vector to the plane defined by the beams. Note that in case (b) there is no component in the vertical direction. Also note that in the interest of clarity, the grating spacing varies between the individual cases.

laser beams, with interesting results.

$$\tilde{\mathbf{E}}_1 = \begin{bmatrix} E_1 \cos\frac{\theta}{2} \\ E_1 \sin\frac{\theta}{2} \end{bmatrix} \text{ and } \tilde{\mathbf{E}}_2 = \begin{bmatrix} E_2 \cos\frac{\theta}{2} \\ -E_2 \sin\frac{\theta}{2} \end{bmatrix} e^{i\Phi}$$

implies that the resultant polarization is given by

$$\begin{aligned} \tilde{\mathbf{E}}_r &= \begin{bmatrix} E_1 \cos\frac{\theta}{2} + E_2 e^{i\Phi} \cos\frac{\theta}{2} \\ E_1 \sin\frac{\theta}{2} - E_2 e^{i\Phi} \sin\frac{\theta}{2} \end{bmatrix} \\ &= \begin{bmatrix} a + be^{i\Phi} \\ c + de^{i\Phi} \end{bmatrix} \\ &= \begin{bmatrix} a+b \\ c+d \end{bmatrix} \text{ for } \Phi = 0 \text{ and} \\ &= \begin{bmatrix} a+bi \\ c+di \end{bmatrix} \text{ for } \Phi = \frac{\pi}{2} \end{aligned}$$

The case $\Phi = 0$ corresponds to linear polarization and the case $\Phi = \frac{\pi}{2}$ corresponds to elliptical polarization, where the principal axes are along $\mathbf{k} = \mathbf{k}_2 \pm \mathbf{k}_1$. The resultant field is shown in Fig. 2.4.

Case c)

$$\tilde{\mathbf{E}}_1 = \begin{bmatrix} 1 \\ 0 \end{bmatrix} \text{ and } \tilde{\mathbf{E}}_2 = \begin{bmatrix} 0 \\ 1 \end{bmatrix} e^{i\Phi}$$

implies that the resultant polarization is given by

$$\hat{\mathbf{E}}_r = \begin{bmatrix} 1 \\ e^{i\Phi} \end{bmatrix}$$

Since Φ varies between 0 and 2π, this grating will vary between linear and elliptical as shown in Fig. 2.4. A very important feature of this case is that the resultant intensity modulation $\triangle I = \sum_{i=x,y,z} E_{1i}E_{2i} = 0$, for all crossing angles θ, since $\mathbf{E}_1$ and $\mathbf{E}_2$ are orthogonal. Hence this will eliminate all intensity effects in the production of the DFWM signal. However there still is a modulation of the resultant direction

of the electric field as shown. Since the two beams are at the same frequency, the grating is stationary and there will be a tendency for the molecules to orient their most polarizable axis along the direction of the electric field. Therefore there will be a refractive modulation due to the birefringence of the molecule. The regions of circular polarization do not contribute to this signal since the RMS direction over one optical cycle is undefined.

Case d) I only show the result in the Fig. 2.4. We have not included the treatment of circularly polarized input beams although this is simply done by setting

$$\begin{aligned} \phi_{1x} &= \phi_{1y} \\ \phi_{2x} &= \phi_{2y} + \frac{\pi}{2} \end{aligned}$$

and repeating the calculations above.

At this stage it must also be noted that two anti-parallel beams also produce a grating. Here $\theta = 180°$ and therefore the spacing is the smallest. However in the DFWM picture this grating does not give rise to a DFWM signal, i.e. a signal anti-parallel to the probe, and hence will not be discussed in this work.

2.3 Material Gratings

A material grating is a periodic modulation of the complex refractive index of a material, which causes an incident optical ray to scatter/diffract from its path. If the refractive index modulation is purely real then only phase changes result, and if it is imaginary, absorption takes place, leading to an effective amplitude modulation. All materials exhibit both although one effect may completely dominate the other. Optical material gratings can be produced mechanically or light-induced by interference as described in the previous section.

There are two possibilities to convert an interference pattern into a physical modulation of the complex refractive index. The conventional process of holography achieves a permanent record of the intensity modulation by storing it in photo-

activated silver halide crystals on a photographic plate and then converting this exposure into an absorption grating via a chemical reduction process. Although this is a slow and sequential, three step process, it has a very large gain and hence allows the use of very low power CW lasers, like a 5 mW HeNe laser.

Alternatively, high power lasers can be used to induce a *material excitation* which results in a complex refractive index modulation. A material excitation is the localized change of a material from its equilibrium state induced by the electric field of the laser beam itself. It is the direct response of the material to the electric field. Examples of these states are the reorientation of molecular dipole orientations, or distortion of electronic cloud distributions or changes in a material's density distribution. These changes result in inhomogeneities in an optical material which causes an incoming ray to scatter. Since the inhomogeneities exhibit order due to the interference pattern which created them, they lead to coherent diffraction much like in conventional holography. This is why DFWM is often referred to as real-time holography. There is no need for a development process and the material usually returns to its original state after the light-matter interaction. The mechanisms which can be used to produce these material gratings are the topic of the next section.

2.4 DFWM Mechanisms

There is a large number of physical effects which can be used to produce a material grating, or conversely, we can use DFWM to determine and study the nature of the physical effects contributing to a material grating. Fig. 2.5 shows a flowchart which organizes these effects into categories, and also shows where this research fits in.

Broadly we can divide these mechanisms into electronic and nonelectronic effects. Electronic implies that the radiation is in resonance with some electronic transition frequency of the material in question. This can be linear absorption [10], ie. one-photon, or nonlinear as is the case for two-photon absorption [9], saturation of absorption [45] or reverse saturable absorption [5]. Resonant electronic nonlinearities are usually very large because of resonant enhancement of the nonlinear

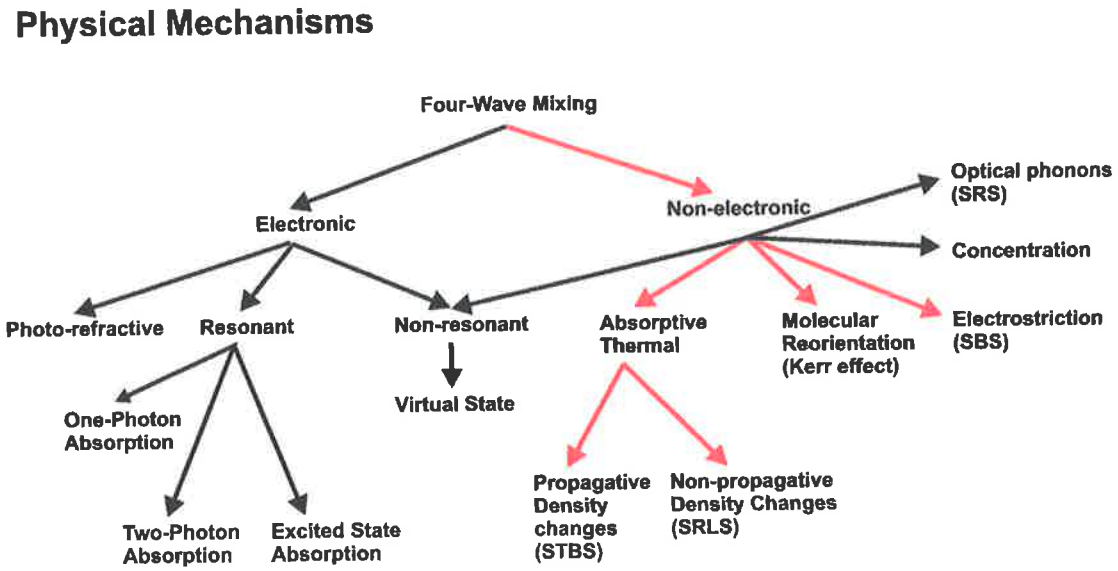

Figure 2.5: Physical mechanisms contributing to DFWM, broken up into their respective categories. Red lines indicate mechanisms relevant to this thesis.

susceptibility. GaAs at 1064 nm is a good example with a nonlinear susceptibility of $\chi^{(3)} = 3.0 \times 10^{-10}$ esu [46] which is three orders of magnitude larger than the nonresonant $\chi^{(3)}$ of CS_2 of 5.6×10^{-13} esu [47]. There is a third class of mechanism which is often referred to as electronic and that is the non-resonant, non-absorptive interaction. This involves virtual electronic states and as such is very small. However energy conservation and the Heisenberg uncertainty principle imply that these transitions are extremely fast, in the order of femtoseconds.

Nonelectronic effects can also give rise to very strong material gratings. If there is any absorption [11], [48], such as a weak vibrational overtone [49] or even strong particle absorption [50] such as in black ink solutions, this will give rise to localized temperature gradients due to radiationless thermal relaxation. This effect can give rise to thermal gratings which will change the refractive index of a material.

2.4.1 Molecular Reorientation Gratings

In an isotropic liquid of anisotropic molecules, such as CS_2 or a liquid crystal like Platinum Ethynyl (Fig. 2.8), polarized light from a high intensity source can induce

realignment of individual molecules [51]. The molecules individually realign their most polarizable axis with the electric field of the laser interference pattern and the net effect is of a modulation of the refractive index along the grating due to the birefringence of each molecule. This is also referred to as the optical Kerr effect [52]. It is usually very fast [53] and picosecond or in the case of CS_2, even sub-picosecond lasers are needed to resolve it. Since the present work uses sub-nanosecond to nanosecond pulses this effect can be considered instantaneous. In the case of weak coupling between molecules the response function (see section 2.6.1) is given by [49]

$$F_{re}(t) = \frac{1}{\tau_{re}} \exp\left(-\frac{t}{\tau_{re}}\right) \tag{2.4}$$

where τ_{re} is the collective molecular reorientational relaxation time.

Random room temperature fluctuations of molecular reorientation are responsible for Rayleigh wing scattering. However for stimulated Rayleigh wing scattering to have sufficient gain, it must by induced by two or more fields with a frequency difference of $\triangle\omega = 1/\tau_{RW}$ [54]. Hence we can safely ignore it in our case because we are dealing with DFWM where all beams have the same frequency.

2.4.2 Electrostrictive Acoustic Gratings

Acoustic gratings are the result of density changes in a liquid duc to electrostrictive forces or thermal expansion. Electrostriction can be described [51] by molecules moving toward a region of high intensity in a laser field, **E**. A molecule in this field experiences a polarization

$$\mathbf{p} = \alpha\mathbf{E}$$

where α is the molecular polarizability. Hence the energy expended on the molecule is

$$u_E = -\int_0^E \mathbf{p}\cdot d\mathbf{E} = -\frac{1}{2}\alpha(\mathbf{E}\cdot\mathbf{E})$$

If the electric field is spatially varying (ie. as it will be in a grating), there will be a force acting on the molecule given by

$$\mathbf{F}_{\text{molecule}} = -\nabla u_E = \frac{1}{2}\alpha\nabla(\mathbf{E}\cdot\mathbf{E})$$

implying that the molecule is pulled towards the region of high intensity. As a result, the density in this region is increased by an amount $\triangle\rho$, which leads to an increase in the dielectric constant and hence the refractive index by an amount

$$\begin{aligned}\triangle\epsilon &= \rho\frac{\partial\epsilon}{\partial\rho}\left(\frac{\partial\rho}{\rho}\right)\\ &= \gamma^e\left(\frac{\partial\rho}{\rho}\right)\end{aligned}$$

where γ^e is the *electrostrictive constant.* If this process gives rise to a propagative density change, a sound wave or *phonon* is the result.

2.4.3 Thermal Gratings

Thermal gratings are due to absorption (linear and nonlinear) and subsequent thermalization via intra- and intermolecular relaxation processes, mostly collisions. This heating leads to localized thermal expansion which opposes electrostriction which is a contractive process.

The dynamics of a thermal grating has been modelled by the use of coupled hydrodynamic equations which describe the light-matter interaction in the presence of absorption [55].

$$\frac{\partial U}{\partial t} = \frac{nc\alpha}{4\pi}E^2 + D\nabla^2 U - \frac{U}{\tau} \tag{2.5}$$

$$\rho_0 C_v\frac{\partial T}{\partial t} - K\nabla^2 T - \frac{T_0 F}{\rho_0}\frac{\partial\rho}{\partial_t} = \frac{U}{\tau} \tag{2.6}$$

$$\frac{\partial^2\rho}{\partial t^2} - \frac{B^T}{\rho_0}\nabla^2\rho - \frac{\eta}{\rho_0}\frac{\partial}{\partial t}(\nabla^2\rho) - F\nabla^2 T = -\frac{\gamma^e}{8\pi}\nabla^2(E^2) \tag{2.7}$$

$$\frac{n^2}{c^2}\frac{\partial^2 \mathbf{E}}{\partial t^2} - \nabla^2 \mathbf{E} = -\frac{4\pi}{c^2}\frac{\partial^2}{\partial t^2}\mathbf{P}_{NL} \tag{2.8}$$

In Eq. 2.5, α is the absorption, U energy density, D diffusion constant and τ the thermalization time. This equation models the absorption of laser radiation by the material and the subsequent delivery of this energy by thermalization to the solution. Eq. 2.6 is the heat-diffusion equation. ρ_0 and T_0 denote the equilibrium values of density and temperature, K is the thermal conductivity and F is a constant, coupling density and temperature. Eq. 2.7 describes the formation of acoustic phonons via electrostriction as well as thermal expansion. η is the effective viscosity, B^T is the bulk modulus and γ^e is the electrostrictive constant of section 2.4.2. Eq. 2.8 is the wave equation, driven by the nonlinear polarization

$$4\pi \mathbf{P}_{NL} = \epsilon_1 \mathbf{E}$$

where ϵ_1 is the change in the dielectric constant ϵ induced by the laser radiation.

2.4.4 Response Times

All these processes have characteristic relaxation times and eventually the material's state will return to equilibrium. This time ranges from femtoseconds for virtual excitations via picoseconds for molecular reorientations to milliseconds for thermal diffusion. Hence the relaxation time can provide information on the type of process involved in the material excitation and conversely, excitation of a specific process allows the tailoring of the duration of the grating. At nanosecond and sub-nanosecond time scales the *non-instantaneous* processes are thermal, pressure and density effects. These are induced by absorption and subsequent heating as well as electrostriction.

2.5 Stimulated Scattering and Diffraction

Once a grating has been established, it can be detected by probing it with a third beam. Note that the time of arrival of this beam can be either before, after, or simultaneous with respect to the write beams. Pre-arrival means that it can be

Scattering Process	Coupling mechanism	material excitation	Relaxation Time
Brillouin (SBS)	propagative pressure wave acoustic phonons	electrostrictive	10^{-9}
thermal Brillouin (STBS)	propagative pressure wave acoustic phonons	thermally induced photon absorption particle absorption	10^{-9}
Rayleigh (STRLS)	non propagative density fluctuation	absorption electrocaloric	10^{-8}
Rayleigh wing (STRLWS)	birefringence of anisotropic molecules	orientation of molecules	10^{-12}
Raman (STRS)	optical phonons	vibrational	10^{-12}

Table 2.1: Scattering Processes and their origins and decay times

used to monitor/observe the formation of the grating. It is not necessary for the read beam to be coherent with the other two, however if it is, coherence can introduce additional effects, such as give rise to electronic nonlinearities.

The generated signal can be monitored in several ways. Two of these are the *transient method* where the temporal pulse shape is measured, and the *time resolved method* where the integrated signal magnitude is measured as a function of 'time of arrival' of the backward pump. The time resolved method gets its name from the fact that it probes the dynamic evolution of the grating.

Scattering usually refers to randomly distributed centers whereas *diffraction* refers to scattering off ordered media, such as crystals or diffraction gratings. Light scattering occurs as a consequence of fluctuations in a material's properties. A completely homogeneous medium can scatter light only in the forward direction (ie. transmit it :) Scattering processes are divided into *spontaneous* ones which occur due to random fluctuations always present in the material and *stimulated* ones which implies that the light itself is the cause of the fluctuations in the material's optical properties. Note that stimulated scattering usually involves ordered scattering centres as opposed to spontaneous scattering.

Nonlinear optical scattering processes, such as DFWM are always referred to as stimulated (or *forced*). The source of the fluctuations define the type of scattering. Common stimulated optical processes are listed in table 2.1.

2.6 DFWM Models

Literature approaches the process of DFWM in two different ways. One uses the nonlinear optical method (NLO) [56] and the other uses *laser induced dynamic gratings (LIDG)* [8], also referred to as *transient real-time holography* (TRTH) [55, 57].

Physically it is easier to picture DFWM using the LIDG picture because it relies on the calculation of the diffraction efficiency produced by the write beams and the subsequent scattering by the read beam.

Mathematically LIDG and NLO are equivalent [8], however their use depends on the type of material excitation giving rise to the process. Electronic processes usually involve the calculation of $\chi^{(3)}$ using multi-level systems and transition rates. They take into account extensive cross coupling between all four beams and thus make use of the NLO method.

When the effect is non-electronic, as for example in thermal or electrostrictive gratings the preferred approach is via LIDG or TRTH.

2.6.1 Nonlinear Polarization

There are some very good texts on nonlinear optics [58, 8, 59, 51, 60]. It is the aim of this section to give a brief overview and to describe those parts that pertain to this work

In the presence of weak electric field, the polarization inside a material is given by the approximation

$$\mathbf{P}_0 = \chi_0 . \mathbf{E} \tag{2.9}$$

In the presence of a time varying optical field

$$\mathbf{E}(\mathbf{r},t) = \mathrm{Re}\{\mathbf{E}(\mathbf{r})e^{-i\omega t}\} = \frac{1}{2}\{\mathbf{E}(\mathbf{r})e^{-i\omega t} + \mathbf{E}(\mathbf{r})e^{i\omega t}\}$$

the time evolution of $\mathbf{P}$ and $\mathbf{E}$ can be calculated using the wave equation

$$\nabla^2\mathbf{E} - \frac{1}{c^2}\frac{\partial^2}{\partial t^2}\mathbf{E} = \frac{4\pi}{c^2}\frac{\partial^2}{\partial t^2}\mathbf{P}$$

However there are important factors which change this simple behavior. For a high intensity optical field, the approximation 2.9 is no longer accurate and higher order components must be considered, namely

$$P_\alpha = \sum_\beta \chi_{\alpha b} E_\beta + \sum_{\beta\gamma} \chi^{(2)}_{\alpha b\gamma} E_\beta E_\gamma + \sum_{\beta\gamma\delta} \chi^{(3)}_{\alpha b\gamma\delta} E_\beta E_\gamma E_\delta + \ldots \tag{2.10}$$

ie. the polarization field is no longer linearly proportional to the incident electric field and hence the term *nonlinear optics.*

In addition matter does not respond instantly to light. The history of any light-matter interaction has to be included in Eq. 2.9. Hence

$$\mathbf{P}(t) = \epsilon_0 \int_{-\infty}^{\infty} \chi(t-\tau)\mathbf{E}(\tau)d(\tau)$$

where causality implies that

$$\chi(t-\tau) = 0 \text{ , for } t-\tau < 0$$

This is simply the convolution of the electric field of the laser beam, $\mathbf{E}(t)$ with the material's temporal response function.

DFWM is a third order nonlinearity because it corresponds to the mixing of three input waves which produce a fourth, signal wave. This is the third order term in Eq. 2.10. Linear and second order effects can occur simultaneously but will not give rise to a DFWM signal and can hence be ignored for our purposes. This leaves the third-order polarization term which is given by

$$P_\alpha(t) = \sum_{\beta\gamma\delta} \chi^{(3)}_{\alpha b\gamma\delta}(t) E_\beta(t) E_\gamma(t) E_\delta(t) + E_\alpha(t) \int_{-\infty}^{\infty} Z(t-\tau)E(\tau)E(\tau)d\tau \tag{2.11}$$

where we have separated the electronic response from the nuclear response contained

in the function $Z(t)$. Higher order effects than this are very much smaller again for nonresonant materials and can also be ignored.

$Z(t)$ is composed of all non-instantaneous effects which can contribute to the DFWM signal, ie.

$$Z = \sum_m F_m \tag{2.12}$$

where F_m represents the response function of a particular physical effect, m. Naturally only dominant effects need to be considered, which in our case are molecular reorientation and density effects.

Eq. 2.11 has two important properties

1. $P^{(3)}_{\max} = k\,|E_{\max}|^3$

2. $P^{(3)}(t) \neq k\,|E(t)|^3$

where k is a constant of proportionality. The latter point implies that the temporal structure of the DFWM signal does not follow the cube of the input radiation for slow mechanisms.

For nonresonant, weakly absorbing systems (and hence low DFWM reflectivities), we can assume that the fourth wave does not contribute to the nonlinear interaction and hence

$$I_4 \propto \left|P^{(3)}\right|^2 \tag{2.13}$$

which is derived from the solution of the *nonlinear wave equation*[58].

$$\nabla^2\mathbf{E} - \frac{1}{c^2}\frac{\partial^2}{\partial t^2}\mathbf{E} - \frac{4\pi}{c^2}\frac{\partial^2}{\partial t^2}\mathbf{P}^{(1)} = \frac{4\pi}{c^2}\frac{\partial^2}{\partial t^2}\mathbf{P}^{(3)} \tag{2.14}$$

Physically this is the well-known result that says that the electric fields of the input beams couple via the nonlinear polarization to produce a fourth wave, ie. the *wave mixing process.*

Combining Eq. 2.11 and 2.13 we get the following important result describing

the temporal nature of the DFWM wave.

$$I_4(t) = I(t)\left|\int_{-\infty}^{t}\sum_m F_m(t-\tau)I(\tau)d\tau\right|^2 \tag{2.15}$$

Note that here we have included all third order nonlinear effects in F_m for simplicity and have labelled the three input pulses $I(t)$, because they originate from the same laser pulse and arrive simultaneously in the material. As we will show in the following sections, F_m can be modelled and thus allows us to model the DFWM response.

In the steady state case, where F_m is the delta function this relation reduces to

$$I_4 = \left(\frac{\omega}{4c^2\epsilon_0 n^2}\right)^2 l^2 I_1 I_2 I_3 \left|\chi^{(3)}_{xxxx}\right|^2 \tag{2.16}$$

where all the variables have their usual meaning. Hence the signal intensity produced by the nonlinear interaction in a non- or weakly absorbing material is proportional to $\left|\chi^{(3)}\right|^2$ and the product of the input intensities [61].

It is also important to realize that $\chi^{(3)}$ is a 4^{th} rank tensor and as such has 81 components, however in an isotropic medium such as a liquid it reduces to all but 4 elements [58] given by $\chi^{(3)}_{xxxx} = \chi^{(3)}_{xxyy} + \chi^{(3)}_{xyxy} + \chi^{(3)}_{xyyx}$. All four can be excited in a DFWM experiment by polarization control of the three input beams [62]. The component $\chi^{(3)}_{xyyx}$ is of special importance, because it corresponds to the case where both pumps are orthogonally polarized to the probe. This implies that there can be no intensity grating written between the pumps and the probe as discussed in section 2.2.

2.6.2 Temporal Response

Note that we should be able to use the measured DFWM pulse shape as well as the laser pulse shape to reconstruct the material's temporal response via a deconvolution

process. Rewriting Eq. 2.15 as

$$\sqrt{\frac{I_4(t)}{I(t)}} = \int_{-\infty}^{t} \sum_m F_m(t-\tau) I(\tau) d\tau$$

and then taking the Fourier Transform (FT) and using the convolution theorem we get

$$FT\left\{\sqrt{\frac{I_4(t)}{I(t)}}\right\} = \hat{I} \sum \hat{F}_m$$

where the $\hat{X}$ denotes the FT of X and hence

$$\sum \hat{F}_m = \frac{FT\left\{\sqrt{\frac{I_4(t)}{I(t)}}\right\}}{\hat{I}}$$

and

$$\sum F_m = FT^{-1}\left\{\frac{FT\left\{\sqrt{\frac{I_4(t)}{I(t)}}\right\}}{\hat{I}}\right\}$$

Hence measurement of the transient response of the DFWM signal should give us the overall response function of the material. If, by polarization control, we can eliminate certain physical mechanisms, as outlined in section 2.2 then we can even separate $\sum F_m$ in Eq. 2.15 for some of the physical effects. We have not done this in this thesis but allude to it in section 6.6 for future work.

2.6.3 Transient Model

Section 2.4 illustrated that in the sub-ns to ns regime molecular reorientation can be considered instantaneous, whereas electrostriction, absorption, thermal and density effects have to be treated as non-instantaneous. The strength of this work lies in the ability to measure both the *transient response* as well as the *dynamic evolution* of the material grating over a *range of pulse lengths*. McEwan et al [49] have developed a model describing the pulse shape of the return wave in a material where absorption dominates over electrostriction using a Q-switched laser at nanosecond time scales. They solve the hydrodynamic equations of section 2.4.3 to obtain the

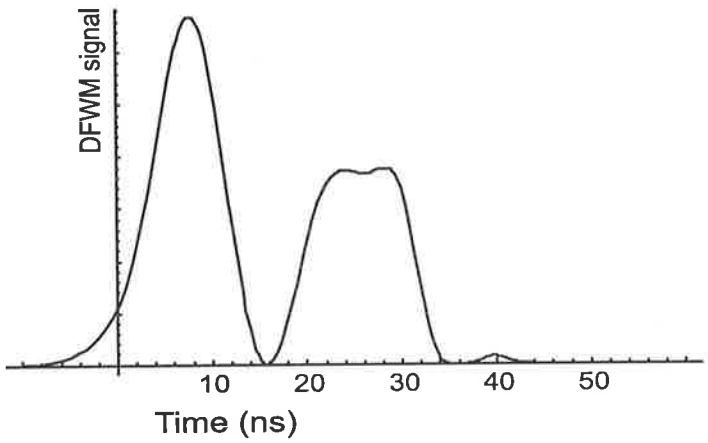

Figure 2.6: This graph illustrates the DFWM signal in a material with a comparable reorientational and thermal nonlinerities. The input pulse was simple Gaussian of length 8ns.

response function F_m of Eq. 2.12which they subsequently use to model the transient DFWM return I_4 in Eq. 2.13.

$$F_m(k,t) = F_{re}(t) + F_{th}(k,t) \tag{2.17}$$

$$F_{th}(k,t) = \frac{1}{\tau_{th}}[-\exp(-D_T k^2 t) + \exp(-D_v k^2 t)\cos(\upsilon_s k t)]$$

The first component describes the decay of the grating by thermal diffusion and the second component describes a sound wave damped by a viscosity D_v. They also include a response function for molecular reorientation

$$F_{re}(k,t) = \frac{1}{\tau_{re}} \exp\left(-\frac{t}{\tau_{re}}\right)$$

where τ_{re} is the molecular reorientation time. In this case the response function is dominated by molecular reorientation as the instantaneous response and thermal density changes as the non-instantaneous response. As an example of the effects of the combination of a reorientational and a thermal nonlinerity, we have calculated the DFWM return using Eqns. 2.15 and 2.17, as shown in Fig. 2.6.

In addition we can use the interference techniques described in section 2.2 to eliminate $F_{th}(k,t)$ from Eq. 2.17 such that the response is dominated entirely by the Kerr effect.

Physically, reorientation and thermal effects are expected to be opposite in sign because localized heating results in expansion and molecular alignment along the electric field results in contraction. The latter is more easily understood when compared the matchbox effect where the alignment of matches allows dense packing. Hence the structure of a DFWM return should reflect this competition.

2.6.4 Picosecond Dynamic Grating Evolution

While the previous section focused on the transient response on a nanosecond scale, we can also probe the transient grating using shorter pulses and measure the maximum intensity of the DFWM response as a function of delay of the backward pump. This examines the time evolution of the dynamic grating and is called the *time resolved method* as discussed in section 2.5.

Nelson et al [63, 64, 65] have developed a model which describes the probing of a material grating with a picosecond laser beam in this fashion. The model takes into account electrostriction and absorptive expansion. It predicts the generation of two counter propagating compressional waves with wave vectors equal to that of the grating. In other words, this process gives rise to acoustic phonons, ie. a sound wave. Due to the symmetry of the sound wave vectors $\pm\mathbf{k}$ a standing wave is the result. The acoustic response due to thermal and electrostrictive effects was shown to be

$$S_{\text{electrostriction}} = -B\cos kx\ (\sin\Omega t) \tag{2.18}$$

$$S_{\text{thermal}} = A\cos kx\ (1-\cos\Omega t) \tag{2.19}$$

where k is the grating vector, Ω is the acoustic frequency, x is the direction along the grating vector defined in Fig. 2.3 and S is the displacement. The diffraction

efficiency of the grating was shown [65] to be related to the displacement by

$$\eta \propto S^2 \tag{2.20}$$

This leads to a very interesting result. In the electrostrictive case, the displacement oscillates between a negative maximum and a positive maximum. Thus the displacement attains a maximum twice per acoustic cycle and therefore, by Eq. 2.20, the diffraction efficiency will as well. However in the case of absorption, thermal diffusion leads to the presence of an additional, static term. Thus the displacement is always positive, varying between a maximum and a null displacement. Therefore the diffraction efficiency attains a maximum only once per acoustic cycle. This behavior is shown in Fig. 2.7 for three cases. If we can measure the speed of sound in the liquid by some other method (Ch. 6), we can determine which mechanism is responsible for the acoustic phonons by measuring the period of oscillation. The latter is given by

$$T_{\text{thermal grating}} = \frac{\Lambda}{v_s} \tag{2.21}$$

$$T_{\text{electrostrictive grating}} = \frac{\Lambda}{2v_s} \tag{2.22}$$

where Λ is the grating spacing given by Eq. 2.1 and v_s is the speed of sound in the material. In chapter 6 we will make use of these results to determine the physical mechanisms of the nonlinear optical interaction in the sub-nanosecond regime.

2.7 Materials

As mentioned briefly in the introduction the motivation behind this work was to investigate the nonlinear scattering and nonlinear refractive properties of an organometallic power limiter, platinum ethynyl (PE). A good review on optical limiting was written by Tutt and Bogess [4]. PE was shown by several groups to be useful in the visible via reverse saturable absorption (RSA) [1, 2]. This material was

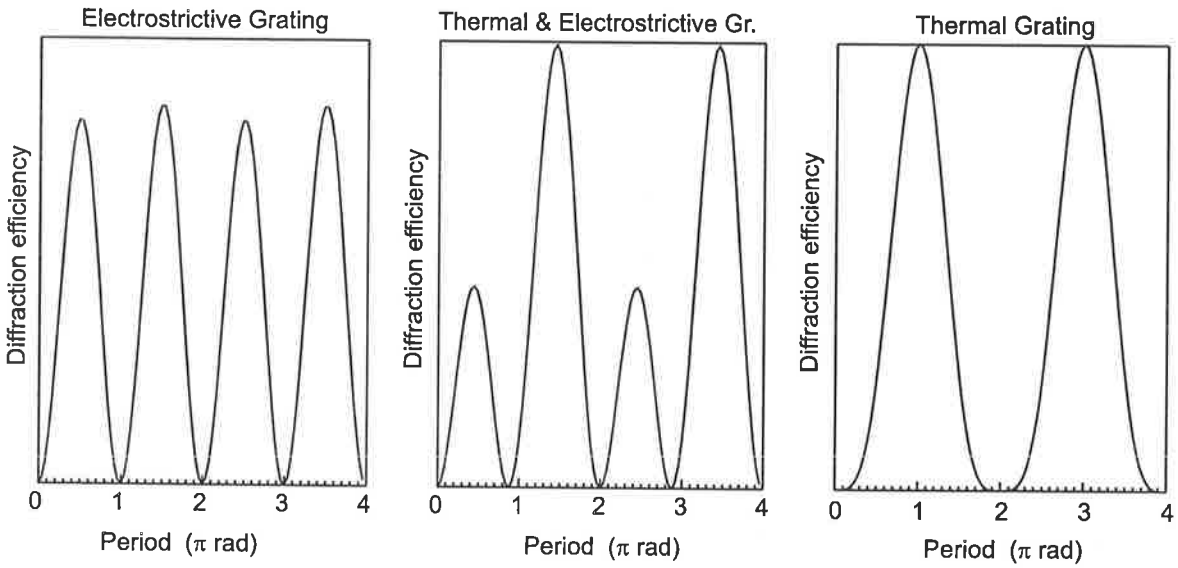

Figure 2.7: Temporal evolution of diffraction efficiency. Comparison between physical mechanisms.

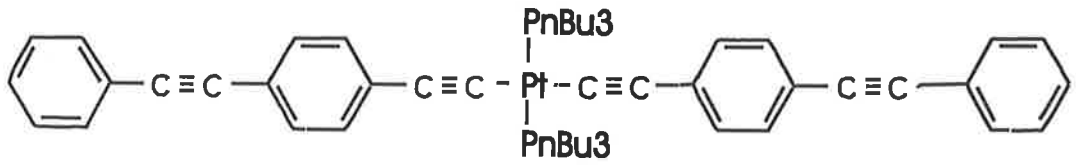

Figure 2.8: Platinum Ethynyl Complex, PE

first synthesized by Takahashi et al [66] and our samples were provided by Julianne Davy of the DSTO[2]. We used it in solutions of THF and at concentrations of 0.08 M. The sample recrystallized at room temperature overnight and was always kept in a refrigerator when not in use. At 1064 nm it exhibits a non-resonant response and thus has a real value of $\chi^{(3)}$ [2].

RSA arises when the excited state of a molecule has a larger absorption cross-section than the ground state, ie. a material which darkens under intense laser radiation. This presents an excellent mechanism for optical limiting. Other mechanisms include self defocusing and light induced scattering. If an optical signal

[2]Defence Science and Technology Organization, South Australia

induces scattering centres in a medium and if this happens on the rising edge of the incoming laser radiation, the signal will be attenuated as it passes through, thus exhibiting optical power limiting properties. Frazier et al [67] and Staromlynska et al [1] demonstrated the existence of nonlinear scattering in PE and hence there was a need to investigate this further. To eliminate RSA effects, this investigation had to be done well away from any possible resonant enhancement and thus was done conveniently at 1064 nm.

To validate our experimental results we used a standard nonlinear optical material, carbon disulfide (CS_2), which also gives rise to a nonresonant nonlinearity at 1064 nm. It has been widely studied and is very commonly used as a reference material and calibration standard. In our experiments we measured the absolute value of its nonlinearity before using it as a calibration standard. This is not usually done because of difficulties involved in measuring absolute values of nonlinear susceptibilities. CS_2 has a large nonlinear susceptibility of $\chi^{(3)}_{xxxx} = 5.6 \times 10^{-13}$ esu [47] which is mainly due to molecular reorientation [53]. Its reorientation time is of the order of 2 ps because it is a small molecule and thus we expect a fast, steady state, non-thermal response at 1064 nm. The major drawback with CS_2 is that it is extremely toxic [68], affecting just about all parts of the human body in some adverse way, even at low concentrations (10 ppm). Thus safety procedures must be in place before it is **purchased**[3]. It is also extremely volatile and flammable, making it difficult to contain. Hence the sample cell had to be chosen such that there was negligible leakage.

The hyperpolarizability of PE has been measured by Guha et al [2] using the optical Kerr effect at 1064 nm with 20 ps pulses. They measured a value of $\gamma = 0.12 \times 10^{-33}$ esu relative to CS_2 for which they used a nonlinear susceptibility value of $\chi^{(3)}_{xxxx} = 30 \times 10^{-13}$ esu [69]. The latter is larger than the value commonly used

[3]We spent quite some time on establishing chemical safety procedures for the laboratory. When using CS_2 this meant: Usage of an amount which if spilled completely did not exceed the safety limit for the size of the room. Transportation in a padded, non-breakable container. Calculation of the complete recirculation time of the air in the laboratory (10 hrs). Long term containment in non-leaking glass container in a fire-proof, well ventilated chemical storage room.

in literature of $\chi^{(3)}_{xxxx} = 5.6 \times 10^{-13}$ esu. $\chi^{(3)}$ and γ are related by

$$\chi^{(3)} = \gamma L^4 N_1$$

where L is the local field correction factor given by

$$L = \frac{n^2 + 2}{3}$$

and N_1 is the number density of the solute in the solution. Guha's value of the hyperpolarizability for PE thus equates to a nonlinear susceptibility of

$$\chi^{(3)} = 2.6 \times 10^{-13} \text{ esu}$$

Since they used a higher value for $\chi^{(3)}$ in CS_2 than Xuan, we will correct it proportionally to reflect the value we used for $\chi^{(3)}$ in CS_2. Hence Guha's value for $\chi^{(3)}$ in PE, relative to a $\chi^{(3)}$ in CS_2 of 5.6×10^{-13} esu is

$$\chi^{(3)}_{PE} = 0.49 \times 10^{-13} \text{ esu.}$$

Chapter 3

Stimulated Brillouin Scattering

3.1 Introduction

We have established in section 2.6.1 that pulse length is a critical parameter in determining the type of physical response in a DFWM experiment. The ability to vary the pulse length with enough dynamic range to access different physical mechanisms would significantly increase the usefulness of a DFWM experiment, or any other nonlinear optical experiment for that matter. If this change can be effected with minimal or no change of any other parameters of the laser system, then the utility of this system would be increased even further because it ensures that all measurements are directly comparable with each other. Most importantly, the alignment of such a system must remain the same for any change in pulse length, because this is one of the most critical parameters in a DFWM experiment (see section 4.1.4). This is very difficult to achieve with the traditional, multiple-laser system approach.

We have accomplished just this by modifying an existing Q-switched Nd:YAG laser to include a phase conjugated mirror and a variable pulse compressor, both of which are based on stimulated Brillouin scattering (SBS) . The different pulse lengths are achieved without disturbing the master oscillator and the systems phase conjugation ensures that the alignment of the DFWM experiment remains unchanged after each change of pulse length. The following review gives a physical account

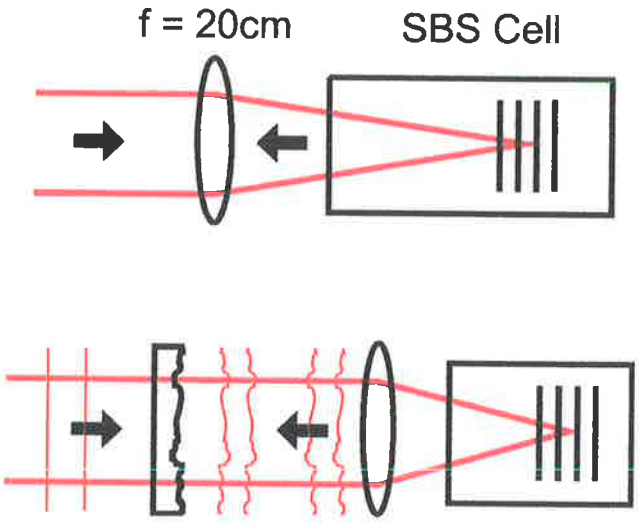

Figure 3.1: (a) Simple SBS mirror setup. The phonon grating is shown inside the SBS cell. (b) shows phase front of an incoming wave being aberrated by, say a piece of shower glass. The SBS mirror reverses this phase wave front and hence all aberrations are "ironed out" after passing back through the aberrator.

of the SBS process. I have given ample references for readers interested in further work.

Stimulated scattering was first demonstrated by Eckhard et al [70] using Raman vibrations in liquids. SBS was demonstrated by Chiao et al [19] and the phase conjugation property was discovered by Zel'dovich et al [71].

In its simplicity and mathematical complexity SBS truly can be called a beautiful process! SBS is stimulated backscattering of a laser beam by an acoustic grating in a medium which is seeded by noise. The onset of SBS is dependent on a threshold intensity given by

$$I_{th}gl = C \tag{3.1}$$

where g is the SBS gain for the material used and C is a numerical constant usually taken to be 25-30 [21]. The interaction length, l, is the shorter of the cell length, coherence length or Rayleigh range [72]. A simple, phase conjugating SBS mirror consists of a lens and a cell filled with a liquid or gas (Fig. 3.1).In the present and most typical applications, where the Rayleigh range of the focused beam is

significantly shorter than both the SBS cell length and the coherence length of the beam, it can be shown [72] that the threshold for SBS is independent of focusing parameters and is given as a threshold power of typically 50-100 kW. This is easily attained with a Q-switched laser.

If the return is generated in the focal region of the lens it is the phase conjugate of the incoming beam and can be used to correct for aberrations in a power amplifier [73, 74].

With proper choice of cell length and focal geometry, SBS also provides a possibility for pulse compression [75, 76]. For optimal compression to occur, both cell and focal lengths must be at least half the length of the input pulse [77]. As with the short cell, the return is initiated in the focal region, but, as the return propagates backwards, the region of maximum reflectivity also moves backward toward the entrance of the cell, compressing the pulse in a bulldozerlike fashion.

The shortest pulse length attainable for high efficiency reflection is limited by the phonon lifetime of the medium [78]. The choice of medium should take this into account as well as ease of use and safety of handling.

Thus a phase conjugated laser system with variable pulse compression has several advantages over a conventional system. These are higher peak power and improved beam quality, as well as operation over a range of pulse lengths while maintaining perfectly the direction of the laser beam.

3.2 The SBS Process

3.2.1 Mechanism

Very good reviews on SBS are given in references [21, 22].

A laser beam incident on a material will experience all kinds of scattering processes as already described in section 2.5. SBS refers to the scattering off acoustic phonons, ie. propagating density fluctuations. In this way it is very similar to SRS which refers to scattering of optical phonons, ie. propagating vibrational fluctuations. In fact SBS materials have to be chosen such that their SBS gain is high, and

their Raman gain is low [59]. These acoustic phonons can have their origin either in thermal or in electrostrictive density fluctuations (see section 2.4). Self-starting SBS distinguishes itself from DFWM in that there is no need for separate pump beams to produce the NLO process.

A small proportion of the incident wave will be scattered backwards by random acoustic fluctuations present in any material at room temperature. This backscattered wave, called the *seed*, will interfere with the input wave and create a near standing wave pattern with a very low amplitude modulation due to the small amplitude of the backscattered wave[1]. Thus an interference grating is established which, provided it is large enough, can give rise to a material excitation much the same way as in section 2.3. It is also important to note that this material excitation is in resonance with the medium because the phonon frequency is a property of the material. This grating acts to increase the *seed*, the backward scattered wave experiences gain and a snowball effect occurs, ie. the more phonons there are the larger the optical grating and the larger the optical grating the larger the material excitation will be[2].

The response time of the SBS process is around 100 picoseconds and therefore a nanosecond pulse will virtually see it as a mirror. Hence the initial part of a nanosecond pulse will be transmitted and once the intensity threshold has been reached, the reflectivity is turned on instantly, resulting in a sharp rise time of the reflected pulse.

The intensity threshold is basically a consequence of the fact that the input beam itself is generating the backscatter. An intensity is needed which is large enough such that *given a constant gain* for a focussed geometry, the return wave is roughly equal in amplitude to the input wave. This is manifested in Eq. 3.1. Only above this intensity is the process actually self starting, below it is not stimulated and we only get spontaneous backscatter.

[1]Note that this backscattered wave will be frequency shifted by the acoustic frequency because of the Doppler effect.

[2]This is why Brillouin induced FWM is such an efficient process. In this case the grating written by the nearly degenerate FWM process is resonant with the material excitation.

3.2.2 Phase Conjugation

Phase conjugation [79, 80] is only achieved if the seed is generated in the *focal region/far field* of the input beam. This is achieved easily with a lens. The reason for this is that the material excitation is either an electrostrictive or a thermal nonlinear optical process which both depend on the intensity of the laser beam. Therefore in order to achieve phase conjugation we need to translate all the phase information of the incoming wave into intensity information. The focal point of a lens corresponds to the spatial power spectrum of the input field and thus provides exactly this mechanism. The gain will be greatest for the wave which exactly retraces its path. Hence it is not necessary for the return to be generated *exactly* at the focus.

If the beam is not focussed, the intensity distribution of the cross section does not contain any phase information and a phase conjugate return is not possible. We may however still get an SBS reflection if the intensity threshold has been exceeded.

3.2.3 Pulse Compression

Pulse compression [81] is another interesting phenomenon which relies on the rapid response time of the process as well as the seeding process of the backward travelling wave. If the pulse is focused deeply into a long cell (say half the pulse length), then the SBS wave is generated as explained before. As it travels backward, the initial part of the pulse itself acts as a seed for further acoustic gratings because of the standing wave pattern that is generated as the pulse is folded onto itself. Hence the centre of reflection is dynamically generated and moves toward the entrance window, "pushing" out the part of the pulse which is still coming in and resulting in an overall compression of the input pulse. The amount of compression is thus limited to the response time of the electrostrictive effect, ie. the speed at which the centre of reflection can follow the leading edge of the pulse.

A two cell arrangement [77] allows for an optimization of this process. In this case one cell, called the oscillator, is used for the seed and the other, the amplifier, is used for compression. This arrangement is usually used for high energy (>1J)

SBS lasers because the SBS seed is generated by the low energy, leading edge of the incoming pulse, thereby avoiding optical breakdown which would be caused if all of the pulse were focused. The seed travels back into the amplifier cell and interacting with the incoming beam. Thus the main portion of the incoming beam is reflected in the amplifier cell, where the beam is collimated and thus has a low intensity. Since our experiment dealt with low energy beams only (approx. 50 mJ) a single cell setup satisfied completely our requirements.

3.2.4 Materials

There were a variety of materials available for SBS [82]. We chose Freon-113 for several, compelling reasons:

Ease of use, cost and importantly, safety of handling: Liquids are easier to contain than gases and require no pressurization. Some good SBS materials like CS_2 are highly toxic and highly volatile. In comparison, Freon-113 is relatively non-toxic. Several liters could be spilled in a laboratory without exceeding dangerous limits[3].

Phonon lifetime (or phonon response time): The extend of pulse compression is limited by the phonon lifetime [78] and hence this needs to be as fast as possible. Freon has a phonon lifetime of 0.8 ns [82] which is faster than most other available materials.

Absorption (linear and nonlinear): A large amount of linear absorption will significantly attenuate the beam in a long cell. Freon-113 has a very low linear absorption at 1064 nm, of less than 10^{-5} cm^{-1} [82]. In addition, if linear or nonlinear absorption are large enough, there will be potential competition between electrostrictive and thermally induced SBS which will lead to instabilities [59].

Gain competition between SBS and SRS: We need the material's Raman gain to be much lower than the Brillouin gain to prevent SRS from reducing the efficiency of the SBS process [83].

[3]Spilling several litres of Freon into the laboratory is unacceptable from an environmental point of view. For this reason, we are in the process of changing to another fluoro-carbon, Flourinert, which is environmentally safe.

Chapter 4

Four-Wave Mixing - Long Pulse Study

4.1 A Preliminary Experiment

We set up a simple, preliminary experiment to establish the operating parameters of DFWM and learn of any practical requirements before commencing with a more versatile and complex experiment.

As discussed in section 2.7 we used CS_2 as a reference material to obtain a transient DFWM signal in the nanosecond and off-resonant regime at 1.064 μm. Prior to the experimental setup we established the requirements to observe a signal:

- Choice of high bandwidth, high sensitivity detectors to record the transient evolution of the signals

- Choice of laser intensity to generate an easily detectable signal with a suitable detector

- Establishment of alignment criteria necessary to observe the DFWM signal

4.1.1 Detection System

Appendix A gives a more detailed description of detector issues. We chose a simple, reverse biased Silicon photodiode[1] for our detection system. This presented a good solution exhibiting good sensitivity, linearity, dynamic range and large bandwidth. Combining this with a 500 MHz digital scope yielded an overall bandwidth of 350 MHz, which gave a pulse rise time of approximately 0.85 ns.

The sensitivity of this diode was about 0.05 A/W at 1064 nm which corresponds to 2.5 V/W into 50 Ω, which was suitable for a pulsed laser with very high peak powers. Assuming a signal to noise ratio of at least 5 and a noise floor of 4 mV, a *minimum detectable signal size* would be around 20 mV which corresponds to 8 mW onto the area of the diode or an intensity of 0.8 W/cm^2.

The laser intensity levels had to be optimized such that the DFWM signal was maximized, while avoiding damage to the optical components and the sample due to optical breakdown.

4.1.2 Estimated Signal size

The magnitude of a nonresonant four-wave mixing signal is given by Eq. 2.16

$$I_4 = \left(\frac{\omega}{4c^2\epsilon_0 n^2}\right)^2 l^2 I_1 I_2 I_3 \left|\chi^{(3)}_{xxxx}\right|^2 \tag{4.1}$$

where l is the overlap length, I_x are the intensities of the pumps, probe and signal beams in that order, and the other symbols have their usual meaning.

The value of $\chi^{(3)}_{xxxx}$ is given by [47].

$$\begin{aligned}
\chi^{(3)}_{CS_2} &= 5.1 \times 10^{-13} \text{ esu} \\
&= (5.1 \times 10^{-13}) \times \frac{4\pi}{(10^{-4}c)^2} \text{ m}^2/\text{ V}^2 \\
&= 7.1 \times 10^{-21} \text{ m}^2/\text{ V}^2
\end{aligned}$$

[1] BPX 65 from RS Electronics

We used the original pulsed Nd:YAG for the preliminary experiment which provided 70 mJ in a 28 ns pulse and a 10 mm diameter beam, which corresponds to a fluence of about 0.1 J/cm^2. Assuming laser intensities of 3.2 MW/cm^2 (32 GW/m^2) for the pumps and 0.32 MW/cm^2 (3.2 GW/m^2) for the probe, a sample 5 mm in length should result in a signal with an intensity of

$$\begin{aligned} I_4 &= \left(\frac{\omega}{4c^2\epsilon_0 n^2}\right)^2 l^2 I_1 I_2 I_3 \left|\chi^{(3)}\right|^2 \\ &\simeq 4.7 \times 10^{16} \times 0.005^2 \times (32 \times 10^9)^2 \times 3.2 \times 10^9 \times (7.1 \times 10^{-21})^2 \text{ W/m}^2 \\ &\simeq 195 \text{ W/m}^2 \\ &\simeq 20 \text{ mW/cm}^2 \end{aligned}$$

which is smaller than the minimum detectable signal of 0.8 W/cm^2. Hence it was necessary to focus the pump beams to achieve more intensity and hence a larger signal. In our calculations, halving the diameter of all beams should increase the signal intensity by a factor of $(2^2)^3 = 64$. We would thus get a power of

$$\begin{aligned} P &= 20 \text{ mW/cm}^2 \times 0.01 \text{ cm}^2 \times 64 \\ &= 12 \text{ mW} \end{aligned}$$

onto the diode, unfocused, which corresponds to a maximum voltage of 30 mV, a detectable signal.

4.1.3 Signal isolation

Another requirement was to isolate the signal from stray light, because the signal level was low and the detector was quite sensitive. Stray light originated from a number of sources including stray beams reflecting off fixtures in the laboratory, and scatter off optical components like beam splitters, and the sample cell itself. Since this scatter was isotropic its intensity diminished quickly with distance. Propagating the signal by a few meters and setting up baffles could thus improve the signal to noise ratio such that there was negligible, detectable scatter for even the most

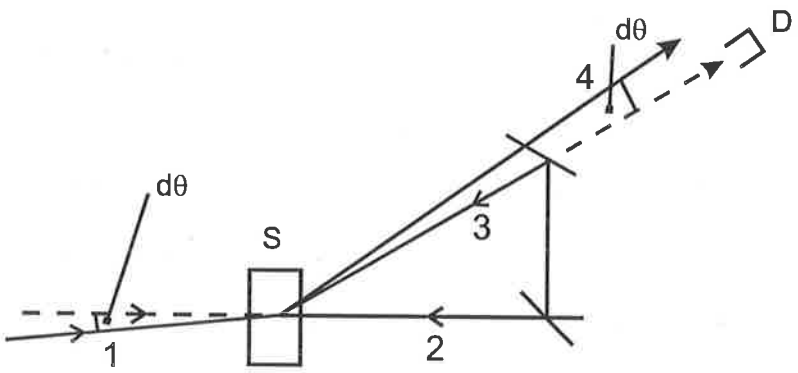

Figure 4.1: Signal direction dependence on backward pump deviation from colinearity

sensitive detector setting. If this was not done however, the DFWM signal would be drowned in the stray scatter.

4.1.4 Alignment

This delay distance rendered the experiment very sensitive to alignment. Hence an alignment procedure had to be established by which we could accurately position the signal detector.

Alignment of the beams had to ensure colinearity of the pumps to within some error factor as well as good overlap of pumps and probe within the sample. *Since the DFWM return would be a weak signal it was essential to know where it was going to be.* Conservation of momentum implied that deviation by an angle dθ by the pumps from colinearity would result in the signal deviating by dθ from the probe path, (see Fig. 4.1) hence missing the signal detector. Therefore the alignment accuracy of the pumps was set by the detector distance and aperture as well as beam diameter. Typical values were 1mm/8m$\simeq$ 0.1mrad.

4.1.5 Experiment

The experiment which satisfied all these requirements is shown in Fig. 4.2.

Good alignment of the pumps was easily achieved by retro-reflecting the back-

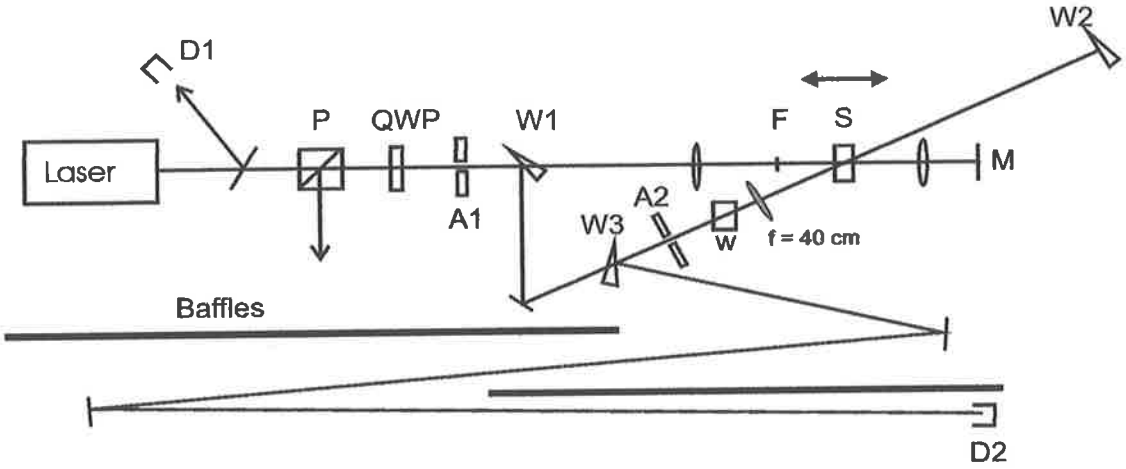

Figure 4.2: Setup for preliminary FWM experiment. The lens shown in red is placed there to verify phase conjugation

ward pump through aperture A1. The lenses ensured the correct beam diameter for the required intensity and sliding the sample along the optical axis of the lens significantly altered the intensities of the pump beams. A polarizer and a quarter wave plate were used to prevent feedback of the pulse into the laser cavity. A wobble plate W was used to scan the interaction region for maximum reflectivity without affecting the angular alignment of the probe. The position of the signal detector could be found by retro-reflecting the probe through aperture A2 by means of wedge W2. *This wedge reflection was also used for calibrating the signal detector by attenuation by a known amount using calibrated, metallic neutral density filters.*

4.1.6 Results

Using CS_2 as the sample, we obtained the signal shown in Fig. 4.3. The magnitude and shape were as expected. The pulse compression was due to the cubic intensity dependence of the DFWM return as shown by Eq. 4.1. The occurrence of four-wave mixing was verified by checking that the return disappeared if any of the three input beams were blocked. We confirmed phase conjugation by inserting a medium focal length lens (0.4 m) in between W3 and the sample. Only a phase conjugated signal would be recollimated after having passed through the lens. A non-phase

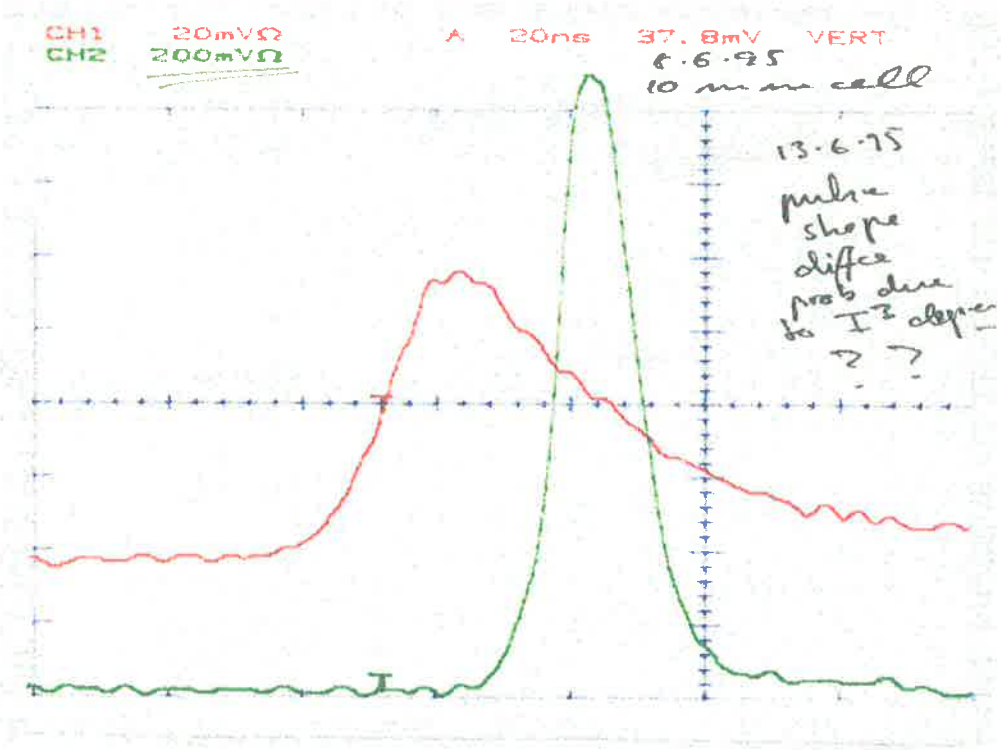

Figure 4.3: Original CRO output plot showing the DFWM signal(green) in CS_2 as well as the corresponding input(red)

conjugated signal would result in a decrease of the received signal intensity because the divergence of the beam would now have been increased and the beam diameter at D2 would be larger. In our experiment, inserting a lens did not change the intensity of the received signal, implying that the return was recollimated and therefore phase conjugated after it had passed through the lens on return.

We repeated the experiment in PE, but could not see a signal.

4.1.7 Discussion

This preliminary experiment validated the proposed requirements. Using CS_2 as a standard reference material we obtained a DFWM signal. The pulse shape was compressed as expected for a cubic nonlinearity and phase conjugation was verified to occur. The signal magnitude compared very well with literature. The experiment was simple to set up and served very well as a preliminary run.

4.2 A Versatile DFWM Experiment

There were a number of important, additional requirements which the previous experiment had not addressed. Hence we set up a more complex experiment which:

- used linear instead of circular polarization in the cell to allow formation of orientational as well as intensity gratings and thus enable measurement of the components of $\chi^{(3)}$,
- permitted temporal coincidence of pulses as well as pre-arrival of the backward pump,
- provided a delay line in order to probe the time evolution of the interaction,
- provided more powerful pulses to observe the weaker nonlinearity in PE.

4.2.1 Experiment

Geometry description

The new setup geometry is shown in Fig. 4.4. All three beams were now split off *before* they entered the cell as opposed to the preliminary experiment (Fig. 4.2) where the backward pump had passed through the sample once already, possibly being modified through nonlinear refraction and/or absorption. In addition this permitted all pulses to arrive simultaneously.

We used halfwave plates and Glan polarizers to control independently the polarization state of each beam and its purity. Note that the insertion of a polarizer into the probe path also enabled us to check the polarization of the return signal.

Delay line

In order to delay the arrival of the backward pump, a delay line was inserted. This posed a problem of alignment because, for all delays, the backward pump had to remain colinear with forward pump as explained in section 4.1.4.

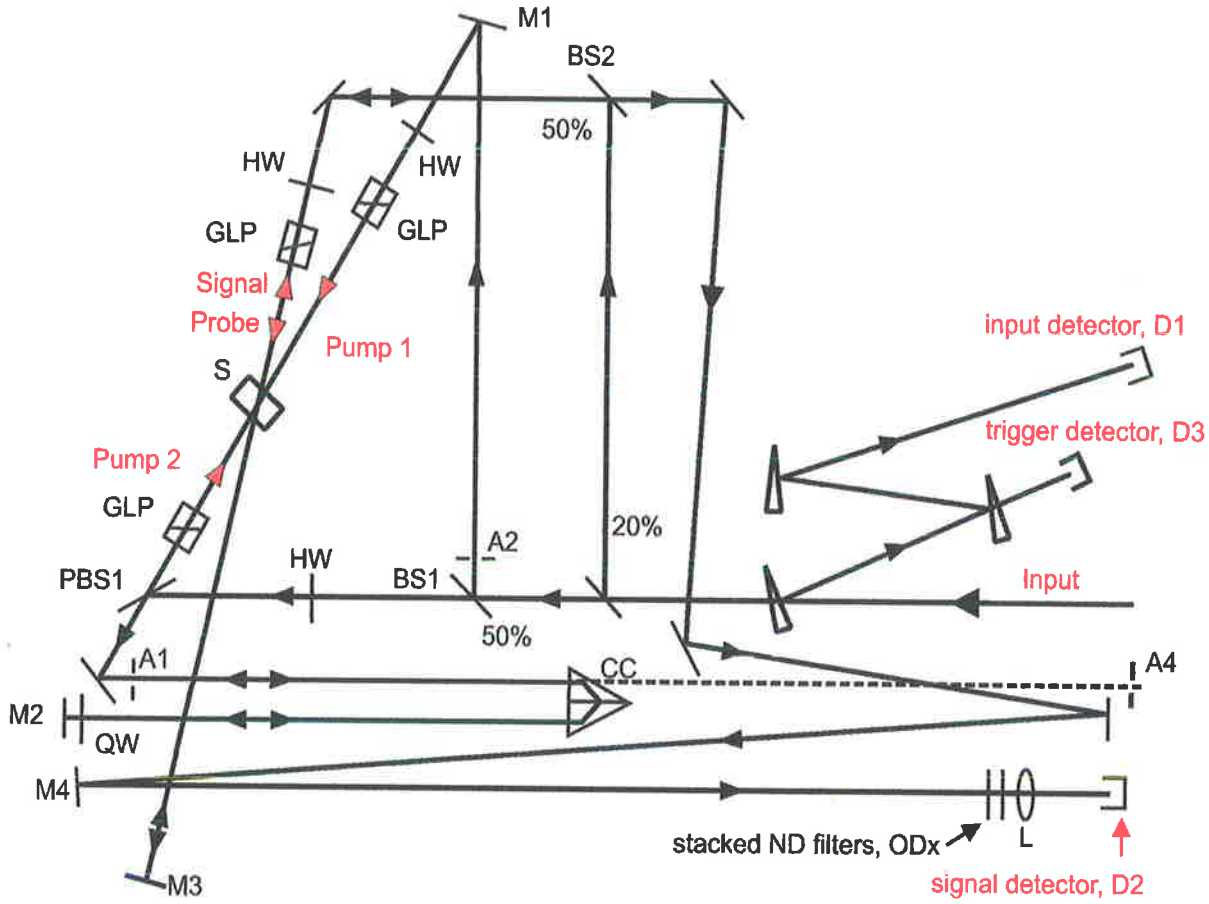

Figure 4.4: Versatile DFWM experiment including a variable delay line, temporally coincident input beams and polarization control. Note the signal is propagated by about 8m to eliminate detectable isotropic scatter from the cell windows.

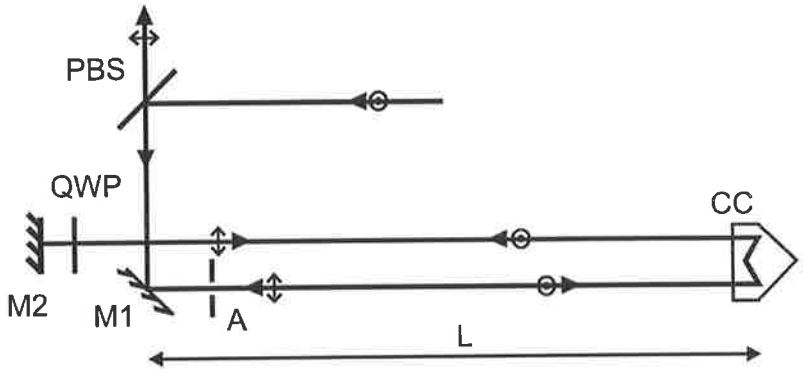

Figure 4.5: Delay line setup, polarization direction as indicated; PBS = polarizing beamsplitter, QWP = quarterwave plate, A = iris type aperture, CC = corner cube, L = delay line distance

Standard delay lines using a corner cube allow parallelism to be conserved, but not colinearity. For this reason I developed a novel type of delay line, shown in Fig. 4.5 with diffraction limited auto-alignment ([84], appendix E).

Alignment

In addition we developed an alignment system, which ensured great accuracy and repeatability in aligning all four beams to the same specifications. This was essential for results to be comparable between experimental runs. Note also that while a HeNe was used for positioning of components, the final alignment was always done at 1.064 μm.

The following explanation refers to Fig. 4.4. Aperture A2 was a 0.4 mm pinhole at the centre of a cross-hair on a white surface. The pinhole was placed at the centre of the forward pump at the position shown. With the help of a CCD camera and a TV set, mirror M1 was aligned to direct the backward pump onto the centre of the cross-hair of A2. Now both pumps had a common point of intersection at A2 to within 0.2 mm accuracy. We now removed the corner cube and used PBS1 to align the forward pump with the backward pump. This was done by centering the backward pump on iris A4 and then passing the forward pump through this as well. Thus there were two points, greater than 4 m apart, coincident to better than 0.2

mm precision. Hence the alignment colinearity was better than 0.2 mm and 5×10^{-5} radians. *This was always repeatable and was performed in the visible AND infrared.*

The signal detector was aligned using a mirror M3 to retroreflect the probe through an aperture (not shown). M3 was blocked and a DFWM signal generated. This signal on the detector was maximized using M4. Then one of the pumps was blocked to remove the DFWM signal and M3 was unblocked to give a simulated signal. This was maximized using the controls of M3. Thus the DFWM signal and M3 were aligned to give maximum signal and consequently were colinear.

The alignment of the delay line is discussed in appendix E.

Detectors and Calibration

We changed the detection system for the complex DFWM setup to give a larger bandwidth and more responsivity. This was effected by using 3 GHz InGaAs photodiodes and a 1 GHz transient digitizer. It is described in more detail in appendix A. To ensure constant and precise triggering we used a photodiode, saturated to give a fast rise time. The signal detector was calibrated using the probe beam to give absolute values for the intensity. Mirror M3 and neutral density filters simulated a weak return. Measuring the energy in the probe beam using a calibrated energy meter, beam diameter and pulse length allowed calculation of the intensity of the beam hitting the detector.

Laser

The laser was modified to improve its beam quality and shorten its pulse length. A complete description of this is given in chapter 5. For now it suffices to state that the beam quality was good (Fig. 4.6) and the pulse length was shortened from 28 ns to 8 ns FWHM (Fig. 4.7). The energy output remained constant and hence the power was increased by a factor of 2.3.

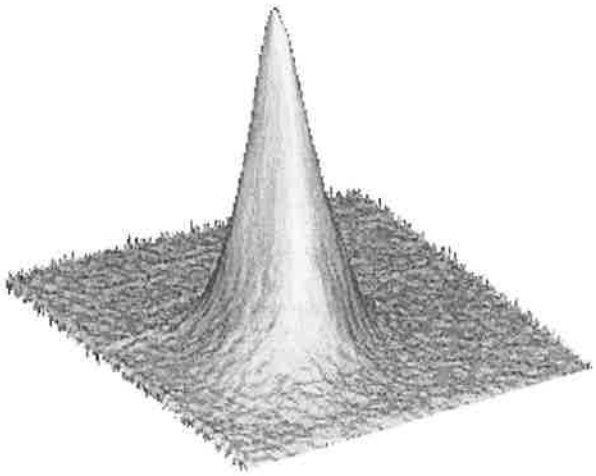

Figure 4.6: Transverse mode of improved Nd:YAG laser

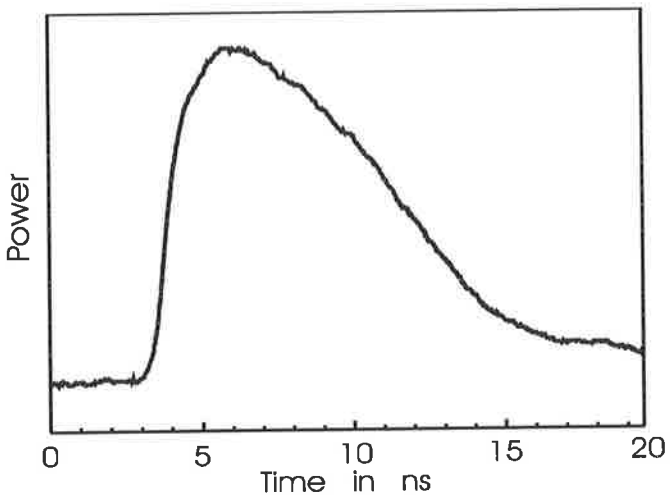

Figure 4.7: Temporal pulse profile of improved Nd:YAG laser

4.2.2 Results

We then measured the DFWM signals for CS_2 and PE in intensity grating and orientation grating configurations. The results are shown in Fig. 4.8. In this diagram I added the calculated cubic return expected for a fast (steady state) DFWM return. We can see that both PE and CS_2 exhibited intensity dependent, transient structure in the DFWM return. Since the transient DFWM return is effectively a measure of the diffraction efficiency of the induced grating (in analogy with TRTH), the grating was destroyed during the laser-matter interaction in both materials. In CS_2 this lead to a truncation of the DFWM pulse by about 1 ns. In PE the grating reformed, leading to a characteristic 'double hump' feature (Fig. 4.8a). While the effect was only small in CS_2 (Fig. 4.8(c)), in PE (Fig. 4.8(a)) both the slow and the fast mechanism appeared to be of equal magnitude. The destruction of the grating in both materials implied that the slow and the fast mechanisms are in direct competition with each other. The DFWM return in PE is very similar to the DFWM return observed by McEwan et al [49] where the slow mechanism was suggested to be due to the build up of a thermal nonlinearity.

The truncation of the CS_2 return, as well as the structure in the PE return disappeared when the intensity modulation of the grating was set to zero in the orientation grating configuration (Fig. 4.8(d & b)). Hence we concluded that this effect was intensity dependent. Since the effect changes the pulse shape from the expected cubic dependency it must have a response time of the order of the pulse length.

Recalling section 2.6.1, the intensity grating signals are examples of a slow, non-steady state DFWM response, whereas the orientation grating signals are examples of a fast, steady state response.

Table 4.1 lists values for $\chi^{(3)}$, calculated using the maximum values of the detected voltages during the pulse according to Eq. 2.16, as well as values given by literature. Refer to App.B for an error analysis of $\chi^{(3)}$ values. We obtained a value for $\chi^{(3)}$ of $(5.3\pm2)\times10^{13}$ esu for CS_2 which is comparable to results obtained by Xuan et al[47] of 5.1×10^{13} esu.

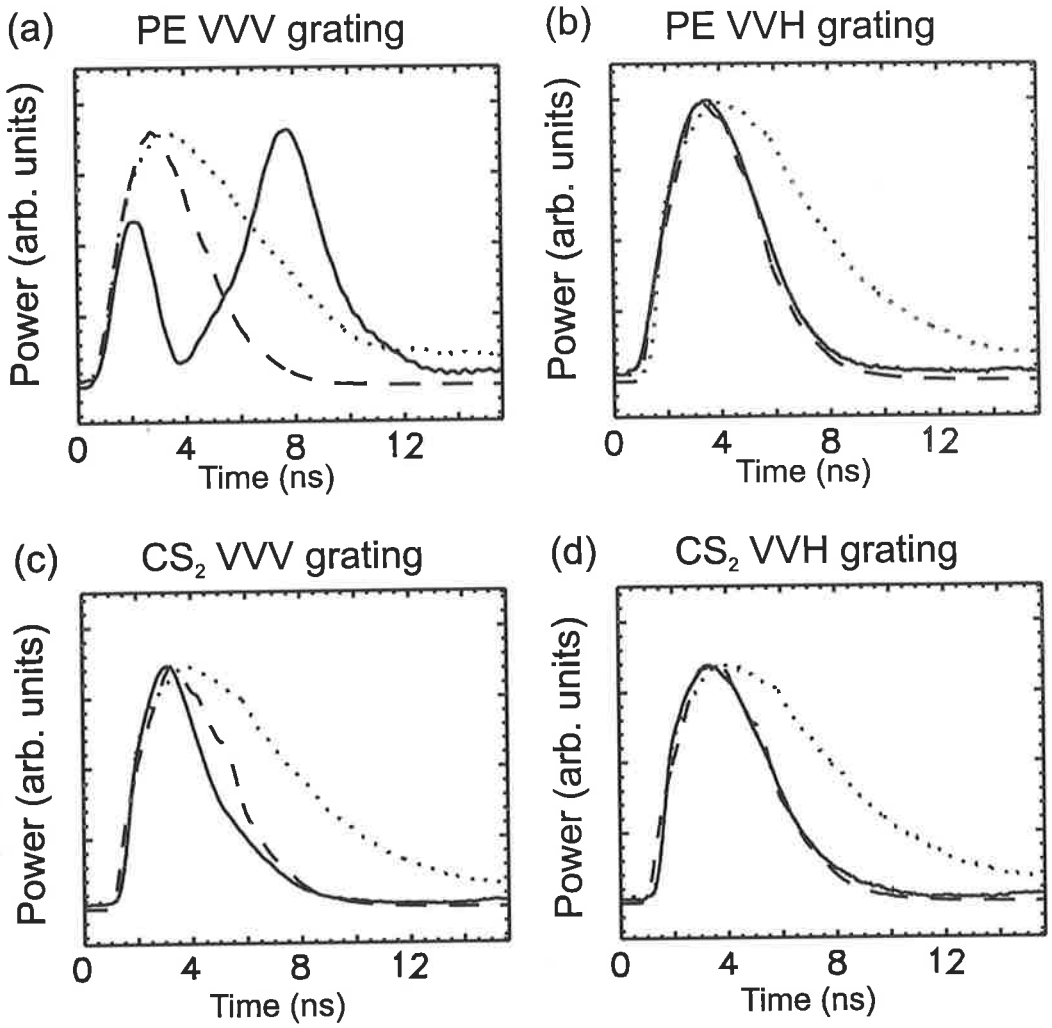

Figure 4.8: DFWM returns for the long pulse input. Dotted line: input pulse; broken line: cubic of input pulse; solid line: DFWM return;
(a) PE intensity grating. (b) PE polarization grating. (c) CS_2, intensity grating. (d) CS_2 polarization grating.

Material	Grating Type	$\chi^{(3)}$ ($\times 10^{-13}$esu)	Lit. $\chi^{(3)}$ ($\times 10^{-13}$esu)
CS_2	VVV	5.3	5.1[47]
CS_2	VVH	3.3	5.1[47]
PE	VVV	1.7	na.
PE	VVH	1.3	na.

Table 4.1: DFWM results for short pulse

4.3 Intensity dependence and grating evolution

In order to characterize further the nonlinear behavior of PE, we investigated the intensity dependence of the DFWM return, as well as the time evolution of the grating that is being written by the probe and the pump beams.

4.3.1 Intensity dependence

We measured the intensity of the DFWM signal as a function of the laser intensity in the intensity grating configuration. The latter was varied by means of the first halfwave plate/polarizer combination as shown in Fig. 4.4. The results are shown in Fig. 4.9. We can see clearly that both CS_2 and PE followed the cubic intensity profile as expected for a DFWM process. Hence there was no significant nonlinear absorption in this intensity regime. If there was any significant nonlinear absorption, this would result in a change of slope over the intensity range. Note that while the *temporal shape* of PE did not follow the cubic profile, the *maximum intensity* of the return did. This is a consequence of Eq. 2.15. Hence this was still a $\chi^{(3)}$ process, but a non steady-state one.

4.3.2 Time evolution of the dynamic grating

We used the delay line described in section 4.2.1 to delay the incidence of the backward pump to probe the time evolution of the grating formed between the probe and the forward pump. The delay was incremented by 1.3 ns each time and for each delay we took 16 consecutive pulses and averaged them to obtain an averaged maximum DFWM intensity while keeping the input intensity fixed. Note that the data sets were corrected for the divergence of the laser which resulted in a decreasing intensity for the backward pump in the overlap region in addition to the acoustic decay of the grating. Hence Figs. 4.10 and 4.11 show the diffraction efficiency as a function of delay for a non-diverging laser beam. This enabled us to see the actual decay of the grating.

The time evolution of the gratings shows a number of important results. As

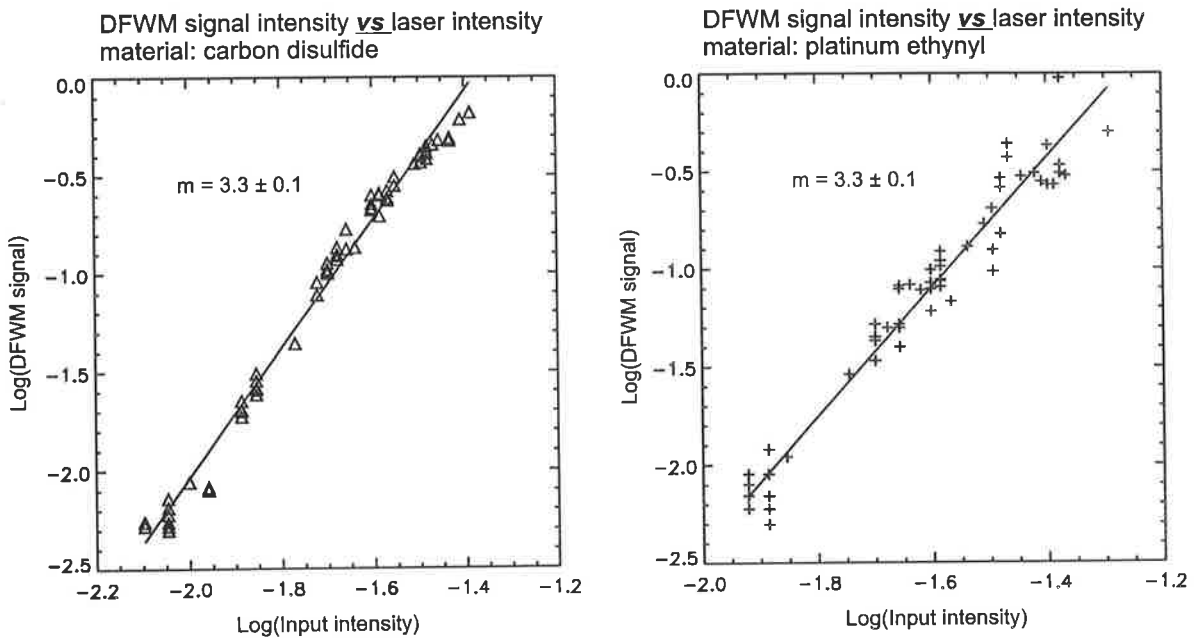

Figure 4.9: DFWM return signal power vs laser output power for both CS_2 and PE. Pulse length=7.5 ns (Line of best fit calculated using method of least squares)

expected, CS_2 exhibited a large steady-state nonlinearity for the duration of overlap of the pumps and the probe, but in addition there was a residual, exponentially decreasing return for time delays greater than the pulse length (ie. beyond 12 ns, see Fig. 4.10). It implied the presence of a slowly decaying refractive index grating which persisted after the 'write' pulses had left the medium. This effect is commonly observed [85, 62] in DFWM using picosecond pulses and is attributed to acoustic phonons (see section 2.6.4). Fig. 4.12(a) shows the pulse shape of the DFWM return for a delay of 18.6 ns and confirmed the presence of acoustic phonons. To my knowledge this measurement has not been done before in CS_2 in the nanosecond regime. It shows the strength of the combination of our detection, alignment and delay line system, that we could still detect this very small signal which is 4 orders of magnitude less than the 'zero delay' signal.

The DFWM return in PE did not exhibit the large, instantaneous nonlinearity of CS_2 (Fig. 4.11). The constant exponential decay of the diffraction efficiency implied that the slow, persistent nonlinearity, seen only late in the grating decay of

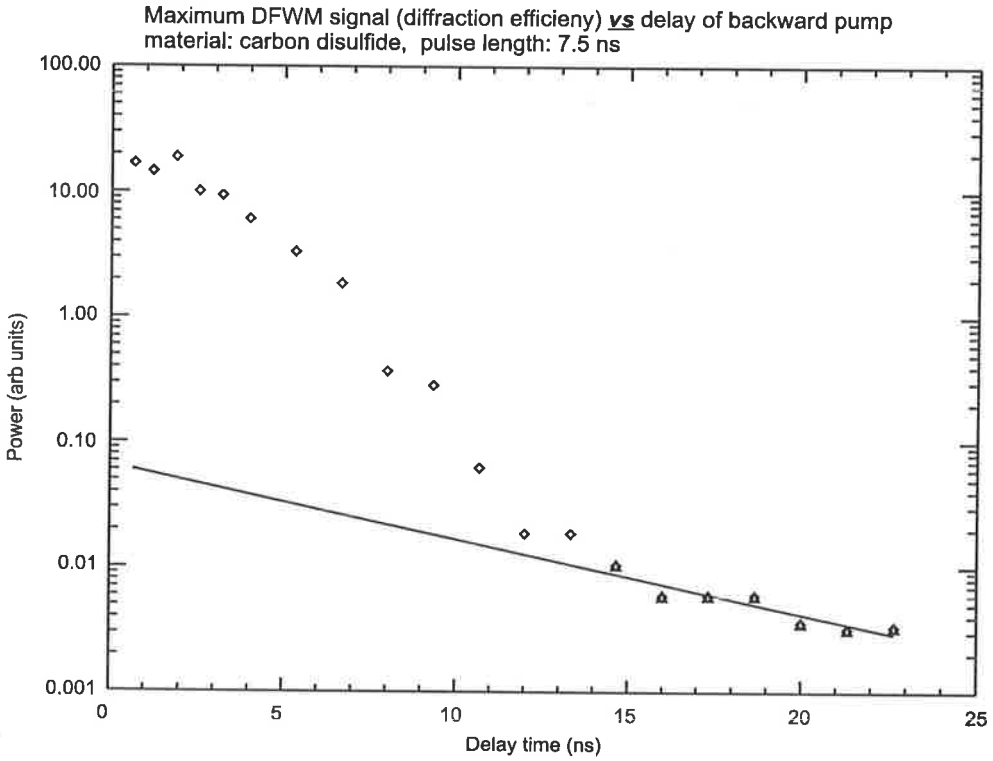

Figure 4.10: Diffraction efficiency vs delay in ns in CS_2. Note the large nonlinearity exhibited by the material while all three beams overlap. This is the steady state response. In addition there is a residual, exponentially decaying nonlinearity if pump 2 reads the grating after pump 1 and the probe have passed.

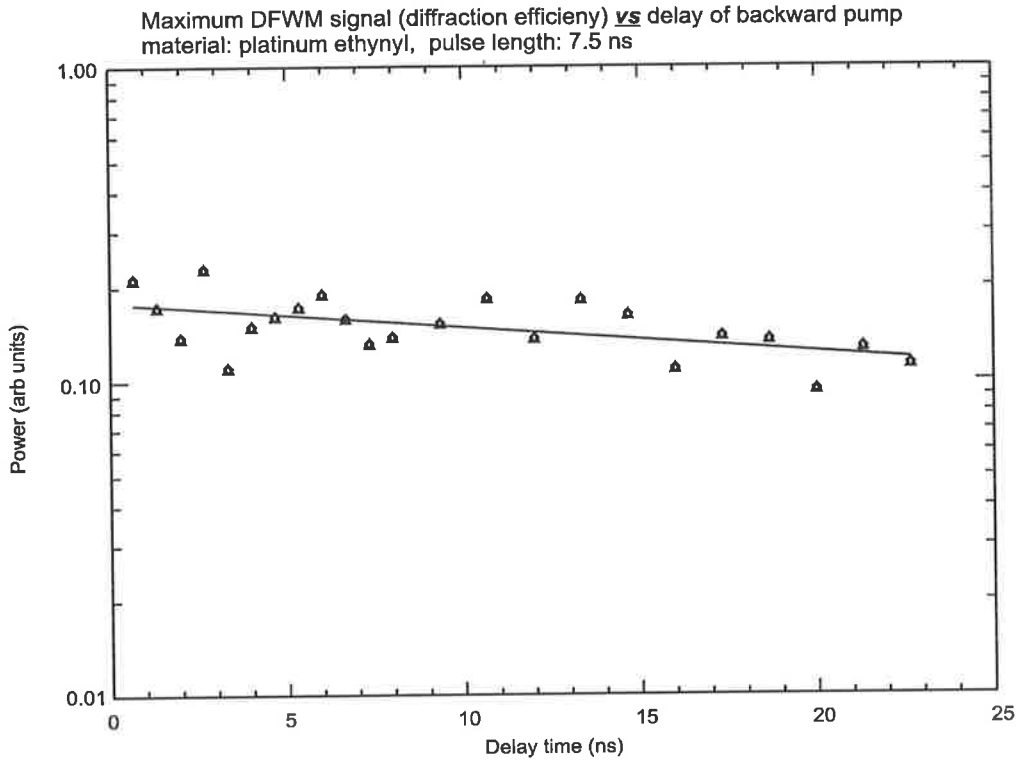

Figure 4.11: Diffraction efficiency vs delay in ns in PE. As can be seen, this nonlinearity is dominated by the transient, slow response.

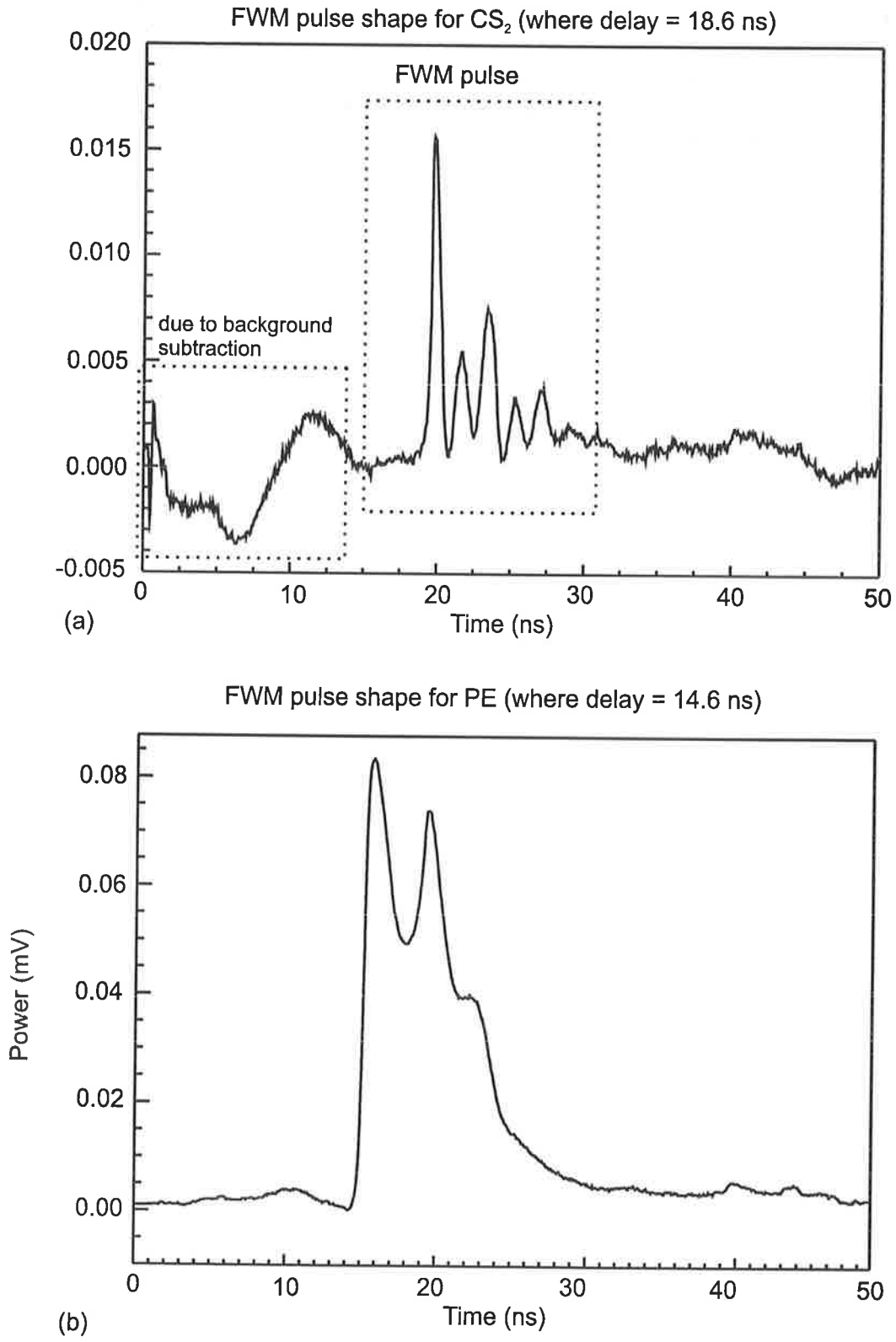

Figure 4.12: DFWM mixing pulse shape for CS_2 and PE for a backward pump delay greater than 12 ns. This case implies that the 'write' beams have left the medium before the 'read' beam enters it. We can see clearly the presence of acoustic oscillations in both pulse shapes. PE also exhibits a static component.

CS_2, dominated the nonlinearity in PE. In fact both the magnitude and decay time for the slow nonlinearity were larger in PE than in CS_2. Over 20 ns the signal in PE dropped by a factor of two only, whereas the signal generated by CS_2 dropped by 4 orders of magnitude. Fig. 4.12(b) indicates that this return was also due to an acoustic grating, as was the case in CS_2.

Fig. 4.13 shows the evolution of the pulse shape of the PE return as a function of delay. The return exhibited an oscillating structure which decayed only very slowly and we can see that this is the same mechanism which gave rise to the structure seen in the PE return in Fig. 4.8(a). The oscillating behavior in each pulse demonstrates very clearly that the structure in the PE return was due to the acoustic phonons generated by the intensity grating. It is important to note that the temporal position of the oscillations was stationary in time as indicated by the vertical lines. This implies that the structure was due only to the probe and the forward pump, and that the backward pump only read this grating, in direct analogy with real time holography.

4.4 Conclusion

We set up a preliminary experiment to determine the operating parameters of DFWM as well as alignment and signal detection criteria. We used this to observe a phase conjugated DFWM signal in CS_2 the magnitude of which agreed well with literature.

Subsequently we set up a complex and more versatile DFWM experiment which allowed variation of intensity and polarization. The alignment was repeatable to a known colinearity and parallelism and was done at the laser wavelength. The backward pump could be delayed by a new type of delay line which allowed diffraction limited auto-alignment. An improved laser system yielded a well defined electric field in the material and high peak powers. The bandwidth of the system was measured to be 750 MHz and the detectors were calibrated to give absolute power readings.

Therefore we were able to measure accurately the values of $\chi^{(3)}_{xxxx}$ and $\chi^{(3)}_{xyyx}$ in

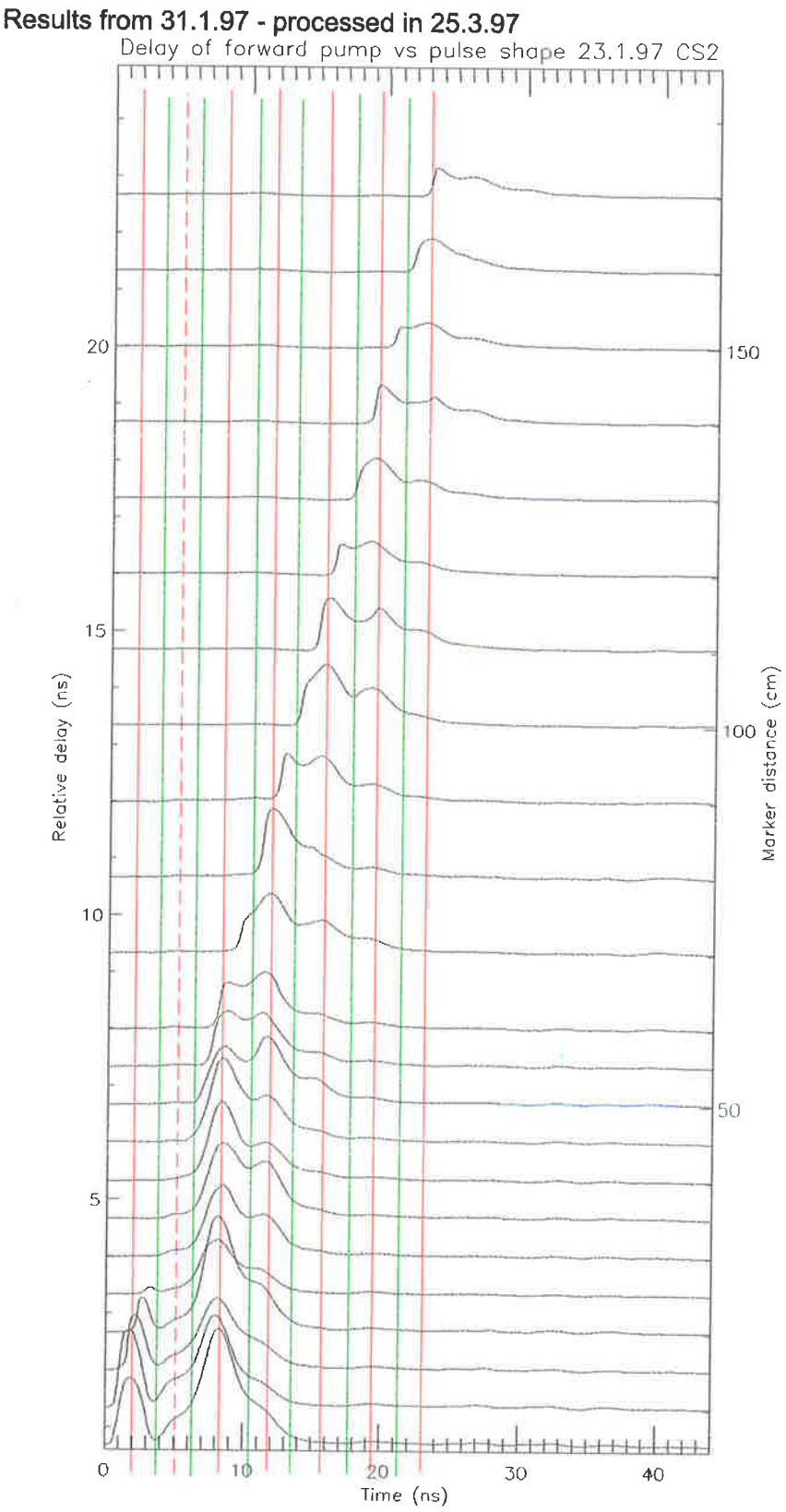

Figure 4.13: Pulse shape of DFWM return in PE as a function of delay. The horizontal axis is the transient time evolution and the vertical axis shows the delay in nanoseconds of the backward pump.

CS_2 and PE. Our values for CS_2 agreed very well with literature and established credibility of our procedures. We found both materials to have a fast steady state response to the polarization grating, indicating molecular reorientation times much faster than the input pulse length of 10 ns.

The intensity grating lead to structure in both the CS_2 and PE DFWM returns. While in CS_2 the effect was small leading to a slight truncation of the DFWM return, PE was dominated by it. Using the delay line to probe the dynamic evolution of the grating we showed that in PE the fast nonlinear response is destroyed during the light-matter interaction by the growth of acoustic phonons. In addition our results suggested that this might be the same mechanism responsible for the structure in the CS_2 response.

Both mechanisms were shown to be third order nonlinearities and nonlinear absorption was ruled out as the cause for the structure in the returns.

The grating in CS_2 decayed by 3 orders of magnitude after 12 ns, after which an acoustic phonon grating became evident which decayed exponentially. PE exhibited an acoustic phonon grating from the start of the interaction, which then decayed exponentially. After 20 ns the signal dropped to half its initial value, indicating a long lived grating.

The long pulse length of the laser did not permit further investigation into the origin of the effects. We thus proceeded to redesign the laser to optimize it for this investigation; this is the subject of the remaining chapters of this work.

Chapter 5

Variable SBS Pulse Compressor

In this chapter I will describe the original laser system, the modifications to convert it into a phase conjugated variable pulse length, master oscillator power amplifier (VPLL, MOPA) system and outline the results of these efforts. This work has been published [86] and [appendix D].

5.1 Original Nd:YAG

The original laser system was a commercial MOPA with an oscillator and a single pass power amplifier. The oscillator was a simple design using a saturable absorber LiF Q-switch, a flashlamp pumped Nd:YAG, a long (1.3 m) resonator with flat end mirrors and a 1 mm intracavity aperture. The output pulse was 2 mJ, 27 ns FWHM in a single longitudinal and transverse mode as shown in Figs. 5.1 and 5.2.

It was then passed through an amplifier, length 78mm and diameter 6mm. The optical quality of this particular amplifier rod was poor, exhibiting much birefringence which resulted in a poor transverse mode as shown in Fig. 5.3, which was obtained using photosensitive paper from Kodak. Magnifying the oscillator beam to fill the volume of the amplifier yielded an energy of 70 mJ.

However the resulting beam profile was unsuitable for DFWM experiments because of the nonuniform intensity profile. In order to make statements about nonlinear behavior, calculate nonlinear susceptibilities and ensure the repeatability of

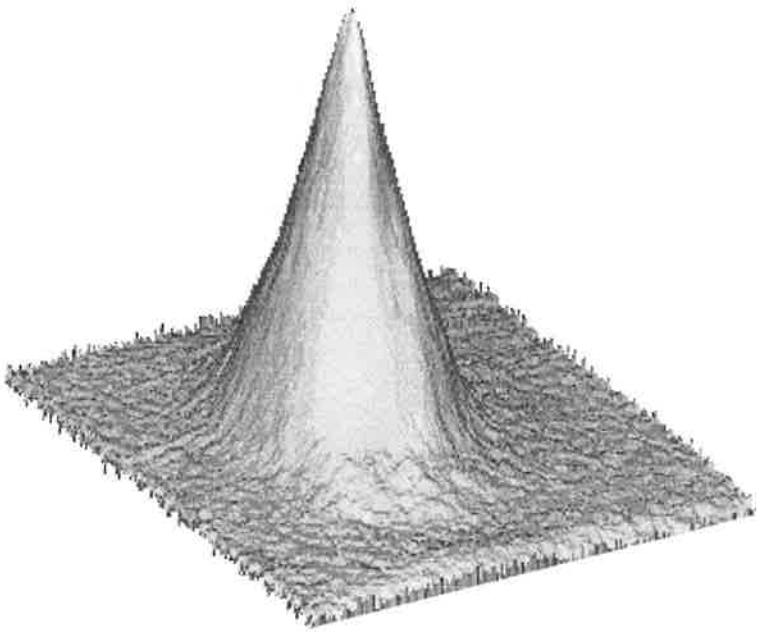

Figure 5.1: Beam profile for oscillator output, measured with a CCD camera, showing power in the vertical direction vs transverse dimensions (in arbitrary units).

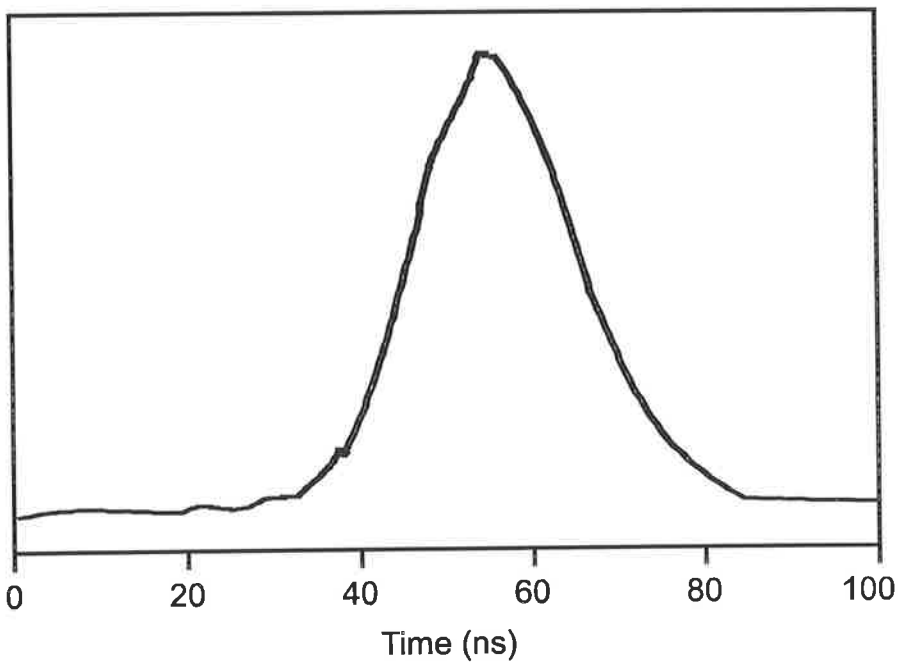

Figure 5.2: Temporal pulse shape of original oscillator beam

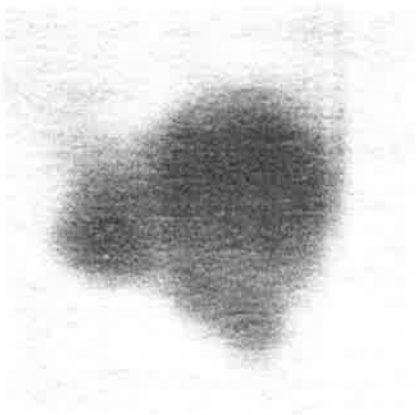

Figure 5.3: Burn pattern of beam profile of single-pass amplifier

the experiment, the electric field distribution inside the material needs to be known accurately, which requires a smooth beam profile such as a Gaussian. Furthermore, as was shown in section 4.1 these power levels are too low to get a sufficiently large DFWM signal out of PE and hence the laser was modified substantially.

5.2 Modified Phase Conjugated MOPA

To begin with the oscillator cavity was shortened to 0.4 m in order to shorten the pulse. This resulted in a pulse length of 12 ns and an energy of 2 mJ. We then set up an SBS cell as a phase conjugated mirror at the output of the laser system as shown in Fig. 5.4. This caused the beam to retroreflect and double pass the amplifier. A halfwave plate/polarizer combination was used to outcouple the beam. Note the latter were thin film plate polarizers utilizing Brewster's angle and were chosen for their high damage threshold (5 J/cm^2, 10 ns pulse). We chose liquid Freon-113 as the SBS medium because it has one of the shortest reported phonon lifetimes (0.84ns [82]), is transparent at 1.064 μm and is easy and safe to handle (see section 3.2.4). A 75 mm lens focused the beam into the liquid which was contained in a glass cell of length 0.3 m with poor optical quality input windows. With "poor quality" we are referring to transparent glass where thickness and curvature vary slightly over the cross section of the beam due to the "all glass" manufacturing process used. This helped to enlarge the aberrated beam waist at the focus thereby increasing the optical breakdown intensity threshold.

Because of the phase conjugating properties of the SBS process, most of the aberrations introduced by the amplifier are removed on the second pass, resulting in a very good (Fig. 5.5) transverse mode of the output beam. We could not use the full volume of the amplifier rod due to its very large amount of birefringence, which this simple SBS approach cannot compensate for [74, 87]. Hence the oscillator beam was not magnified to fill the amplifier volume, keeping distortions to a minimum. Fig. 5.5 shows the beam profiles obtained using the SBS cell, as well as the beam profile obtained when this cell is replaced by an ordinary mirror. We obtained a

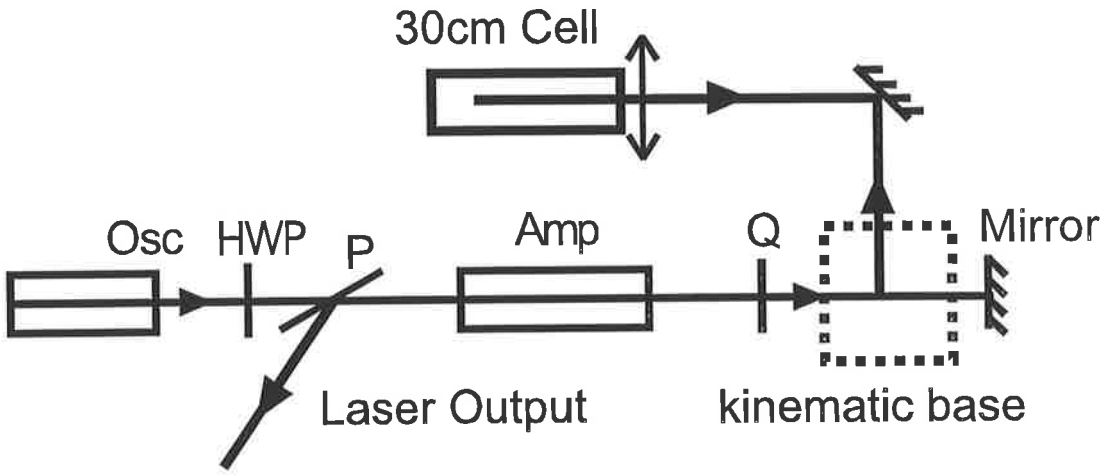

Figure 5.4: Simple phase conjugated MOPA with short (0.3m) SBS cell containing Freon-113

reflectivity of 92% for the short SBS cell, with an energy of 53 mJ.

5.3 Variable Pulse Compression

The pulse lengths obtained with this system allowed a nanosecond investigation of the third-order nonlinear optical properties of PE, but as initial results had shown, even shorter pulse lengths were necessary to resolve some of the physical mechanisms. Hence we further modified the laser system to include SBS pulse compression (Fig. 5.6). A kinematic mirror was used to direct the beam towards a long cell made of a copper pipe fitted with uncoated, O-ring sealed glass windows and containing Freon-113. The beam was magnified by a factor of 1.5 and focused using a telescope of focal length of 2 m. The magnification factor had to be chosen such that the SBS threshold was not attained before the beam reached the focus, otherwise a non-phase conjugated return would result (section 3.2.2). It was also important that this long cell reached thermal equilibrium because any localized changes in temperature resulted in large angular deviations of the beam due to refractive index changes.

The results for pulse length and energies are shown in Tab. 5.1 and Fig. 5.8. We achieved a maximum compression factor of 15, reducing the pulse width on average

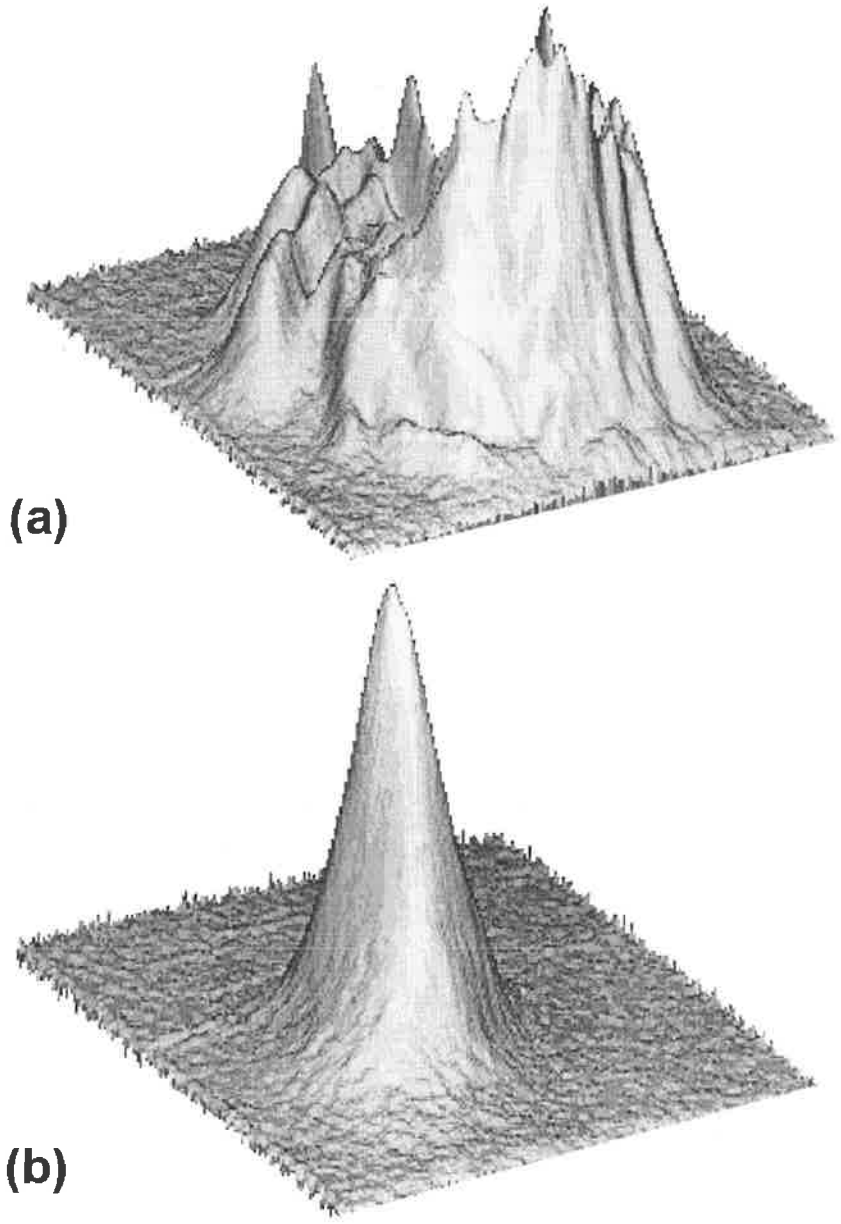

Figure 5.5: Beam profiles obtained using the SBS cell (b), as well as the beam profile obtained when this cell is replaced by an ordinary mirror (a).

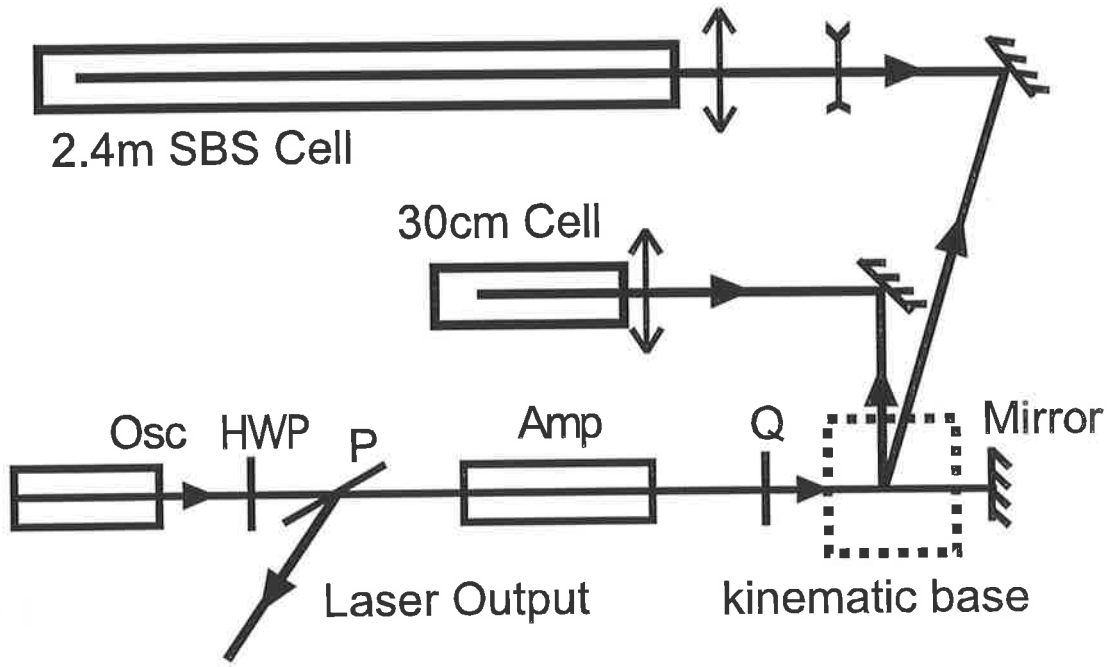

Figure 5.6: Experimental setup for variable pulse compression

Mirror Type	Pulse width (ns)	Energy (mJ)	Intensity (GW/cm^2)	Reflectivity
Conventional	11.3	60	0.03	>99%
Short SBS cell	7.5	53	0.22	92%
Long SBS cell	0.75	40	1.7	83%

Table 5.1: Pulse compression results and laser system output. The energies were measured at the output of the laser system. Intensities were calculated using the beam diameter and reflectivities were calculated using the input energy and the transmitted energy

from 11.3 ns to 0.75 ns, while maintaining phase conjugation. Very good pulse-to-pulse stability was achieved as shown in Fig. 5.7.

As shown in Fig. 5.8, intermediate pulse lengths could also be produced by varying the depth of focus in the long cell using the telescope. In order to achieve pulse lengths between 4 and 7 ns, we also found it necessary to lower the energy of the pulse entering the SBS cell by 30%. This was done using a halfwave plate, inserted before the outcoupling polarizer before the power amplifier as shown in Fig. 5.6. Without this adjustment, the short pulses often displayed a secondary maximum on

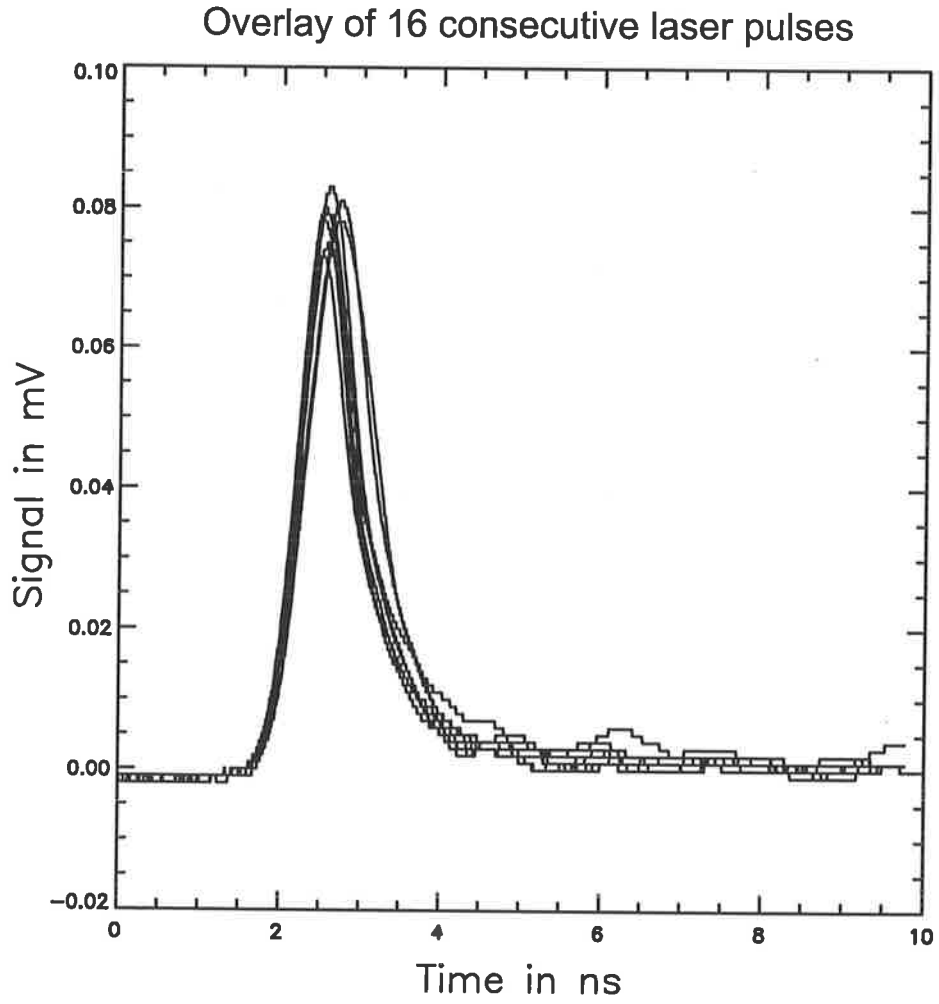

Figure 5.7: 16 consecutive laser pulses in the 0.7 ns regime demonstrating excellent pulse-to-pulse stability

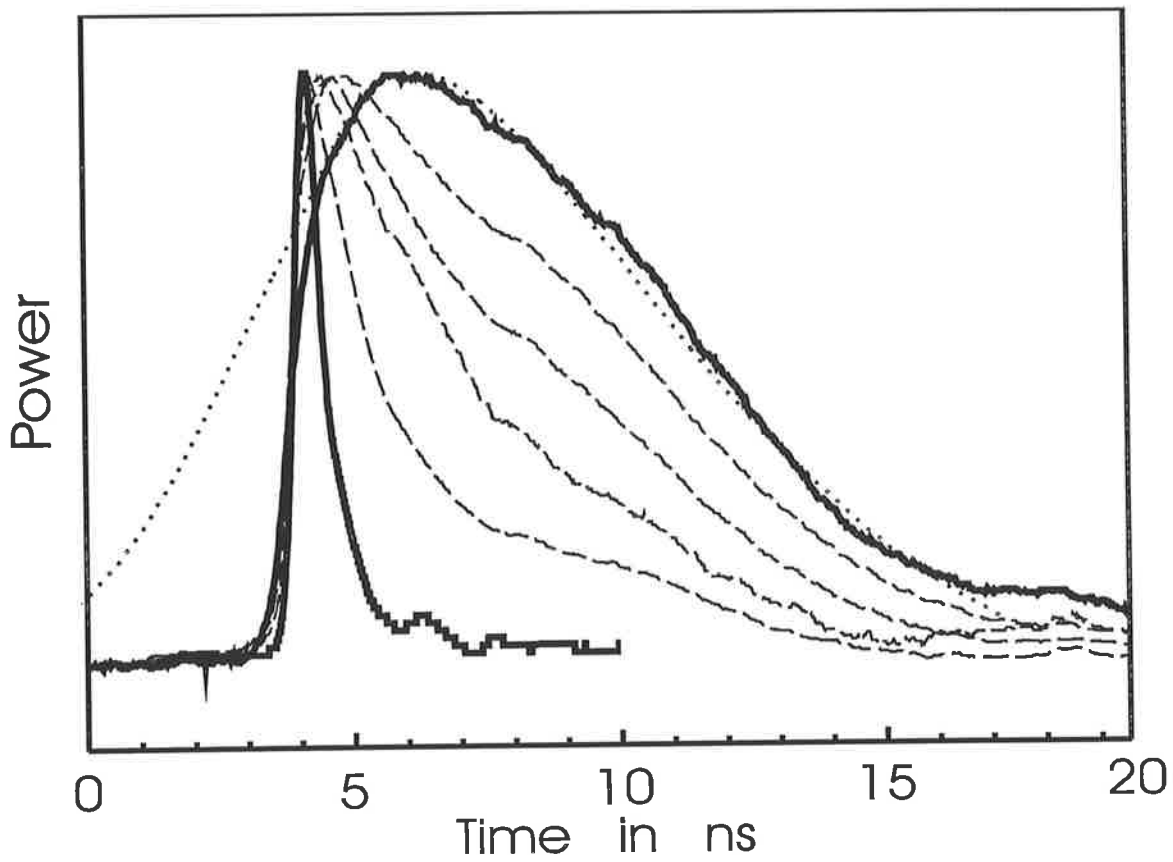

Figure 5.8: Pulse length results. All pulses are normalised in power to indicate temporal shape. The dotted line indicates the oscillator pulse. The solid lines show the pulses obtained with the long and the short cell. The broken lines show the pulses obtained by varying the focal length and energy into the long cell.

the trailing edge of the pulse. This occurs as a consequence of SBS gain depletion. The intensity of the Stokes wave rises rapidly during pulse compression and depletes the SBS gain which results in a rapid, transient decrease of reflectivity. The rest of the incoming pulse then causes the SBS process to recover, generating a secondary reflection.

To increase reflectivity and avoid optical breakdown in the SBS cells, the Freon was distilled once to remove impurities and suspended particles. We observed no visible degradation in the material over a period of eight months

Note that energy values of up to 260 mJ have been achieved when all the amplifier volume was used. For the purpose of the DFWM experiment however, 50 mJ was

sufficient. Note that our amplifier rod was of poorer quality than is typical and the aberration correction shown in Fig. 5.5 was thus essential. However most modern laser systems can benefit to some extend from beam profile improvement, but it may not be essential. Nevertheless while in some systems aberration correction may be of lesser importance, phase conjugation was still essential in the experiment to maintain auto-alignment while changing pulse lengths.

5.4 Conclusion

We converted an existing Q-switched laser into a phase conjugated MOPA based on SBS which is capable of producing pulses continuously variable between the 0.6 ns and 10 ns. The modifications to the laser were inexpensive and simple. SBS phase conjugation ensured excellent beam quality, leading to a very well defined electric field distribution, which is essential nonlinear optical experiments. Phase conjugation also guaranteed auto-alignment of the experiment while changing pulse length. Since our DFWM experiments had very stringent alignment criteria this was essential. Auto-alignment also implied that all measurements would be directly comparable with each other. In addition, pulse compression lead to much higher peak power densities, which increases the magnitude of any nonlinear signal.

Sub-nanosecond pulse lengths neatly access a time-scale commonly unavailable in commercial lasers which operate either in the nanosecond or the picosecond regime. This enables us to access different physical mechanisms in a material and probe the continuous transition between them.

Chapter 6

Variable Pulse Compressor applied to DFWM

6.1 Simple Transient Measurement

We repeated the DFWM experiment shown in Fig. 4.4 with the 0.75 ns pulses provided by the SBS pulse compressor. The results for this are shown in Figs. 6.1 and 6.2. These figures show that the structure has disappeared from the PE signal (within the bandwidth of the detector system). The CS_2 and PE returns now look identical, suggesting that we eliminated any significant, non-instantaneous effects at these time scales.

Tab. 6.1 gives the $\chi^{(3)}$ values obtained with the short pulses as well as those obtained using the 10 ns pulses in chapter 4. Refer to App.B for an error analysis of $\chi^{(3)}$ values. Again, the CS_2 values agree well with literature. As was also observed by Xuan et al [47] the CS_2 $\chi^{(3)}$ value for the short pulse intensity grating was slightly larger than the $\chi^{(3)}$ value for the long pulse. Note that the $\chi^{(3)}$ value for the polarization grating is in between those for the intensity grating and the value measured by Xuan using 20 ps laser pulses. This seems reasonable seeing that our laser operates at 650 ps.

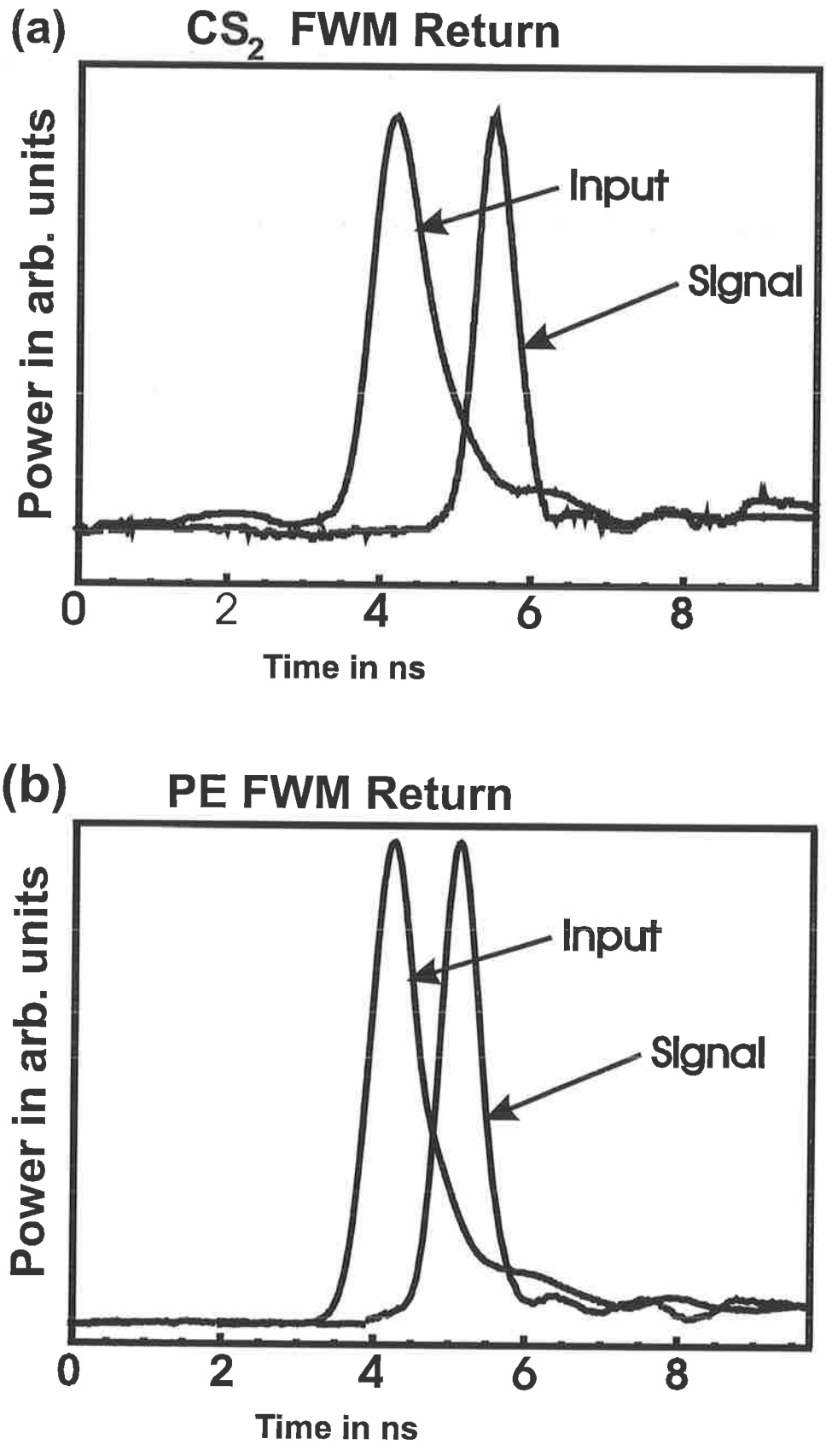

Figure 6.1: FWM returns for intensity grating, short pulse (a) CS_2, (b) PE

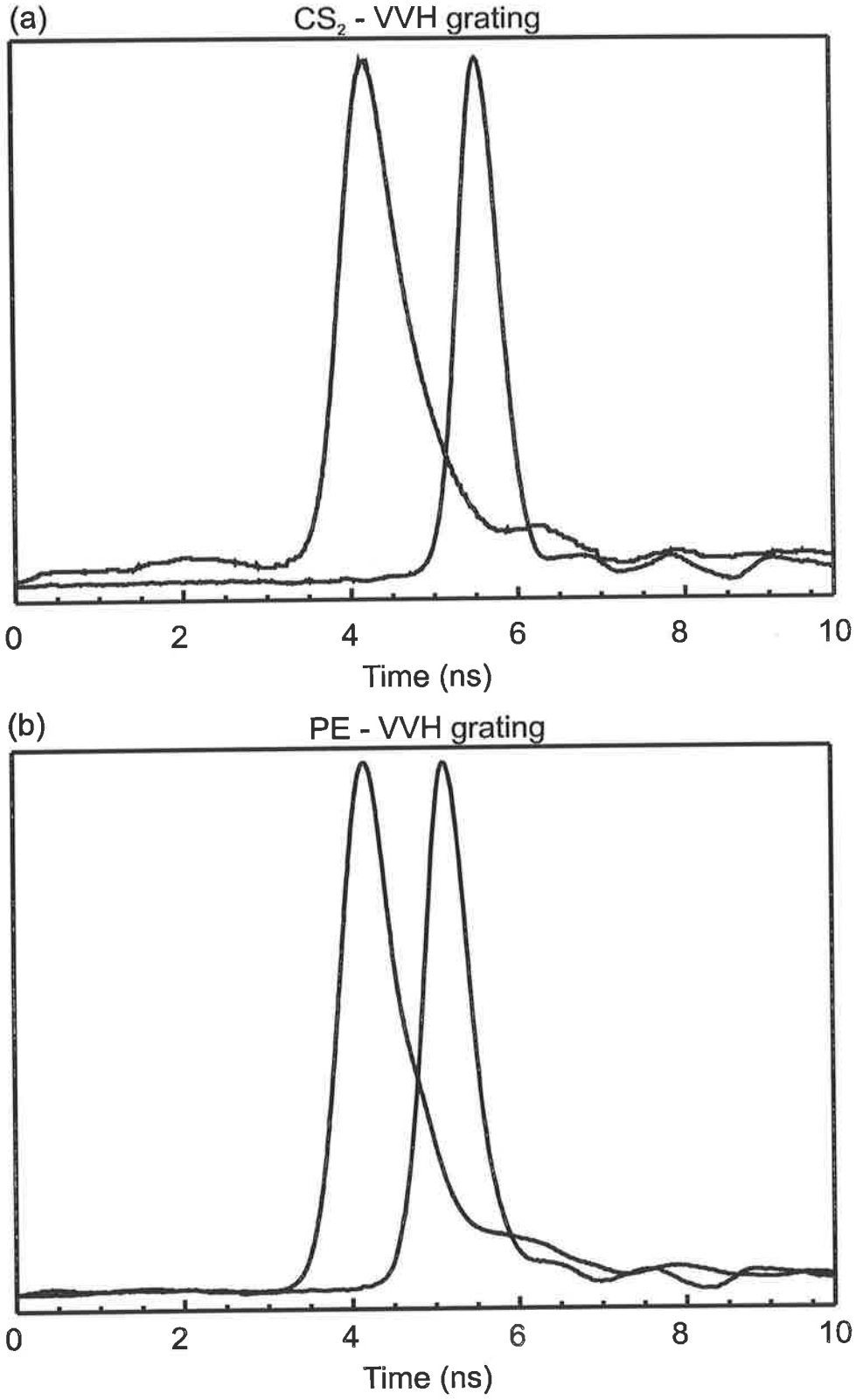

Figure 6.2: FWM returns for orientation grating, short pulse (a) CS_2, (b) PE

Material	Grating Type	$\chi^{(3)}$ $\times 10^{13}$ esu	Lit. $\chi^{(3)}$ $\times 10^{-13}$esu
CS_2	VVV	6.3 (5.3)	6.8 [47] (5.1) [47]
CS_2	VVH	3.7 (3.3)	0.76 [47] (5.1) [47]
PE	VVV	1.3 (1.7)	na. na.
PE	VVH	0.55 (1.3)	0.26 [10]* na.

Table 6.1: DFWM results for short pulse. For reference the long pulse values from chapter 4 are given in brackets. (* this value is given relative to their $\chi^{(3)}$ value for CS_2)

6.2 Intensity Dependence

As in section 4.3.1 we measured the intensity dependence of the DFWM return. The results for this are shown in Fig. 6.3. Both CS_2 and PE exhibit slopes of 3.1 ± 0.1 and 3.2 ± 0.1 which agree very well with the cubic intensity dependence expected of a DFWM return as shown in Eq. 2.16.

There is no significant change in the slopes over the input power range which rules out nonlinear absorption as the cause of the nonlinearities observed.

6.3 Dynamic Grating Evolution

Having separated the slow from the fast processes in the sub-nanosecond regime, we proceeded to examine the dynamic evolution of the DFWM grating in order to determine the origin of the slow effect which gave rise to the structure of the PE return in Fig. 4.8(a).

In accordance with section 2.6.4, a pulsed laser system should establish an acoustic grating within the DFWM material. A graph of the diffraction efficiency vs the optical delay of backward pump should verify this. We did this with both CS_2 and PE. The results shown in Fig.6.4 clearly demonstrate the presence of a standing density wave, giving rise to an oscillation in the diffraction efficiency. Note that Fig. 6.4 and Fig. 6.5 have been corrected for the decrease of intensity due to the laser beam

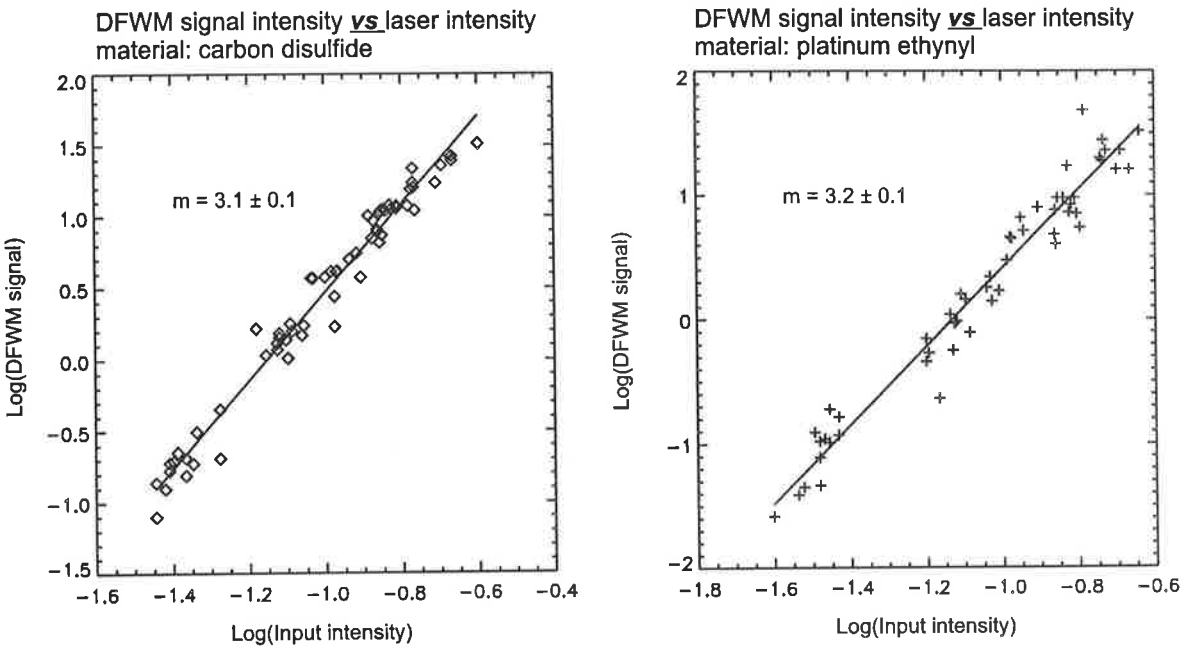

Figure 6.3: DFWM return signal power vs laser output power for both CS_2 and PE. Pulse length=0.75 ns (Line of best fit calculated using method of least squares)

divergence (0.73 mrad) as the delay is increased. In other words they represent the hypothetical case of zero laser divergence. Numerical results are shown in Tab. 6.2. The angle within the cell between the probe and forward pump was 9°. The period of oscillation was measured to be 1.8 ns. CS_2 has a refractive index of 1.60 [88]. This corresponds to a grating period of

$$\begin{aligned} \Lambda &= \frac{\lambda}{2\eta \sin\left(\frac{\theta}{2}\right)} \\ &= 3.93\ \mu\text{m} \end{aligned}$$

and a speed of sound of

$$\begin{aligned} v &= \frac{\Lambda}{2T} \\ &= 1.09 \times 10^3\ \text{m/s} \end{aligned}$$

Material	Period ns	Grating spacing μm	Speed of sound $\times 10^3$ m/s	Speed of sound (lit.) $\times 10^3$ m/s	Mech.	Grating lifetime ns	Phonon lifetime ns	Phonon lifetime (Lit.) ns
CS_2	1.8	3.9	1.1	1.15	E	7.8±1	7.8	6.5
PE	3.8	4.1	0.54 (1.1)	na.	E (T)	17±4	6.4	na.

Table 6.2: Results for Dynamic Grating Decay. Lit. values were taken from [88]. E=electrostriction, T=thermal

in CS_2.

This calculation assumes that the underlying physical effect giving rise to the acoustic oscillations was electrostriction and hence the occurrence of period halving (in accordance with section 2.6.4). This compared very well with the value given in literature of 1.15×10^3 m/s and confirms the validity of our technique as well as electrostriction as the mechanism for phonon creation.

Turning to Fig. 6.5, the PE grating evolution, we note that the period of oscillations was 3.8 ns. The doubling of the oscillation period compared to CS_2 would imply either that stimulated thermal Brillouin scattering (STBS) is responsible for the acoustic grating rather than SBS, or that the speed of sound in PE is half that of CS_2. Hence we needed to measure the speed of sound in both materials (see section 6.4). Assuming for now that STBS is responsible for the oscillation and a refractive index of PE/THF (tetrahydrofurane) of 1.55, the grating spacing is given by 4.1 μm and the velocity of sound is 1.07×10^3 m/s or 98% of that in CS_2.

There are a few more results of note in these graphs: The ratio of the acoustic signal to the steady-state signal is larger in PE than in CS_2 hence nonlinear scattering is the dominant nonlinearity in PE at this wavelength. As a result there was strong competition between the fast nonlinear response and nonlinear scattering in the long pulse return of Fig. 4.8(s).

Furthermore, we can calculate the phonon lifetime as well as the grating lifetime from Fig. 6.4 and Fig. 6.5. The measured voltage of the acoustic maxima in these

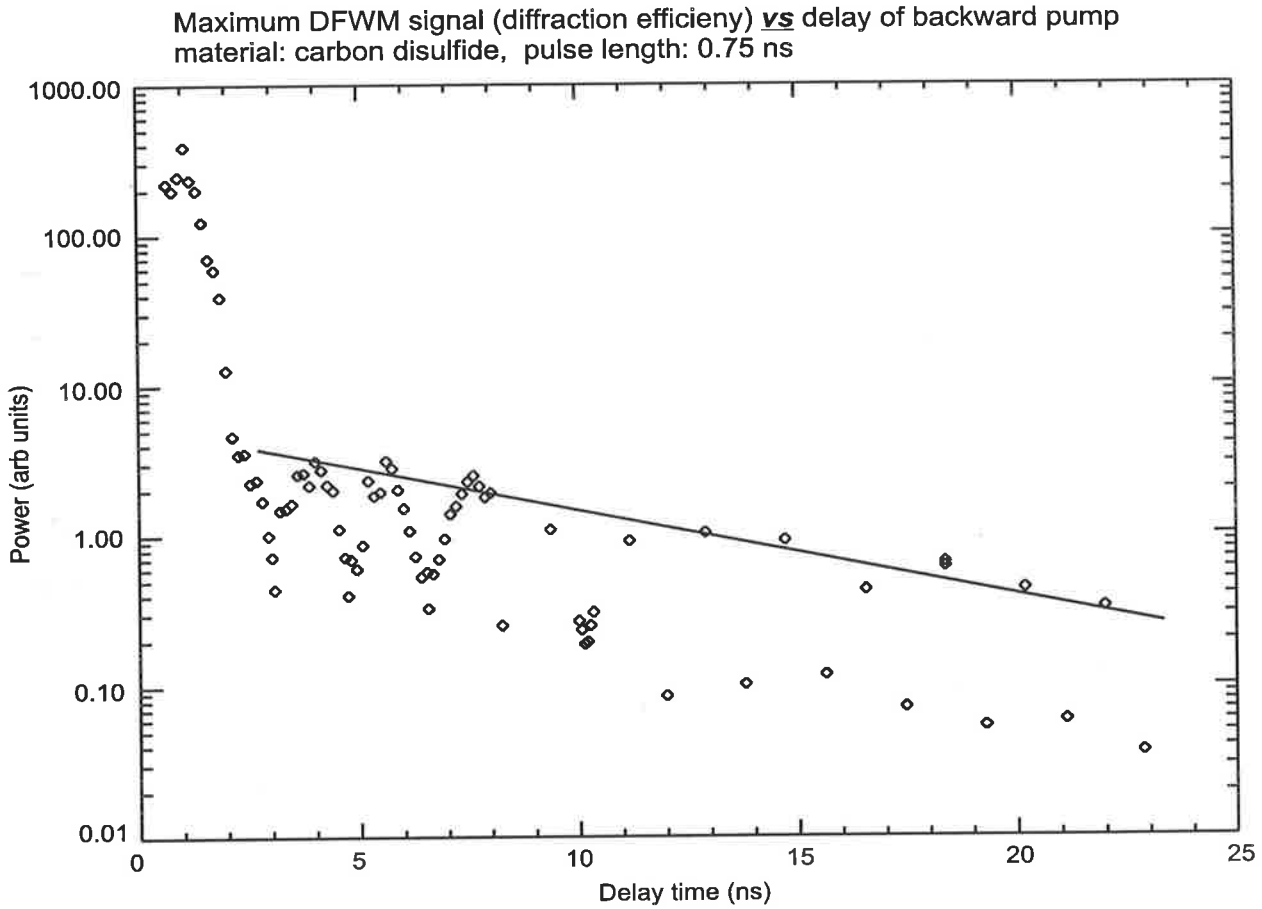

Figure 6.4: FWM signal maxima vs delay of backward pump clearly demonstrates acoustic oscillations

figures certainly seems to follow exponential form given by

$$V = V_0 \exp(-\frac{t}{\tau})$$

where τ is the decay constant. This can be rewritten as follows

$$\ln V = \ln V_0 - \frac{t}{\tau}$$

which, of course, is the equation of a straight line

$$y = a + bt$$

The grating lifetime in PE was much longer (17ns) than in CS_2 (7.8 ns). Thus, while the effective $\chi^{(3)}$ of PE is less than that for CS_2, it is much longer lasting, even for sub-nanosecond pulses. Note also that within the bandwidth of the detection system, the grating decay in CS_2 was equal to the phonon lifetime, while in PE the phonon lifetime was much shorter (6.5 ns) than the grating lifetime (17 ns). This behaviour has been observed and modelled by Genberg *et al* [89] and was shown to occur if the thermalization time is of the same order as the acoustic period. The thermalization time is a result of the delay in energy deposition via non-radiative relaxation into a thermal grating.

6.4 Heterodyne Speed of Sound Measurement

As pointed out in the previous section, we could not conclude from Fig. 6.5 that the dominant nonlinear mechanism for PE is thermal, unless the speed of sound in the material was known. We addressed this problem by measuring the speed of sound experimentally using a standard heterodyne technique as shown in Fig. 6.6.

The laser beam was split by a 50% beam splitter. One part reflected in an SBS cell, the other part reflected of a mirror. Recombination of the two signals on a detector yielded the sum of the two pulses including a superimposed frequency beat.

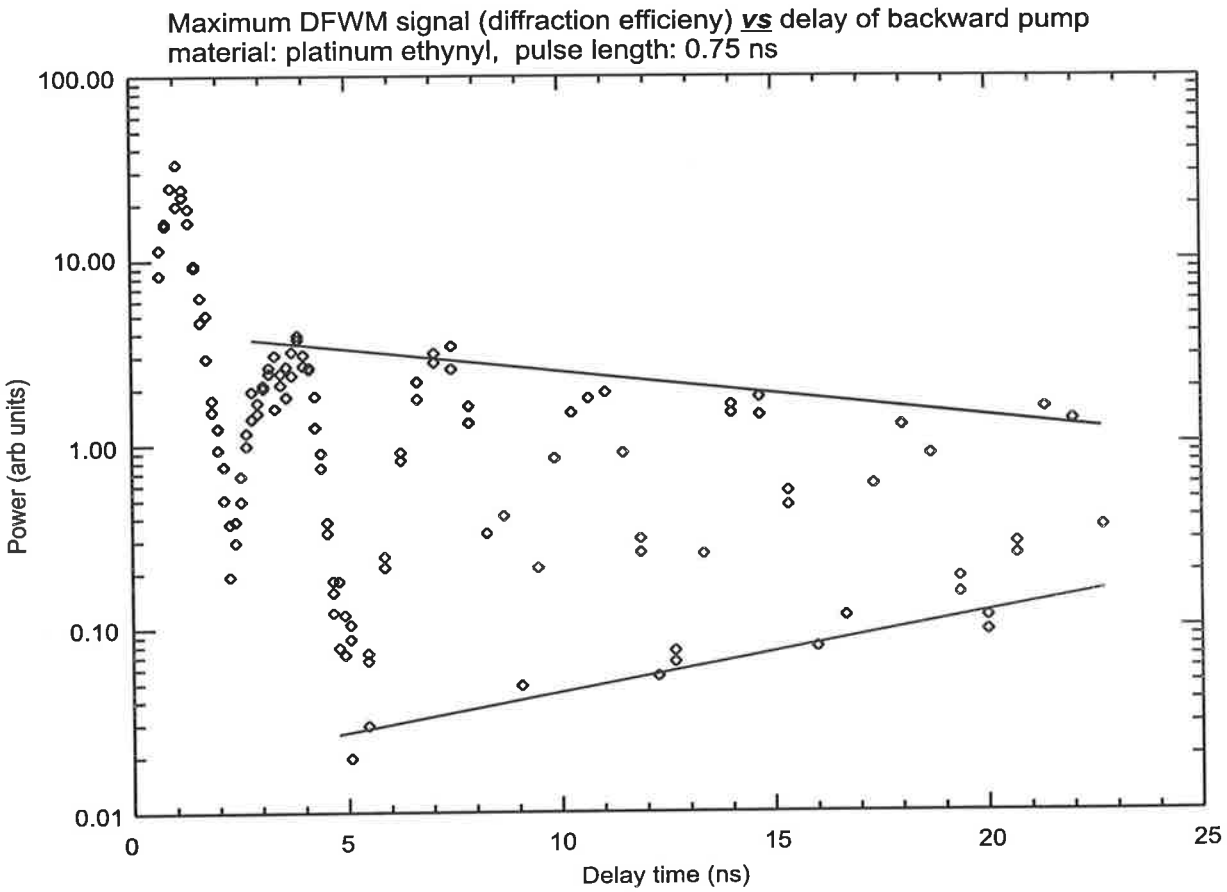

Figure 6.5: FWM signal maxima vs delay of backward pump clearly demonstrates acoustic oscillations. Note the period has doubled when compared to the CS_2 case.

The latter was due to frequency shift caused by an SBS return. This is simply the Doppler effect due to the propagative sound grating. Measurement of this frequency beat allowed us to measure the speed of sound in the material in question from

$$f_{doppler} = \frac{2\eta v_s}{\lambda} \tag{6.1}$$

Variable attenuators were used to equalize the intensities in of the reflected beams.

Note that this formula is similar to Eq. 2.1 which can be rewritten using Eq. 2.21 as

$$f_{spacing} = \frac{4\eta v_s \sin\left(\frac{\theta}{2}\right)}{\lambda}$$

However Eq. 6.1 is independent of the mechanism which gives rise to the nonlinearity

because it represents a velocity induced frequency shift. Hence we could find a value for ηv_s[1] using both methods. It is important to note that they are entirely different techniques. The DFWM method does not give rise to a frequency shift, because a *standing* wave gives rise to the return (section 2.6.4). In self-induced SBS the interference grating is moving at the speed of sound, thereby downshifting the frequency of the laser.

From the previous section we believed CS_2 and PE to have similar speeds of sound. The frequency shift of CS_2 is given by 3.8 GHz [90]. The bandwidth of our detection system was 1 GHz and hence we did not expect to see any frequency shift above 2 GHz. To overcome this problem we used Freon as an intermediate frequency reference, because it exhibits an SBS shift of 1.86 GHz [90]. In other words, we first measured the Freon frequency shift against a mirror and then the CS_2 and PE frequency shifts against the Freon frequency shift.

The results of this experiment are shown in Fig. 6.7 and Tab. 6.3.

As can be seen our values compare very well with literature, which lends credibility to our approach. Using these results to obtain a value for ηv_s in PE.

$$\begin{aligned} \eta v_s &= \frac{\lambda f_{doppler}}{2} \\ &= 1.74 \times 10^3 \text{ m/s} \end{aligned}$$

Likewise, using Eqs. ?? we obtain a value for ηv_s of

$$\begin{aligned} \eta v_s &= \frac{\lambda f_{spacing}}{4 \sin\left(\frac{9^\circ}{2}\right)} \\ &= 1.66 \times 10^3 \text{ m/s} \end{aligned}$$

As can be seen, these results agree[2] to within 5%, which confirms that the speed of sound in PE is close to that of CS_2.

[1]Note that we do not need to know the refractive index to compare the results for both methods which both yield a value for $v\eta$.

[2]We took great pleasure in the fact that these results were so close considering we measured ηv_s with two entirely different methods. Physics always takes care of itself!

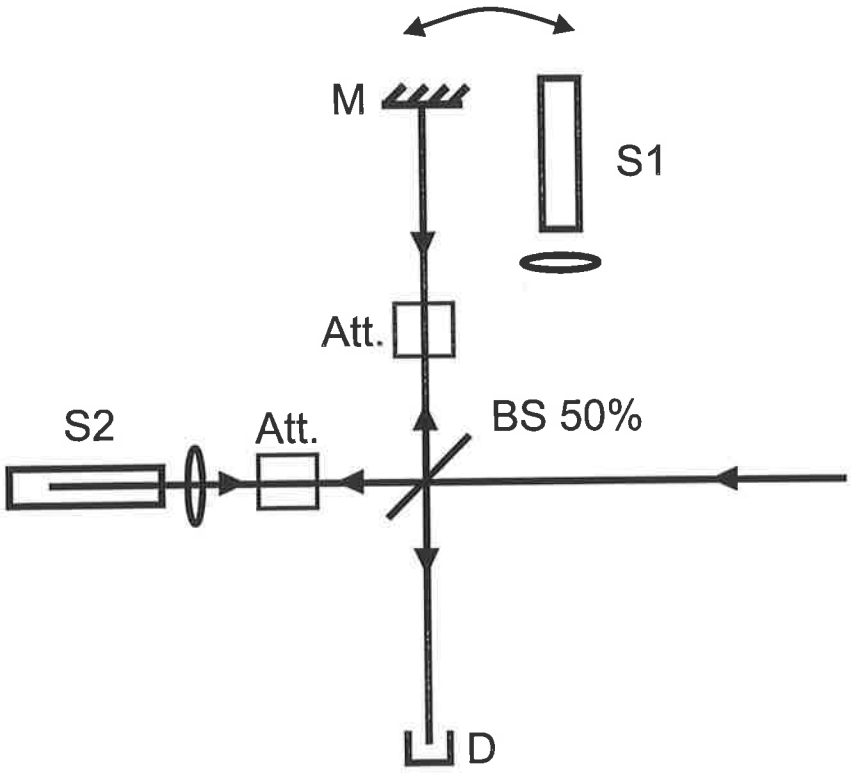

Figure 6.6: Heterodyne experiment to measure Doppler shift of SBS return. S1, S2: SBS samples; Att.: attenuators to achieve equal return intensities; BS: 50% nonpolarizing beam splitter; M: mirror used as non frequency shifting reference; D: Fast detector

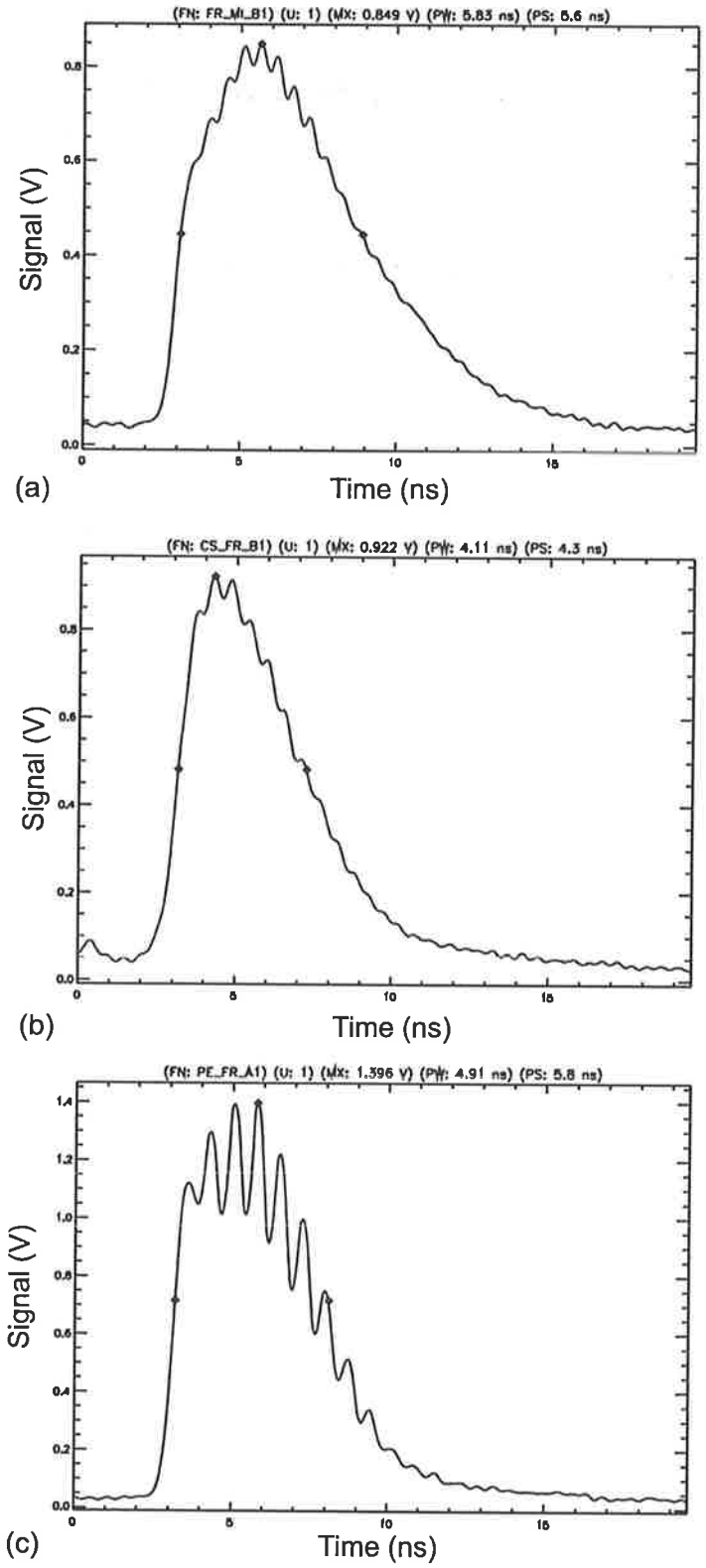

Figure 6.7: Heterodyne frequency beats between SBS returns of various materials. (a) Freon-plain mirror (b) CS_2-Freon (c) PE-Freon

Material	T (ns)	FrEq. shift (GHz)	Literature Value
Freon-Mirror	0.507	1.97	1.86
CS_2-Freon	0.523	1.91 (+1.97 = 3.88)	3.8
PE-Freon	0.731	1.37 (+1.97 = 3.34)	n.a.

Table 6.3: Heterodyne Frequency shifts - Relative beat Frequencies

6.5 Discussion

In chapter 4 we established the physical mechanism which gave rise to the transient shape of the DFWM return in PE, namely the buildup of an acoustic phonon grating, which destroyed the fast reorientational grating. In this chapter we established the origin of the acoustic phonons to be due to linear absorption and subsequent, localized thermal expansion.

In fact this mechanism also explains the pulse truncation in the CS_2 nanosecond DFWM return. We saw that in the sub-nanosecond regime, the CS_2 response was reorientational, followed by acoustic phonons. We established those phonons to be purely of electrostrictive origin, because of their period. Fig. 6.8 (same as Fig. 4.12a) shows the DFWM return of CS_2 in the acoustic region, probed with an 8 ns pulse and it can be seen that the peaks alternate in height. In accordance with section 2.6.4, and Fig. 2.7 on page 33 this implies increased competition from thermal expansion.

This shows that the thermal response was stronger in the nanosecond than in the sub-nanosecond regime in CS_2, which would cause the transient shape of CS_2 to be truncated slightly via the same mechanism as in PE. Both our nanosecond and sub-nanosecond results showed that this effect is much stronger in PE than in CS_2, which explains that in CS_2 the DFWM return was truncated only, while in PE the thermal nonlinearity dominated later in the pulse.

6.6 Pulse Length Transition Regime

We also used variable pulse compression to observe the transition dynamics of the nonlinearity in PE from the short pulse to the long pulse regime. The input was varied according to Fig. 5.8 and the resulting DFWM signal is shown in Fig. 6.9.

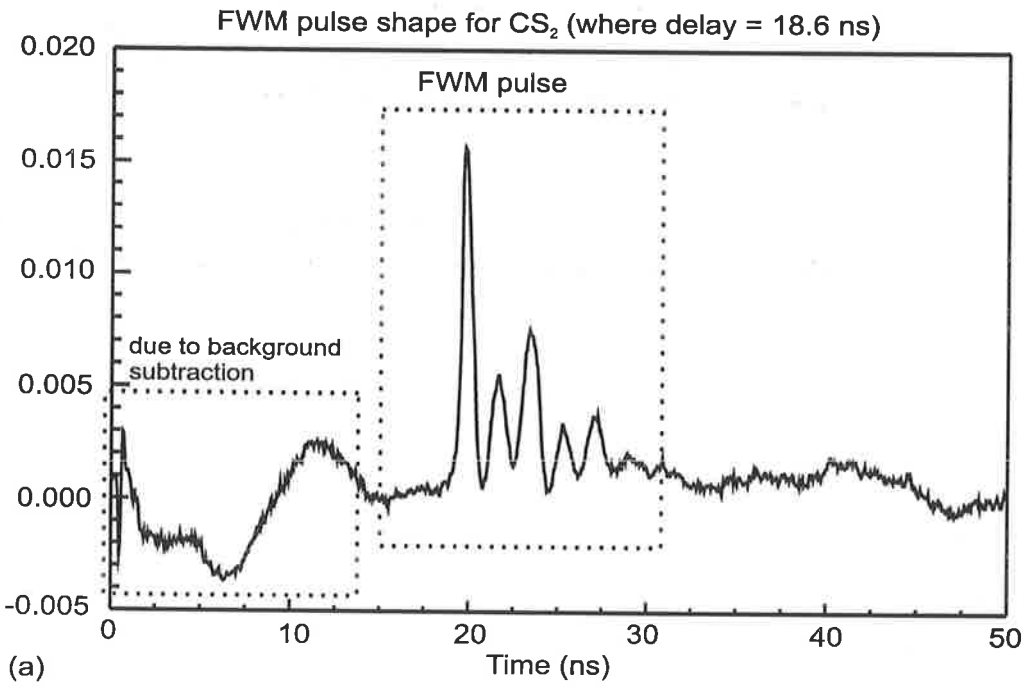

Figure 6.8: DFWM mixing pulse shape for CS_2 for a backward pump delay greater than 12 ns. This case implies that the 'write' beam left the medium before the 'read' beam entered it. We can see clearly the presence of acoustic oscillations. In addition each peak alternates in height indicating increasing competition from STBS.

This demonstrates clearly the domination of molecular reorientation in the sub-nanosecond regime, the subsequent 'competition regime' where both effects are of equal magnitude, and in the 10 ns regime, the domination of the thermal nonlinearity.We believe this to be the first time to have been done in the time regime of Q-switched lasers. Furthermore we believe this feature will be very important in modelling the dynamics of the nonlinear interaction. This belief is well-founded because the DFWM interaction is given by the temporal convolution of the input beams and application of a deconvolution to the DFWM pulse should yield the temporal response function. This was discussed briefly in section 2.6.2. Combining this with variable pulse length response, should give us the nonlinear dynamics as a function of input pulse duration.

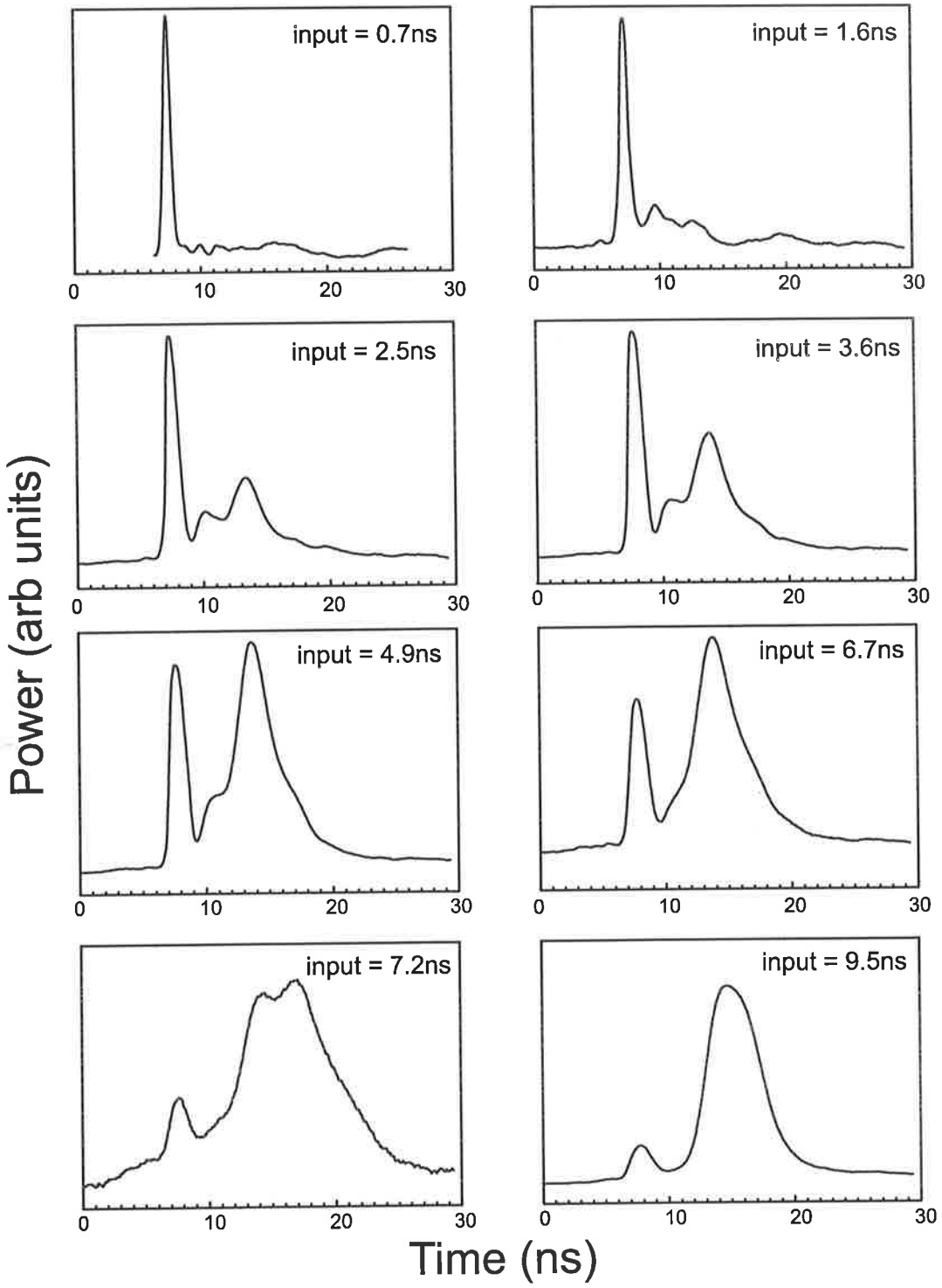

Figure 6.9: DFWM return for transition regime between reorientational and thermal nonlinearity.

6.7 Conclusion

Using the sub-nanosecond pulses generated by the SBS laser, we eliminated the structure present in the long pulse PE DFWM return, and measured $\chi^{(3)}$ for PE and CS_2. We established that the return was still purely third-order in nature and that there was no nonlinear absorption present.

The observation of the dynamic grating evolution confirmed the presence of acoustic oscillations in both materials. We found that the period of the oscillations in PE was approximately twice that of CS_2 for the same experimental arrangement. Using the Doppler shift caused by acoustic phonons in self-induced SBS we measured the speed of sound in PE and CS_2. We found the speeds in both materials to be approximately equal and therefore we established that the nonlinear response of PE at 1064 nm is dominated by thermally induced nonlinear scattering. Therefore this was the cause of the transient shape of the nanosecond response in PE, namely the fast response of a reorientational nonlinearity and its subsequent destruction by the buildup of a thermal grating. We also established this to be the cause of the pulse truncation in CS_2, which showed an increased thermal competition in the 10 ns regime.

Our measured CS_2 $\chi^{(3)}$ values and the speed of sound in CS_2 and Freon agreed very well with literature which validated our experiments.

We also established nonlinear scattering parameters for CS_2 and PE, including speed of sound, phonon lifetime, grating lifetime and scattering mechanism origin. Our results showed that while the refractive nonlinearity in PE is smaller than that of CS_2, the nonlinear scattering effect is comparably stronger and much longer lasting.

In addition we used the continuous variability of the SBS laser to access the transition between the instantaneous and the non-instantaneous response in PE. This will be very useful for the intended future modelling of the impulse response of PE.

Chapter 7

Conclusion

We have developed a new method to access nonlinear optical dynamics and characterize nonlinear optical materials. This entailed the construction of a laser system based on SBS which is capable of producing pulses continuously variable between the 0.65 ns and 9.5 ns. SBS phase conjugation provided excellent beam quality and auto-alignment, both essential to nonlinear optical experiments. Using this laser system we carried out experiments usually reserved for multiple laser systems. The combination of these experiments allowed us to characterize in detail the nonlinear scattering properties of an optical power limiter.

We setup a sophisticated DFWM experiment which included highly accurate alignment, the ability to measure transient signals and absolute power values in addition to other conventional control parameters such as intensity, polarization and time of arrival control. However our laser system provided the additional ability to access different physical regimes in the nonlinear material by varying the pulse duration. We made full use of this facility by first characterizing the transient dynamics of the power limiter in the long pulse regime and subsequently determining the physical mechanisms and their origins using the short pulses.

This included the demonstration of laser-induced acoustic gratings in the sub-ns regime and mechanism competition in the ns regime. By use of a new type of delay line which allowed diffraction limited auto-alignment we were able to establish that nonlinear thermal scattering was the dominant cause of the DFWM signal in the

power limiter at 1.06 μm in the nanosecond regime, whereas molecular reorientation dominated in the sub-ns regime. We also found CS_2 to be affected by a thermal nonlinearity in the nanosecond regime. Our results showed that while the refractive nonlinearity in PE is smaller than that of CS_2, the nonlinear scattering effect is comparably stronger and much longer lasting. However the effective nonlinear susceptibility is smaller than that of CS_2. Hence PE would not be an effective optical power limiter at 1064nm against threat pulses in the nanosecond and subnanosecond regime.

In addition the continuous variability of the laser pulse duration enabled us to observe the transition between opto-mechanical and microscopic nonlinearities and hence determine directly the time scales for which effects such as electrostrictively and thermally induced acoustic scattering become dominant.

We confirmed the validity of our measurements and experiments by comparing the CS_2 $\chi^{(3)}$ values to those found in literature and by verifying other DFWM properties such as phase conjugation and third order signal dependence.

We believe our laser system to be ideally positioned to study the transient behavior of thermally and electrostrictively induced nonlinear scattering processes.

7.1 Future work

We now suggest further improvements to the system which will allow exciting new measurements to be made. They are:

- Further reduction of pulse length will increase the dynamic range of pulse lengths over which nonlinear materials can be probed, it will increase the resolution of acoustic scattering parameters and possibly extend the range of nonlinear optical mechanisms which can be probed to include bulk molecular reorientation. Other experiments [91, 92, 78, 93] have achieved SBS pulse compression to less than 200ps.

- Increase of the SBS reflectivity in order to achieve constant laser output energies. This would allow for the direct probing of fluence dependent effects

in materials, such as excited state absorption. In this case the energy into the SBS cell would be constant, and the pulse length would vary. Thus the intensity would be variable, and the fluence would be constant. A two stage pulse compressor [93] may make possible to achieve constant reflectivity.

- The continuous variability of pulse length poses an ideal way of testing dynamic models of the nonlinear impulse response of optical materials via the deconvolution method outlined in section 2.6.2. We have done a dynamic analysis by visual inspection of the DFWM return as a function of pulse length which provided us with all the information we needed, namely the time regimes for which each mechanism was dominant. In order to obtain exact values for the thermal parameters, a full digital deconvolution analysis would be preferable.

Appendix A

Detectors

We spent some time finding suitable photodetectors. Our requirements were good linearity, 1 GHz bandwidth, large dynamic range, high sensitivity and reasonable pricing. Commercially available products all failed one or more of the requirements outlined above and in the end we decided to build our own detectors and test them.

The schematic is shown in Fig. A.1 along with two pictures in Figs. A.2.

We used reverse biased, 0.1 mm diameter, 3 GHz InGaAs photodiodes from EG&G (CE30617E). Their responsivity is about 0.5 A/W at 1064 nm. The 9V battery sets the operating point in the I-V diagram of the diode, which determines the linearity of the detector. The voltage supplied by the battery served to sweep the electron-hole pairs out of the active area of the diode at a much faster rate than in an unbiased circuit. The inductor was made up of a few turns around a ferrite coil and served to isolate the 9V battery from the rest of the circuit for AC currents. The surface mount capacitor provided the charge for the photocurrent generated in the diode. This substitutes the internal resistance of the battery with that of the capacitor which is much less, which improves linearity and speed. Great care was taken to produce a detector circuit that was as small as physically possible to reduce stray capacitances and inductances which may introduce unwanted resonances. To get more light onto the diode, the beam is focussed as shown in Fig. A.2(b). A piece of ground glass 3 mm in front of the diode protects the diode and samples the whole area of the beam over the active area of the diode. The detector was isolated

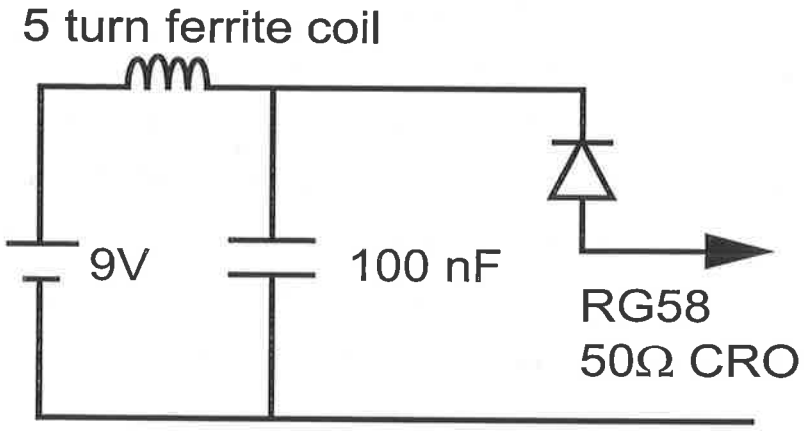

Figure A.1: Photodetector circuit: BW 750 MHz, Lin 0.005V-2.0V.

electrically from the table by a sheet of plastic (overhead transparency) to avoid any earth loops which may have picked up noise from the laser power supplies.

We measured the detector to be linear from 1 mV to 2.0 V and the shortest pulse width measured was 0.44 ns. This included the bandwidth of 1GHz of the transient digitizer TDS1000 from Tektronix. We used two identically constructed photodetectors connected to two transient digitizers to record the input and DFWM pulses. The digitizers were triggered by the signal of a separate, photodetector, saturated to give a fast risetime. This allowed accurate, 'relative time of arrival' measurements to about 100 ps. This can be seen in Fig. A.3 which shows 16 consecutive pulses. This figure also demonstrates the pulse to pulse stability of the laser output.For comparison Fig. A.4 shows the same pulses measured with a 1 GHz commercial photodetector (ET2000) which made use of an non-amplified Si photodiode. In this diagram we compare both detectors to a 6 GHz, amplified, Si photodetector from New Focus. The cost of the detectors was \$100, \$500, \$3000 for the home built, ET2000, New Focus detectors respectively.

The transient digitizers were controlled by a Pentium computer running Windows 95, via Labview from National Instruments and GPIB-interface protocol. Before we switched to Labview we wrote a program in C to do the same thing. However Labview allowed easy instrument interchange via instrument device drivers. Hence we were able to use digital CROs and the transient digitizers interchangeably. All

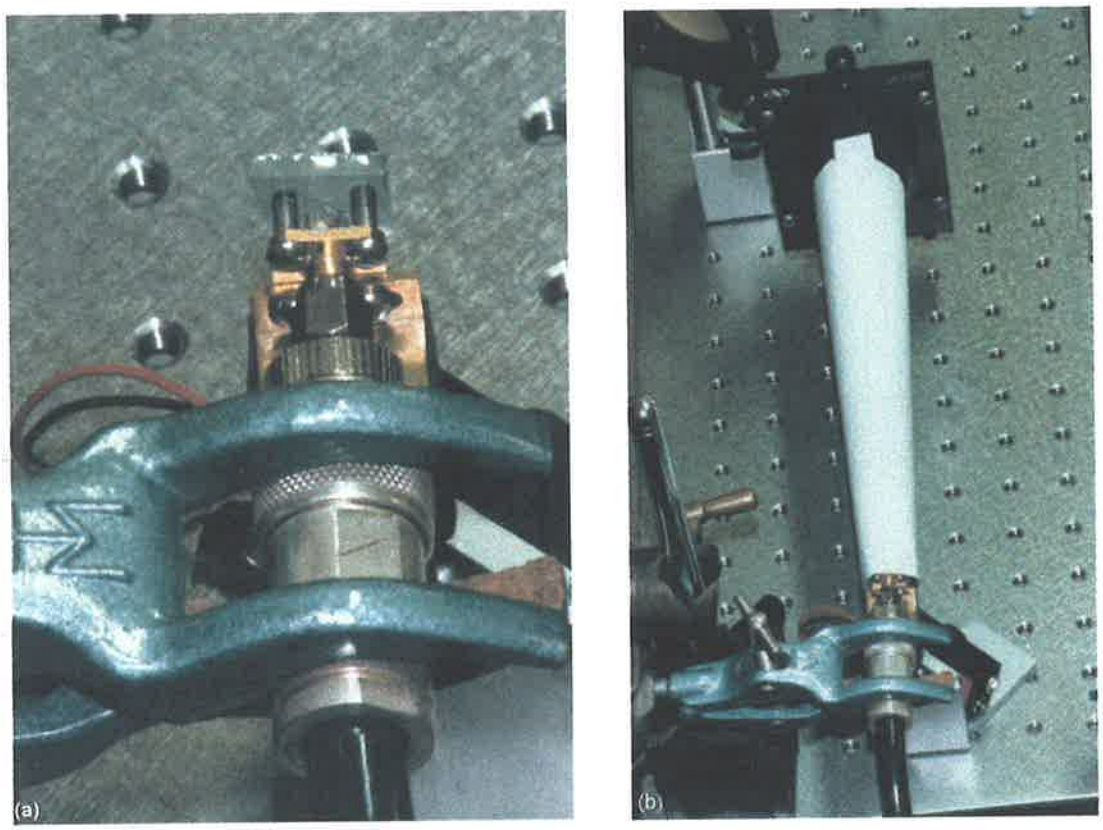

Figure A.2: (a) Photodetector construction. The diode was mounted on an SMA connector. This connector was then adapted to an N-type coaxial cable for maximum bandwidth/length. A piece of ground glass was used to protect the diode and sample the entire cross-section of the beam. The diode was mounted on a brass block fastened to a pole. The latter was held in place by a three point mount. A clamp on a separate mount was used to secure the cables. Both mounts were electrically isolated from the table using plastic sheets. (b) We focused the beam onto the detector to increase the intensity. The tube was used as a baffle to eliminate stray light.

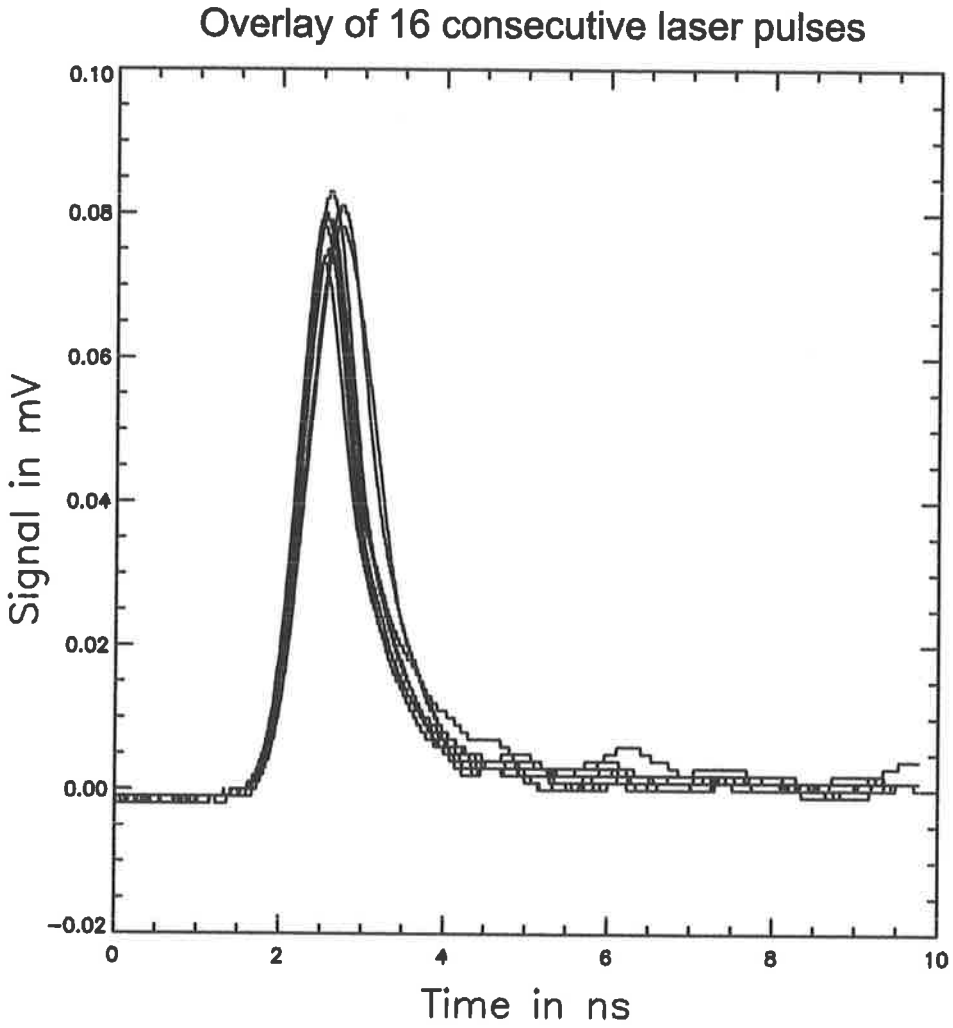

Figure A.3: 16 consecutive laser pulses, demonstrating good pulse stability and accurate, repeatable triggering.

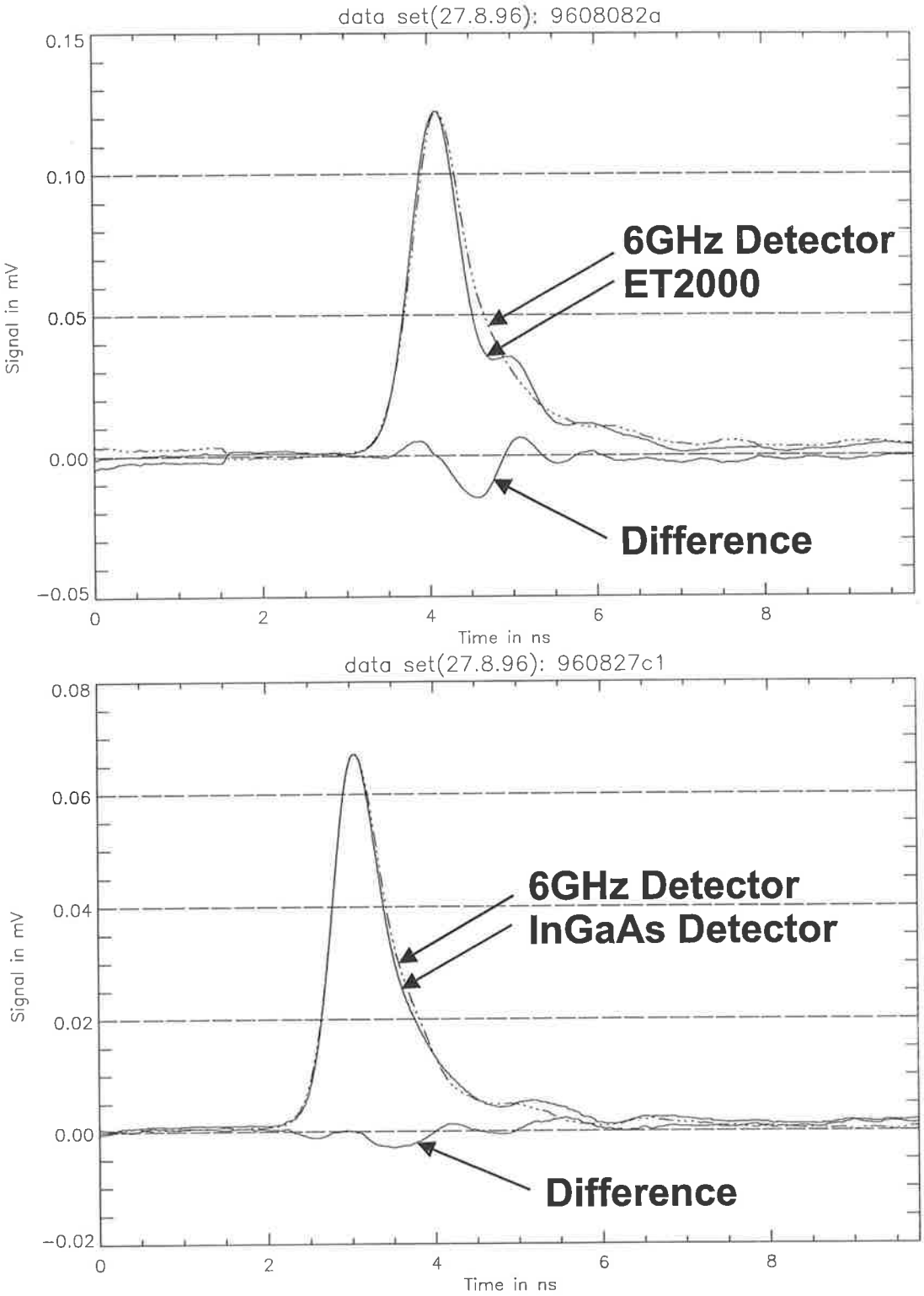

Figure A.4: Comparison of our detector (and commercial ET2000) to commercial 6 GHz detector from New Focus.

data was saved always and compressed using PKZIP.

Appendix B

Nonlinear susceptibility error analysis

This appendix demonstrates an error analysis of the $\chi^{(3)}$ measurements given in this thesis. $\chi^{(3)}$ is given by the following formula.

$$I_4 = \left(\frac{\omega}{4c^2\epsilon_0 n^2}\right)^2 l^2 I_1 I_2 I_3 \left|\chi^{(3)}_{xxxx}\right|^2$$

Rewriting this to solve for $\chi^{(3)}$ yields

$$\left|\chi^{(3)}\right| = \left(\frac{4c^2\epsilon_0 n^2}{\omega}\right) \frac{1}{l} \sqrt{\frac{1}{I_1 I_2} \frac{I_4}{I_3}} \tag{B.1}$$

Given that $I = I_1 = I_2$ and $I_3 = sI_1$ where $s = 0.25$ and $I_4 = RI_3$ (where R is the reflectivity of the DFWM process), we can rewrite this equation as

$$\begin{aligned} \left|\chi^{(3)}\right| &= B\frac{1}{lI}\sqrt{\frac{I_4}{I_3}} \\ &= Bl^{-1}I_4^{\frac{1}{2}}I^{-\frac{3}{2}}s^{-\frac{1}{2}} \end{aligned}$$

where

$$B = \frac{4c^2\epsilon_0 n^2}{\omega}$$

Hence we can now evaluate the error in $\chi^{(3)}$ using standard error analysis techniques, ie. implicit differentiation.

$$\begin{aligned}
\triangle\left|\chi^{(3)}\right| &= \left|\triangle\{Bl^{-1}I_4^{\frac{1}{2}}I^{-\frac{3}{2}}s^{-\frac{1}{2}}\}\right| \\
&= Bs^{-\frac{1}{2}}l^{-2}I_4^{1/2}I^{-3/2}\triangle l \\
&\quad +\frac{1}{2}Bs^{-\frac{1}{2}}l^{-1}I_4^{-1/2}I^{-3/2}\triangle I_4 \\
&\quad +\frac{3}{2}Bs^{-\frac{1}{2}}l^{-1}I_4^{1/2}I^{-5/2}\triangle I
\end{aligned}$$

We have values for the length and respective intensities, but we do not have error values for the intensities. These are given by

$$I = \frac{E}{t.A}$$

where the symbols have their usual meaning. The error in the intensity value is given by

$$\triangle I = t^{-1}A^{-1}\triangle E + t^{-2}A^{-1}E\triangle t + t^{-1}A^{-2}E\triangle A$$

and the error in the area is given by

$$\begin{aligned}
\triangle A &= \triangle\{\pi r^2\} \\
&= 2\pi r\triangle r
\end{aligned}$$

Assuming the following values for the above parameters

$$\begin{aligned}
l &= (5.0 \pm 0.25) \times 10^{-3} \text{ m} \\
t &= (0.75 \pm 0.05) \times 10^{-9} \text{ s} \\
E &= (35 \pm 1) \times 10^{-3} \text{ J} \\
r &= (1.5 \pm 0.08) \times 10^{-3} \text{ m} \\
s &= 0.25 \\
B &= 4.6 \times 10^{-9} \text{ [units]}
\end{aligned}$$

then we get a value for $\chi^{(3)}$ of

$$\chi^{(3)} = (6.3 \pm 2.3) \times 10^{-13} \text{ esu}$$

which corresponds to a 37% error. We can trace this back to a 20% uncertainty in I, which in turn is due to a 10% error in the area of the beam due to the 5% uncertainty in the radius of the beam. While this seems like a large uncertainty in the value of the nonlinear susceptibility, it must be noted that uncertainties in $\chi^{(3)}$ are almost never published, and it is the order of $\chi^{(3)}$ which is important, not its precise value. The order is the important because researchers are interested in large values of $\chi^{(3)}$ (eg. 10^{-9} esu) to achieve strong nonlinear effects.

Appendix C

Experiment Photographs

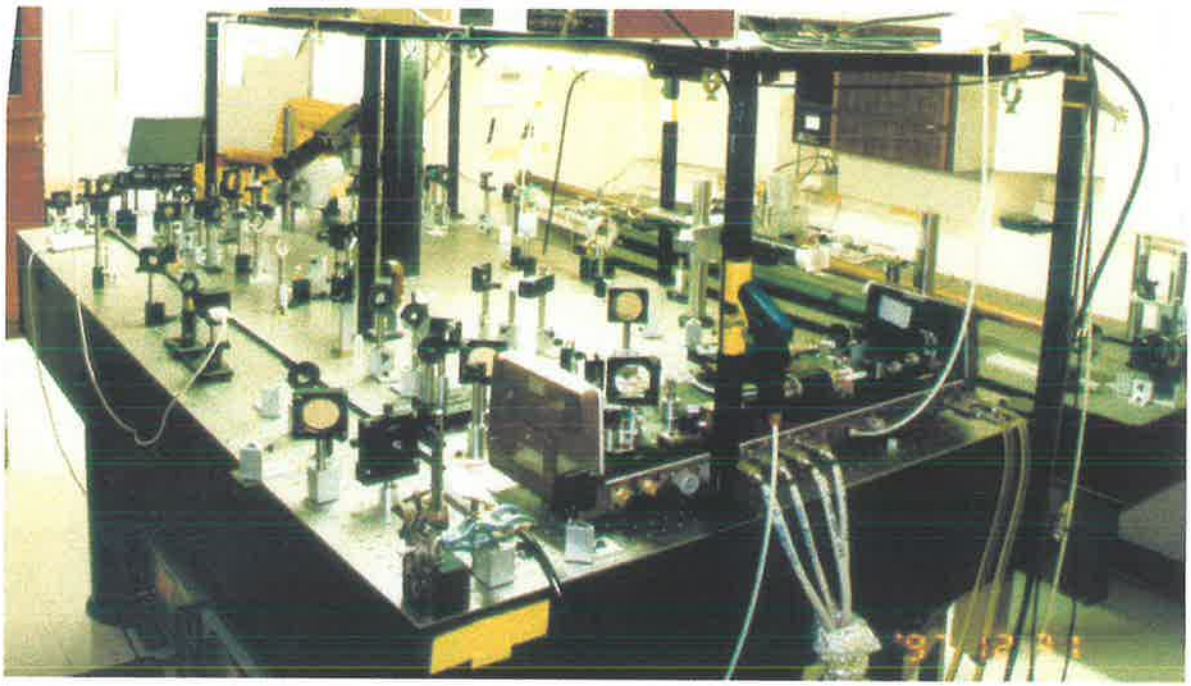

Figure C.1: Large table: Laser and DFWM; small table: SBS pulse compresssion. SBS phase conjugation makes it possible to link one experiment between two tables without alignment problems.

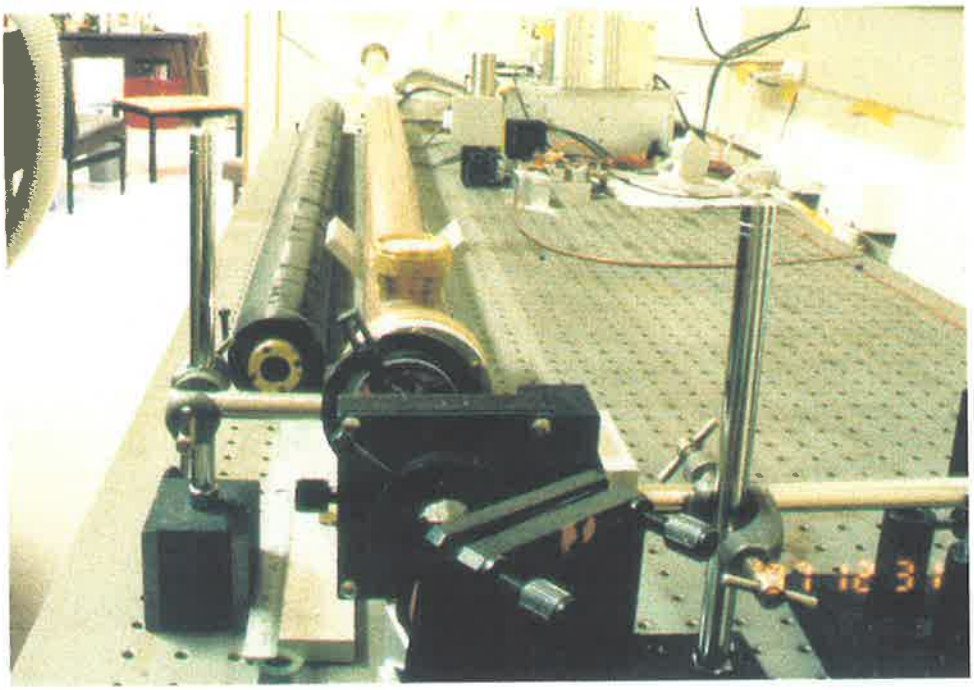

Figure C.2: SBS pulse compressor: The telescope is shown at the bottom, followed by a 2.4 m copper cell. Next to this cell is a smaller (1800x30 mm) cell which was used earlier. We found it necessary to thermally insulate the small cell to prevent thermal refractive index changes directing the beam toward the cell walls. The large cell had a large enough volume to make it less susceptible to changes in temperature. We did not use the small cell after initial trials because its size was impractical from an experimental point of view. For example the small aperture size made it cumbersome to direct the beam through it.

Appendix D

Paper 1

P. Klövekorn and J. Munch (1997) Variable stimulated Brillouin scattering pulse compressor for nonlinear optical measurements.
Applied Optics, v. 36 (24), pp. 5913-5917, August 1997

Appendix E

Paper 2

"Variable optical delay line with diffraction-limited autoalignment"

Applied Optics, April 1998

P. Klövekorn and J. Munch (1998) Variable optical delay line with diffraction-limited autoalignment.
Applied Optics, v. 37 (10), pp. 1903-1904, April 1998

Appendix F

Paper 3

submitted J. Quantum Electron.

"Investigation of transient nonlinear optical mechanisms using a variable pulse-length laser"

I. Abstract

We show a variable pulse length laser to be extremely useful when investigating the dynamics and parameters of opto-mechanical nonlinearities in optical materials. Pulse length variability allows observation of the transient nonlinear behaviour using nanosecond pulses and determination of the underlying physical mechanisms using sub-nanosecond pulses. It also enables observation of the transition response between the two time regimes where intrinsic polarizabilities compete with opto-mechanical effects. We examine the transient nonlinear scattering properties of an optical power limiter, platinum ethynyl, in comparison to carbon disulfide using degenerate four-wave mixing. Intensity, polarization and pulse length control allow us to measure acoustic scattering and decay parameters, $\chi^{(3)}$ magnitudes and the transient, laser-induced grating behaviour.

II. Introduction

Characterization of nonlinear properties of optical materials is central to present day optical devices. The dynamic response and magnitudes of nonlinear susceptibilities of optical materials are very sensitive to the pulse length of the laser used[1]. This is due to the multitude of physical mechanisms which can contribute to the nonlinear optical (NLO) interaction. These mechanisms are usually classified as either intrinsic or bulk nonlinearities. Intrinsic nonlinearities, such as resonant excitation [2, 3, 4] and molecular reorientation [5, 6], are due to the polarizability of a single molecule. Bulk nonlinearities are due mainly to opto-mechanical effects such as electrostriction [7, 8], thermo-optic phase gratings[9] and collective molecular reorientation of liquid crystals [10]. Due to their microscopic scale, intrinsic effects typically occur at timescales of picoseconds or faster, whereas macroscopic, bulk effects occur at subnanoseconds or slower. It is therefore important to understand both the mechanisms and the transient dynamics which contribute to the measurement of a nonlinear signal.

The sensitivity of NLO parameters to laser pulse length suggests that the laser be chosen to fit the requirements of the interaction of interest. However, we frequently require knowledge of the response of a material over a range of pulse lengths. Examples include the characterization of optical power limiters [11, 12, 13], where the duration of a potential threat pulse is unknown, and the investigation of the damage threshold of optical materials[14, 15].

We recently demonstrated a variable pulse length laser (VPLL) as a source for a degenerate four-wave mixing (DFWM) experiment[16]. In this paper we present the results of detailed experiments aimed at characterizing the dynamic response of an optical power limiter, platinum ethynyl (PE), in comparison with carbon disulfide in the sub-nanosecond to nanosecond regime. Continuous variability of the pulse length from 0.7 ns to 10 ns significantly enlarges the amount of experimental control of DFWM. The VPLL allows us to separate the intrinsic nonlinearities from the optomechanical nonlinearities and determine the physical mechanisms giving rise to the NLO response. In addition we also determine the transient response as a function of pulse length which demonstrates clearly the competition between nonlinear optical mechanisms at different timescales.

III. Theory

Since DFWM [5, 17, 9, 18, 19] was first proposed by Hellwarth[20] and successfully demonstrated by Bloom and Bjorklund[21], the technique has emerged as an important tool in transient nonlinear spectroscopy [22]. DFWM is especially useful due to the great amount of experimental control which can be exercised, with selective access to various physical mechanisms of the nonlinear interaction. This can be achieved by careful selection of the laser [3, 23, 24], geometry[25, 18, 2], intensity[26] and polarization[27, 28]. We add continuous pulse length control in the subnanosecond to nanosecond time regime to this list of variable parameters.

Fig. 1 shows the general DFWM geometry. The two colinear and antiparallel laser beams,

I_1 and I_2, are referred to as the pump beams. The third beam, I_3, is the probe and leads to generation of the fourth beam, I_S, the signal beam and the phase conjugate of the probe [29]. The forward pump and probe intersect at an angle θ in a material with refractive index n. The phase difference between the two beams at any point x along the grating vector $\mathbf{k}$ is given by $\Phi(x) = |\mathbf{k}|\, x$ where

$$|\mathbf{k}| = \frac{4\pi}{n\lambda} \sin\frac{\theta}{2}$$

In the case of S-polarized beams, this produces an S-polarized electric field modulation and intensity distribution as shown. Since the beams have the same optical frequency, this modulation is stationary in space for the duration of the overlap of the beams[30]. In the presence of a material, this stationary but dynamically evolving interference pattern induces a polarization which depends on the nonlinear optical susceptibility of the material, $\chi^{(3)}$. This process is known as a material excitation[18] and leads to localized changes in the complex refractive index, resulting in a dynamic material grating with spacing Λ, given by

$$\Lambda = \frac{2\pi}{|\mathbf{k}|} \tag{1}$$

Scattering or diffraction of one of the pumps by this material grating generates the signal. In the steady state case, for a non-absorbing material for which the reponse time is fast compared to the length of the laser pulse, the DFWM signal is given by[31]

$$I_S(t) = \left(\frac{\omega}{4c^2\epsilon_0 n^2}\right)^2 l^2 I_1(t) I_2(t) I_3(t) \left|\chi^{(3)}(\omega)\right|^2 \tag{2}$$

where ω, c, ϵ_0 and n have their usual meaning and l is the interaction length of the pumps I_1 and I_2 and the probe I_3. If the pumps and the probe all originate from the same laser, ie. $I(t) = I_1(t) = I_2(t) = aI_3(t)$, Eq.2 is written

$$I_S(t) = \left(\frac{\omega}{4c^2\epsilon_0 n^2}\right)^2 l^2 a I(t)^3 \left|\chi^{(3)}(\omega)\right|^2 \tag{3}$$

showing the cubic intensity dependence of this third order, nonlinear process.

In the transient regime for which the response time of the material is of the order of the pulse length, Eq.2 is replaced by

$$I_S(t) \propto I(t) \left| \int_{-\infty}^{t} \sum_m F_m(t-\tau) I(\tau) d\tau \right|^2 \tag{4}$$

where F_m represents the response function of a particular physical effect, denoted m [32]. Hence the signal is given by the convolution of the input pulse intensity with the temporal response function of the material and its dominant mechanisms[19]. Note that although Eq.4 implies that the temporal profile of the DFWM signal may have a completely different shape than the input, the signal still shows the third-order dependence on the laser intensity. Also Eq.4 reduces to Eq. 3 if the temporal response of a material is instantaneous compared to the laser pulse length [19].

In the time regime of nanoseconds or longer, bulk optomechanical effects play an increasingly dominant role and hence the DFWM signal is given by the sum of the fast, intrinsic effect (Eq. 3) as well as the slower, bulk effect (Eq. 4). Hence the DFWM signal provides a direct probe of the dynamics of the interaction.

All DFWM configurations give rise to intrinsic polarization effects due to the microscopic polarizability of each molecule. However polarization control can eliminate the major source of opto-mechanical nonlinear effects, namely thermally and electrostrictively induced refractive index changes[31]. As shown before, vertical polarization of all beams, denoted SSS, results in an intensity grating. Alternatively the probe can be polarized parallel to the plane of intersection and orthogonal to the pumps, denoted SSP. In this case the intensity remains constant along $\mathbf{k}$ since the polarization of pumps and probe are always orthogonal, however the phase difference Φ still varies linearly along $\mathbf{k}$. Therefore the resultant polarization will vary between circular and linear as shown in Fig.2. Note that this polarization has components in x, y and z directions. For each grating period there will be two orthogonal states of linear polarization. In an isotropic liquid, the molecules are free to move and will have a

tendency to realign their most polarizable axis with those two linear polarization directions. Hence this configuration is commonly called a polarization or reorientation grating[31, 6]. Since there is no intensity modulation along the grating direction, intensity dependent opto-mechanical effects cannot give rise to a DFWM signal in this configuration.

In order to establish the physical mechanisms which give rise to the DFWM response, it is necessary to determine the dynamic evolution of the grating. Nelson *et al*[7, 33, 34] have modelled the evolution of the diffraction efficiency of a laser induced grating when probed with a picosecond laser. This technique has received much attention recently for its application in dynamic chemical reaction analysis[35, 36], transient nonlinear spectroscopy [37] and thin-film analysis [38]. The model takes into account electrostriction and absorptive expansion which cause density changes that persist longer than the optical interaction, and hence give rise to a refractive index grating with a characteristic decay. It predicts the generation of two counter propagating compressional waves with wave vectors equal to that of the grating, resulting in a standing wave. This acoustic response was shown to be given by

$$S_{\text{electrostriction}} = -B \cos kx \ (\sin \Omega t) \tag{5}$$

$$S_{\text{thermal}} = A \cos kx \ (1 - \cos \Omega t) \tag{6}$$

where Ω is the acoustic frequency, x is the direction along the grating vector $\mathbf{k}$, defined in Fig. 1 and S is the displacement. The diffraction efficiency, η, of the grating was shown [34] to be related to the displacement by

$$\eta \propto S^2 \tag{7}$$

Thus, in the electrostrictive case, the displacement oscillates between maxima in the positive and negative direction, the displacement and the diffraction efficiency attaining an absolute maximum twice per acoustic cycle. In the case of absorption, however, thermal diffusion leads to the presence of an additional static term and the displacement varies between a positive

maximum and a null displacement. The diffraction efficiency thus attains a maximum only once per acoustic cycle. This behavior is shown in Fig. 3 for three cases. The acoustic period thus depends on the driving mechanism and is given by

$$T_{\text{thermal grating}} = \frac{\Lambda}{v_s} \tag{8}$$

$$T_{\text{electrostrictive grating}} = \frac{\Lambda}{2v_s} \tag{9}$$

where Λ is the grating spacing given by Eq. 1 and v_s is the speed of sound in the material.

By measuring v_s in the liquid, the mechanism responsible for the acoustic phonons can be determined by measuring the period of oscillation.

IV. Materials

The motivation behind this work was to investigate the nonlinear scattering and nonlinear refractive properties of an organometallic optical power limiter, platinum ethynyl (PE, Fig.4). Good reviews on optical limiting are available [39, 40]. PE exhibits optical limiting behaviour in the visible wavelenghts using reverse saturable absorption (RSA) [41, 23]. RSA arises when the excited state of a molecule has a larger absorption cross-section than the ground state, causing the material to darken under intense laser radiation. This presents an excellent mechanism for optical limiting. Other mechanisms are self-defocusing and light induced nonlinear scattering. Nonlinear scattering (NLS) and absorption (NLA) have been shown to exist at 1064 nm[41, 42]. To eliminate RSA effects, our investigation was done at 1064 nm, well away from any possible resonant enhancement[23]. This approach complemented experiments done in the resonant regime and allowed us investigate other mechanisms such as NLA and NLS.

Our previous experiments [16] in the nanosecond time regime showed PE to exhibit an unexpected nonlinear response at 1064 nm, the origin of which is presently resolved. We used PE in solutions of tetrahydrofurane (THF) and at concentrations of 0.08 M. The sample

recrystallized at room temperature overnight and was always kept in a refrigerator when not in use. We compared its response with that of carbon disulfide (CS_2) which also gives rise to a nonresonant nonlinearity at 1064 nm. CS_2 has a large intrinsic nonlinear susceptibility of $\chi^{(3)}_{xxxx} = 5.1\times10^{-13}$ esu [1] which is due mainly to molecular reorientation [6]. Its reorientation time is of the order of 2 ps because it is a small molecule and thus we expected a fast, steady state, non-thermal response at 1064 nm. We measured the absolute value of its nonlinearity before using it as a calibration standard.

V. Experiment

The VPLL was described in Ref.[16]. It supplies single transverse mode pulses with continuously selectable pulse lengths between 0.7 ns and 9.5 ns at 1064 nm as shown in Fig.5. Phase conjugation by stimulated Brillouin scattering (SBS) in Freon-113 guaranteed diffraction limited Gaussian beams and hence well known laser field distributions. The DFWM setup, shown in Fig.6, is similar to that in our earlier experiments[16] but includes a self-aligning variable delay line. Energy was controlled with a halfwave plate/polarizer combination (not shown) and the input pulses were monitored with detector D1 (bandwidth > 1GHz). Probe and pumps were split off with wedged, thin film beamsplitters and independent polarization control of each beam was achieved with halfwave plates and Glan polarizers attaining a polarization purity of greater than $1{:}10^{-3}$. The samples were contained in cells with 5 mm optical pathlengths. The DFWM signal was allowed to propagate by 7 m behind baffles to minimize detection of scatter by the optical components used, especially the sample cell. We set up a variable delay line in the backward pump to probe the temporal evolution of the DFWM grating. The alignment of this delay line was independent of the mechanical quality of the track[43], which greatly simplefied the experiment. We therefore needed only to account for the laser divergence, which was measured to be 0.73 mrad.

An alignment technique was also developed for the pump beams to guarantee their colin-

earity to 0.1 mm and 10^{-4} rad and was performed at 1064 nm. This excluded the possibility of misalignment due to slight variations in sample cells and other adjustments such as polarizer rotation.

To measure the DFWM signal we focused it onto a piece of ground glass, mounted 3 mm in front of a fast (bandwidth > 1 GHz), InGaAs photodetector D2. The ground glass allowed sampling of the entire cross-section of the beam and focusing increased the experimental sensitivity to a minimum detectable reflectivity of 10^{-7}. The signals of D1 and D2 were recorded by two transient digitizers with a bandwidth greater than 1 GHz. The bandwidth-limited pulse of this dectection system was measured to be 0.44 ns (FWHM). A saturated photodiode signal with a sharp rise time was used to trigger both digitizers which ensured temporal pulse to pulse coincidence to an accuracy of 30 ps. Each data set consisted of averaging 16 consecutive pulses.

We chose the intensity ratios of the pump beams and the probe beam to be 4:4:1. The low reflectivity ($<10^{-2}$) in our experiments ensured that the DFWM signal did not affect the nonlinear interaction.

VI. Characterization of the optical response

A. Nanosecond transient $\chi^{(3)}$ response

In Ref.[16] we reported the nanosecond transient response of PE and CS_2 in a DFWM experiment in the intensity grating configuration. We include those results here in Fig.7(a) and (c) as well as the calculated signals for a fast, nonresonant, steady state nonlinearity. As can be seen, both materials deviate from the expected cubic intensity dependence, indicating the presence of a slow mechanism in accordance with Eq.4. Keeping in mind that the DFWM signal is a direct probe of the diffraction efficiency of the material grating, we see that in both cases the grating was destroyed during the pulse. In CS_2 this lead to a truncation of the

DFWM pulse by about 1 ns. In PE the grating reformed, leading to a distinctive double peak structure. The destruction of the grating implies that the slow and fast mechanisms were in direct competition with each other. Note that the DFWM signal in PE is very similiar to that observed by McEwan et al [32] where the slow effect was modelled to be due to the build up of a thermal nonlinearity.

When the intensity modulation of the grating was set to zero using the orientation grating configuration, the DFWM signal in both materials changed to the steady state response as shown in Fig. 7(b) and (d). The slow response shown in Figs. 7(a) and (c) was therefore an intensity dependent effect.

After calibration of our detectors we obtained values for $\chi^{(3)}$ of $(5.3 \pm 2.1) \times 10^{13}$ esu and $(1.7 \pm 0.7) \times 10^{-13}$ esu for CS_2 and PE respectively. The value for CS_2 compares well with the literature value [1] of 5.1×10^{13} esu. Fig.8 shows the DFWM signal as a function of intensity of the input beams. We calculate slopes of 3.3 ± 0.1 for CS_2 and 3.3 ± 0.1 for PE, confirming the dominance of the third-order nonlinearity, as expected from Eq. 4.

B. Nanosecond dynamic grating evolution

We measured the maximum diffraction efficiency of each pulse as a function of delay of the backward pump. The optical delay was incremented in 1.3 ns steps and for each delay we averaged 16 consecutive pulses to obtain an averaged maximum DFWM intensity while keeping the input intensity fixed. The divergence of the laser beam caused the intensity of the backward pump in the material to decrease with increasing optical delay. We corrected the measured signal intensities for this decrease. Hence Figs. 9 and 10 show the diffraction efficiency as a function of delay for a non-diverging laser beam and illustrate the actual decay of the grating. Grating parameters are given in Tab. 1.

The time evolution of the gratings shows a number of important results. As expected, CS_2 exhibited a large steady state nonlinearity for the duration of overlap of the pumps and

the probe. For time delays greater than the pulse length we observed a residual, exponentially decreasing signal which implied the presence of a decaying refractive index grating. Fig. 11(a) shows the pulse shape of the DFWM signal at a fixed optical delay of 18.6 ns. The oscillations in this signal confirmed the presence of an acoustic phase grating.

In contrast to CS_2, the DFWM signal in PE exhibited a constant exponential decay as shown in Fig. 10, irrespective of the time of arrival of the backward pump. The pulse shape of the DFWM signal at a fixed optical delay of 14.6 ns is shown in Fig. 11(b) and indicates the presence of an acoustic phase grating, as was the case in CS_2.

To determine whether the structure seen in the 'zero delay' transient DFWM signal (Fig. 7 a) was associated with this acoustic phase grating, we measured the evolution of the pulse shape as a function of optical delay. This is shown in Fig. 12 which reveals that the second peak of Fig 7(a) was part of the series of peaks which constitute the acoustic phase grating. The first peak did not seem to due to the same mechanism, because there was a small suppressed peak at the position of the broken line in Fig. 12. The temporal positions of the oscillations were stationary in time as indicated by the solid vertical lines, implying that the oscillations were due only to the probe and the forward pump, and that the backward pump only read this grating, in direct analogy with real time holography.

Hence the DFWM signal in PE was due mainly to the opto-mechanical response of the fluid to the radiation whereas in CS_2 the signal was due to the intrinsic polarizability of the molecules. Note also that over 20 ns the signal in PE dropped by a factor of only two, whereas the signal generated in CS_2 dropped by 10^4.

C. Sub-nanosecond dynamic grating evolution

The nanosecond, transient DFWM structure exhibited by both materials was shown to be a combination of the photo-acoustic response and the intrinsic polarizability. It remained to determine the source of the acoustic phonons, which could be either electrostrictive or

thermal. We repeated the previous experiment with the 0.7 ns laser pulses provided by the VPLL. Fig. 13 and 14 show the resulting maximum diffraction efficiency as a function of optical delay of the backward pump for CS_2 and PE respectively. The oscillation in the diffraction efficiency demonstrates the presence of a standing wave, phase grating due to acoustic phonons. In both graphs the first peak, which corresponds to temporal coincidence of all three input beams, is much larger than the subsequent ones. Therefore we effectively separated the fast intrinsic polarizability from the opto-mechanical phase grating effects using the 0.7 ns pulses. This is a significant change from the grating decay of Fig.9 and 10 which was measured using 7.5 ns pulses.

Tab. 2 gives numerical values for the acoustic parameters obtained. Using Eq. 1 and 9 we arrive at values for the speed of sound, v_s, in CS_2 and PE which depend on the mechanism driving the excitation. The results compare well with literature which, in turn, confirms electrostrictive SBS (SEBS) as the physical mechanism generating the CS_2 phonons. We found the acoustic period in PE to be approximately twice that of CS_2, however since v_s has not been measured in PE, the acoustic mechanism remains unknown. If v_s in the two materials were equal, the phonons in PE would be of thermal origin

An interesting point about the grating decay in PE is that while the acoustic grating decays, Fig.14 shows a non-oscillating background term, increasing with the delay of the backward pump. Hence there are two values for the grating decay in Tab. 2. This behaviour has been observed and modelled by Genberg *et al* [44] and was shown to occur if the thermalization time is of the same order as the acoustic period. The thermalization time is a result of the delay in energy deposition via non-radiative relaxation into a thermal grating.

D. Heterodyne SBS speed of sound measurement

In order to determine the nature of the nonlinear mechanism involved, we measured the speed of sound in both materials using a different method. A self-induced SBS reflection in

a material gives rise to a Doppler shift in the optical frequency due to scattering by a sound wave. This frequency shift is given by

$$f_{Doppler} = \frac{2\eta v_s}{\lambda} \tag{10}$$

and can be measured directly by heterodyne detection[45]. Hence we could find a value for ηv_s[1] using both this and the DFWM method. Note that DFWM does not give rise to a frequency shift, because the signal is scattered by a standing, acoustic wave.

Fig.15 shows the setup used. The laser beam was split by a 50% beam splitter. One part was reflected by an SBS cell, the other by a mirror. Recombination of the two signals on a detector yielded the superposition of the two pulses which consequently exhibited a frequency beat. Variable attenuators were used to equalize the signal intensities returned by each arm of the experiment and maximize the modulation amplitude. For CS_2 the frequency shift is expected to be 3.8 GHz[46], which was beyond the bandwidth of our detection system. Hence we used Freon-113 which induces an SBS shift of 1.86 GHz[46] as an intermediate frequency reference. We first measured the beat signal produced between Freon and a plain mirror, then between Freon and CS_2 and finally between Freon and PE.

The results of this experiment are shown in Fig. 16 and Tab. 3.

As can be seen our values compare very well with literature. Using these results we obtain a value for ηv_s in PE.

$$\begin{aligned} \eta v_s &= \frac{\lambda f_{doppler}}{2} \\ &= 1.74 \times 10^3 \text{ m/s} \end{aligned}$$

Likewise, using the DFWM method with Eqs. 1 and 8 we obtain a value for ηv_s of

$$\begin{aligned} \eta v_s &= \frac{\lambda f_{spacing}}{4 \sin\left(\frac{9^\circ}{2}\right)} \\ &= 1.66 \times 10^3 \text{ m/s} \end{aligned}$$

[1]Note that we do not need to know the refractive index to compare the results for both methods which both yield a value for $v\eta$.

based on STBS as the phonon generation mechanism. As can be seen, these results agree to within 5%, which confirms that the speed of sound in PE is close to that of CS_2. This, in turn, confirms by direct experimental evidence using the VPLL, that STBS is the origin of the non-instantaneous nonlinearity in PE.

E. Pulse Length Transition Regime

We also used variable pulse compression to observe the transition dynamics of the nonlinearity in PE from the short pulse to the long pulse regime. The input was varied according to Fig. 5 and the resulting DFWM signal is shown in Fig. 17. This demonstrates clearly the dominance of the intrinsic nonlinearity in the sub-nanosecond regime, the subsequent 'competition regime' where both effects are of equal magnitude, and in the 10 ns regime, the dominance of the bulk, thermal nonlinearity.

Since the thermal nonlinearity starts growing significantly for pulses larger than 3 ns, we can assume the thermalization time to be of that order. This is in agreement with the observed grating decay measured with subnanosecond pulses. In that section we established that the thermalization time must be of the order of the acoustic period, namely 3.8 ns.

VII. Discussion

Both PE and CS_2 showed deviation from the expected, steady state DFWM signal in the nanosecond regime. In PE this deviation was large compared to the steady state nonlinearity and imposed significant structure on the transient DFWM signal. The dynamic evolution of the transient grating showed that this structure was due to a acoustic phase grating established during the pulse. An independent measurement of the speed of sound proved that the phonons were driven by thermal expansion. Therefore the transient DFWM signal in PE was characterized by the fast response of the intrinsic polarizability which was subsequently destroyed by the growth of a thermally excited acoustic phase grating. The absorption

mechanism was determined to be linear since there was no change in the slope nor in pulse shape over the entire dynamic intensity range of the laser as shown in Fig. 8.

In contrast, CS_2 was dominated by the large intrinsic polarizability of the molecule which was two orders of magnitude larger than the acoustic phase grating. The sub-nanosecond pulses showed the phonons were driven by the electrostrictive effect, as expected. At first glance this did not seem to explain the truncation of the nanosecond CS_2 signal of Fig.7(c). CS_2 gave rise to a purely electrostrictive grating at sub-nanosecond time scales, as shown by the exponential decay of the magnitude of the acoustic peaks of the grating evolution in Fig. 13. However, Fig. 11(a) shows the pulse shape of the DFWM signal at nanosecond time scales for an optical delay of the backward pump of 18.6 ns. The alternating height of the acoustic peaks implied increased competition from thermal expansion for nanosecond pulses in accordance with Fig. 3 and Eq. 6. Hence the transient, nanosecond DFWM signal was truncated because of competion from a thermal phase grating. This was the same mechanism as for PE, only much smaller and is in qualitative agreement with the relative magnitudes of the optomechanical and intrinsic nonlinearities observed in Fig. 9.

In conclusion, we have shown a VPLL to be extremely useful when investigating the dynamics and parameters of opto-mechanical nonlinarities.

VIII. Acknowledgements

This work was supported in part by grants from the Australian Research Council (ARC) and the Defence Science and Technology Organisation, DSTO. The Platinum Ethynyl compound was prepared by J.R.Davy (DSTO).

References

[1] N. P. Xuan, J. L. Ferrier, J. Gazengel, and G. Rivoire, "Picosecond measurement of the third-order susceptibility tensor in liquids," *Opt. Comm.*, vol. 51, pp. 433–437, 1984.

[2] M. Samoc and P. Prasad, "Dynamics of resonant third-order optical nonlinearity in perylene tetracarboxylic dianhydride studied by monitoring first and second order diffractions in subpicosecond degenerate four-wave mixing," *J. Chem. Phys.*, vol. 91, pp. 6643–6649, 1989.

[3] H. Fei, Y. Yang, Z. Wei, L. Han, Y. Che, P. Wu, and G. Sun, "Degenerate four-wave mixing based on excited-state absorption in azo-dye-doped polymer films," *Appl. Phys. B*, vol. 62, pp. 299–302, 1996.

[4] A. Agnesi, G. P. Banfi, M. Ghigliazza, and G. C. Reali, "Picosecond nonlinear optical characterization of GaAs," *Opt. Comm.*, vol. 92, pp. 300–306, 1992.

[5] I.-C. Khoo, *Liquid Crystals: Physical Properties and Nonlinear Optical Phenomena.* John Wiley and Sons, 1995.

[6] J. R. Lalanne, J. Buchert, and S. Kielich, "Fast molecular reorientation in liquid crystals probed by nonlinear optics," *Adv. Chem. Phys. Ser.*, vol. 85, pp. 159–215, 1993.

[7] K. A. Nelson, D. R. Lutz, M. D. Fayer, and L. Madison, "Laser-induced phonon spectroscopy. optical generation of ultrasonic waves and investigation of electronic excited state interactions in solids," *Phys. Rev. B*, vol. 24, pp. 3261–3275, 1981.

[8] J. M. Nunzi and D. Grec, "Picosecond phase conjugation in polydiacetylene gels," *J. Appl. Phys.*, vol. 62, pp. 2198–2202, 1987.

[9] H. J. Hoffman, "Thermally induced phase conjugation by transient real-time holography: A review," *J. Opt. Soc. Am. B*, vol. 3, pp. 253–273, 1986.

[10] G. K. L. Wong and Y. R. Shen, "Study of pretransitional behavior of laser-field induced molecular alignment in isotropic nematic substances," *Phys. Rev. A*, vol. 10, p. 1277, 1974.

[11] K. Mansour, M. J. Soileau, and E. W. V. Stryland, "Nonlinear optical properties of carbon-black suspensions (ink)," *J. Opt. Soc. Am. B*, vol. 9, pp. 1100–1109, 1992.

[12] K. J. McEwan and P. A. Madden, "Transient grating effects in absorbing colloidal suspensions," *J. Chem. Phys.*, vol. 97, pp. 8748–8759, 1992.

[13] W. Ji, J. J. Du, S. H. Tang, and S. Shi, "Nanosecond reverse saturable absorption in cubanelike transition-metal clusters," *J. Opt. Soc. Am. B*, vol. 12, pp. 876–881, 1995.

[14] D. X. Hammer, E. D. Jansen, M. Frenz, G. D. Noojin, R. J. Thomas, J. Noak, A. Vogel, B. A. Rockwell, and A. J. Welch, "Shielding properties of laser-induced breakdown in water for pulse durations from 5 ns to 125 fs," *Appl. Opt.*, vol. 36, pp. 5630–5640, 1997.

[15] A. A. Said, T. Xia, A. Dogariu, D. J. Hagan, M. J. Soileau, E. W. V. Stryland, and M. Mohebi, "Measurement of the damage threshold in fused quartz," *Appl. Opt.*, vol. 34, pp. 3374–3376, 1995.

[16] P. Klövekorn and J. Munch, "Variable SBS pulsecompressor for nonlinear optical measurements" *App. Opt.*, vol. 36, pp. 5913–5917, 1997.

[17] Y. R. Shen, "Basic considerations of four-wave mixing and dynamic gratings," *IEEE J. Quantum Electron.*, vol. 22, pp. 1196–1203, 1986.

[18] H. J. Eichler and P. Günter, *Laser-Induced Dynamic Gratings.* Springer-Verlag, 1986.

[19] R. W. Hellwarth, "Third-order optical susceptibilities of liquids and solids," *Prog. Quantum Electron.*, vol. 5, pp. 2–68, 1977.

[20] R. W. Hellwarth, "Generation of time-reversed wave fronts by nonlinear refraction," *J.Opt.Soc.Am*, vol. 67, pp. 1–3, 1977.

[21] D. M. Bloom and G. C. Bjorklund, "Conjugate wave-front generation and image reconstruction by four wave mixing," *Appl. Phys. Lett*, vol. 31, pp. 592–594, 1977.

[22] M. D. Levenson and S. S. Kano, *Introduction to Nonlinear Laser Spectroscopy, Revised Edition.* Academic Press, 1988.

[23] S. Guha, K. Kang, P. Porter, J. F. Roach, D. E. Remy, F. J. Aranda, and D. V. G. L. N. Rao, "Third-order optical nonlinearities of metallotetrabenzoporphyrins and a platinum poly-yne," *Opt. Lett.*, vol. 17, pp. 264–266, 1992.

[24] T. Steffen and K. Duppen, "Time resolved four- and six-wave mixing in liquids. ii. experiments," *J. Chem. Phys.*, vol. 106, pp. 3854–3864, 1997.

[25] A. M. Scott and M. S. Hazell, "High-efficiency scattering in transient Brillouin-enhanced four-wave mixing," *IEEE J. Quantum Electron.*, vol. 22, pp. 1248–1257, 1986.

[26] S. Guha and P. Conner, "Degenerate four-wave mixing in Kerr media in the presence of nonlinear refraction, pump depletion and linear absorption," *Optics Comm.*, vol. 89, pp. 107–118, 1992.

[27] W. M. Dennis and W. Blau, "Thermal effects in picosecond optical phase conjugation in soluble polydiacetylene," *Opt. Comm.*, vol. 57, pp. 371–374, 1986.

[28] D. J. McGraw, A. E. Siegman, G. M. Wallraff, and R. D. Miller, "Resolution of the nuclear and electronic contributions to the optical nonlinearity in polysilanes," *Appl. Phys. Lett.*, vol. 54, pp. 1713–1715, 1989.

[29] A. Yariv, "Phase conjugate optics and real-time holography," *IEEE J. Quantum Electron.*, vol. 14, pp. 650–656, 1978.

[30] Y. R. Shen, *The Principles of Nonlinear Optics.* New York: John Wiley and Sons, 1984.

[31] C. Maloney and W. Blau, "Resonant third-order hyperpolarizabilities of large molecules," *J.Opt.Soc.Am.B*, vol. 4, pp. 1035–1039, 1987.

[32] K. J. McEwan, K. J. Harrison, and P. A. Madden, "Polarisation and material dependence of degenerate four-wave mixing transients in molecular fluids," *Molecular Physics*, vol. 69, pp. 1025–1042, 1990.

[33] K. A. Nelson, R. Casalegno, R. J. D. Miller, and M. D. Fayer, "Laser-induced excited state and ultrasonic wave gratings: Amplitude and phase grating contributions to diffraction," *J. Chem. Phys.*, vol. 77, pp. 1144–1152, 1982.

[34] K. A. Nelson, R. J. D. Miller, D. R. Lutz, and M. D. Fayer, "Optical generation of tunable ultrasonic waves," *J. Appl. Phys.*, vol. 53, pp. 1144–1149, 1982.

[35] T. Hara, N. Hirota, and M. Terazima, "New application of the transient grating method to a photochemical reaction: The enthalphy, reaction volume change, and partial molar volume measurements," *J. Phys. Chem.*, vol. 100, pp. 10194–10200, 1996.

[36] E. Vauthey and A. Henseler, "Picosecond transient thermal phase grating study of a photoinduced electron transfer reaction in solution," *J. Phys. Chem*, vol. 99, pp. 8652–8660, 1995.

[37] M. Takezaki, N. Hirota, and M. Terazima, "Excited state dynamics of 9,10-diazaphenanthrene studied by the time-resolved transient grating method," *J. Phys. Chem.*, vol. 100, pp. 10015–10020, 1996.

[38] A. R. Duggal, J. A. Rogers, K. A. Nelson, and M. Rothschild, "Real-time characterization of acoustic modes of polyamide thin-film coatings using impulse stimulated thermal scattering," *Appl. Phys. Lett*, vol. 60, pp. 692–694, 1992.

[39] L. W. Tutt and T. F. Bogess, "A review of optical limiting mechanisms and devices using organics, fullerenes, semiconductors and other materials," *Prog. Quant. Electr.*, vol. 17, pp. 299–338, 1993.

[40] J. S. J. A. Hermann, "Trends in optical switches, limiters and discriminators," *International Journal of Nonlinear Optical Physics*, vol. 2, pp. 271–337, 1993.

[41] J. Staromlynska, P. B. Chapple, J. R. Davy, and T. J. McKay, "A platinum ethynyl compound for optical limiting," *Proc. SPIE*, vol. 2229, pp. 59–66, 1994.

[42] C. C. Frazier, S. Guha, P. L. Porter, and P. M. Cockerham, "Nonlinear optical properties of transition metal poly-ynes," *SPIE*, vol. 971, pp. 186–195, 1988.

[43] P. Klövekorn and J. Munch, "Variable optical delay line with diffraction-limited autoalignment," *App. Opt.*, vol. 37, pp. 1903–1904, 1998.

[44] L. Genberg, Q. Bao, S. Gracewski, and R. J. D. Miller, "Picosecond transient thermal phase grating spectroscopy: A new approach to the study of vibrational energy relaxation processes in proteins," *Chem. Phys.*, vol. 131, pp. 81–97, 1989.

[45] D. A. Jennings and H. Takuma, "Optical heterodyne detection of the forward-stimulated Brillouin scattering," *Appl. Phys. Lett.*, vol. 5, pp. 241–242, 1964.

[46] M. J. Weber, *CRC Handbook of Laser Science and Technology, Supplement 2: Optical Materials*, ch. 12, p. 471. CRC Press, 1995.

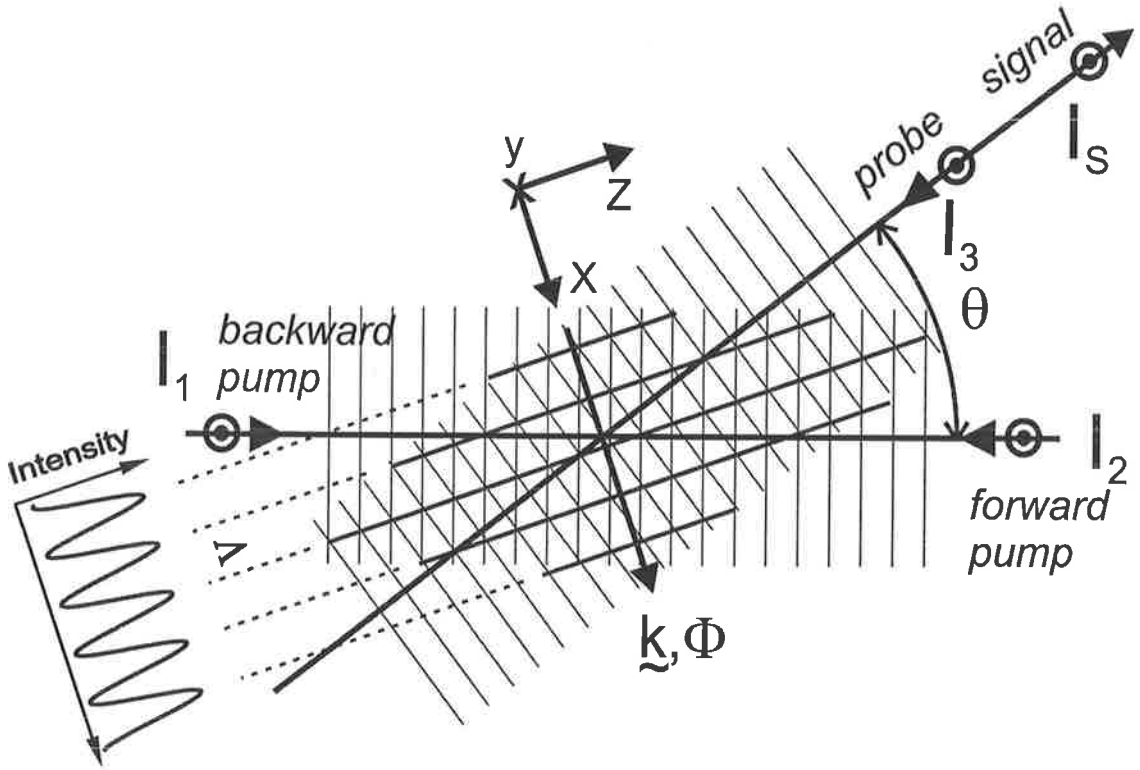

Figure 1: DFWM interference produced between two beams, I_2 and I_3, intersecting in a material at angle θ, giving rise to intensity distribution as shown.

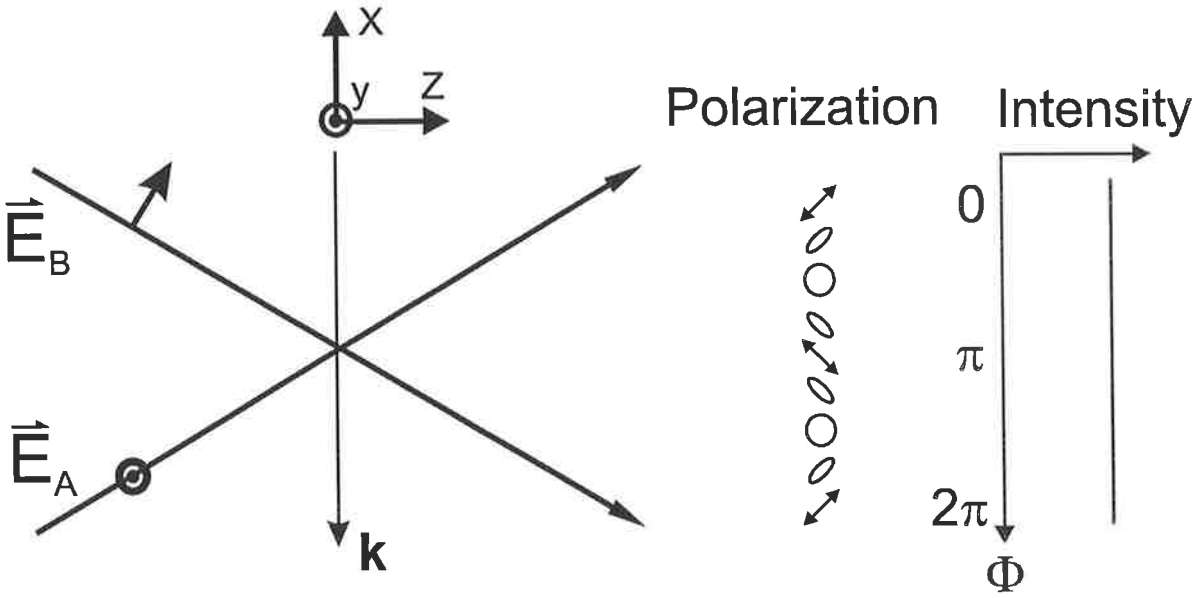

Figure 2: Interference between two, orthogonally polarized beams showing grating direction **k**, the phase difference Φ at any point along x between the beams and the resultant polarization and intensity distributions. Note that the resultant polarization has components in each of the x,y and z directions.

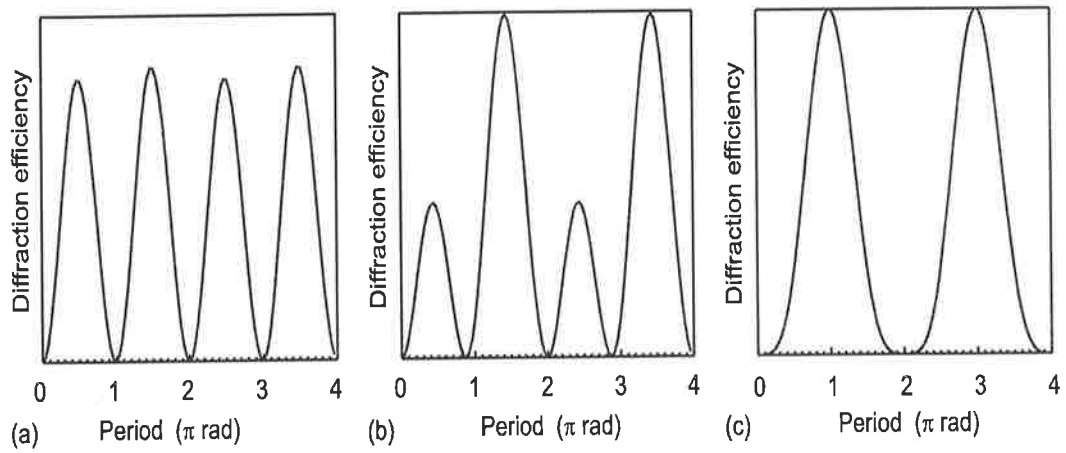

Figure 3: Comparison of the temporal evolution of the diffraction efficiency of material gratings driven by (a) electrostriction only, (b) electrostriction and thermal expansion, (c) thermal expansion only.

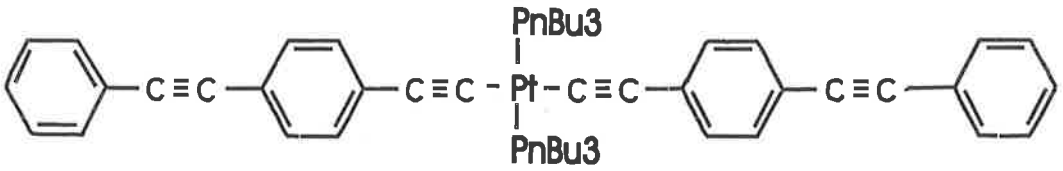

Figure 4: Platinum Ethynyl, PE

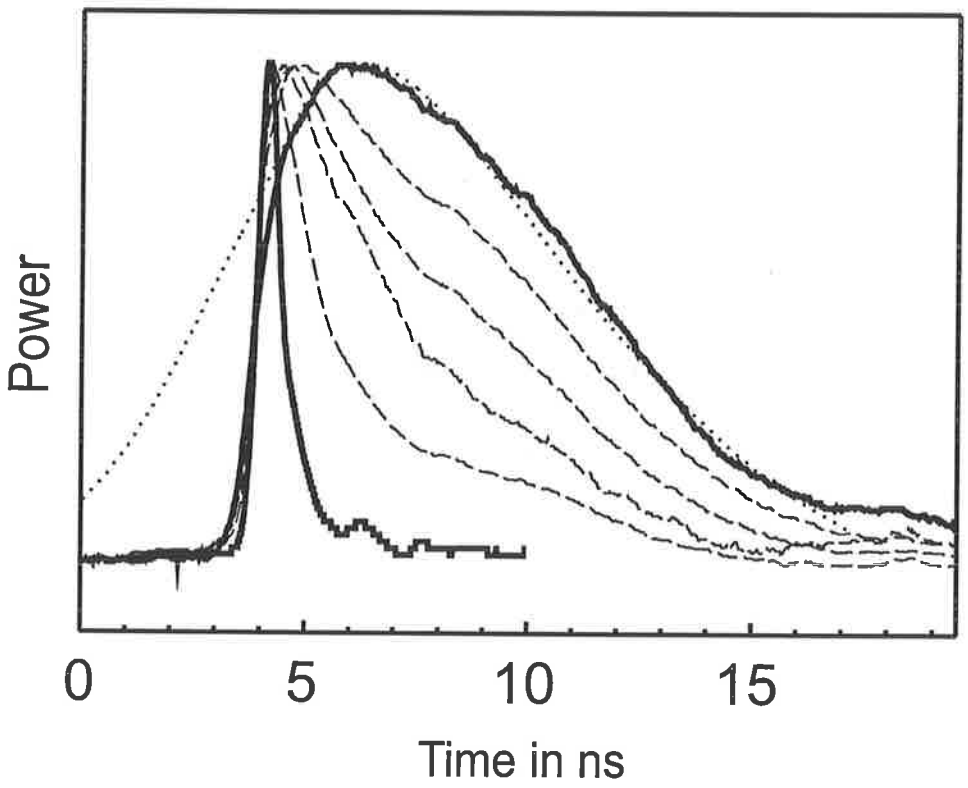

Figure 5: Pulse length results. All pulses are normalised in power to indicate temporal shape. The dotted line indicates the oscillator pulse. The solid lines show the pulses obtained with the long and the short cell. The broken lines show the pulses obtained by varying the focal length and energy into the long cell.

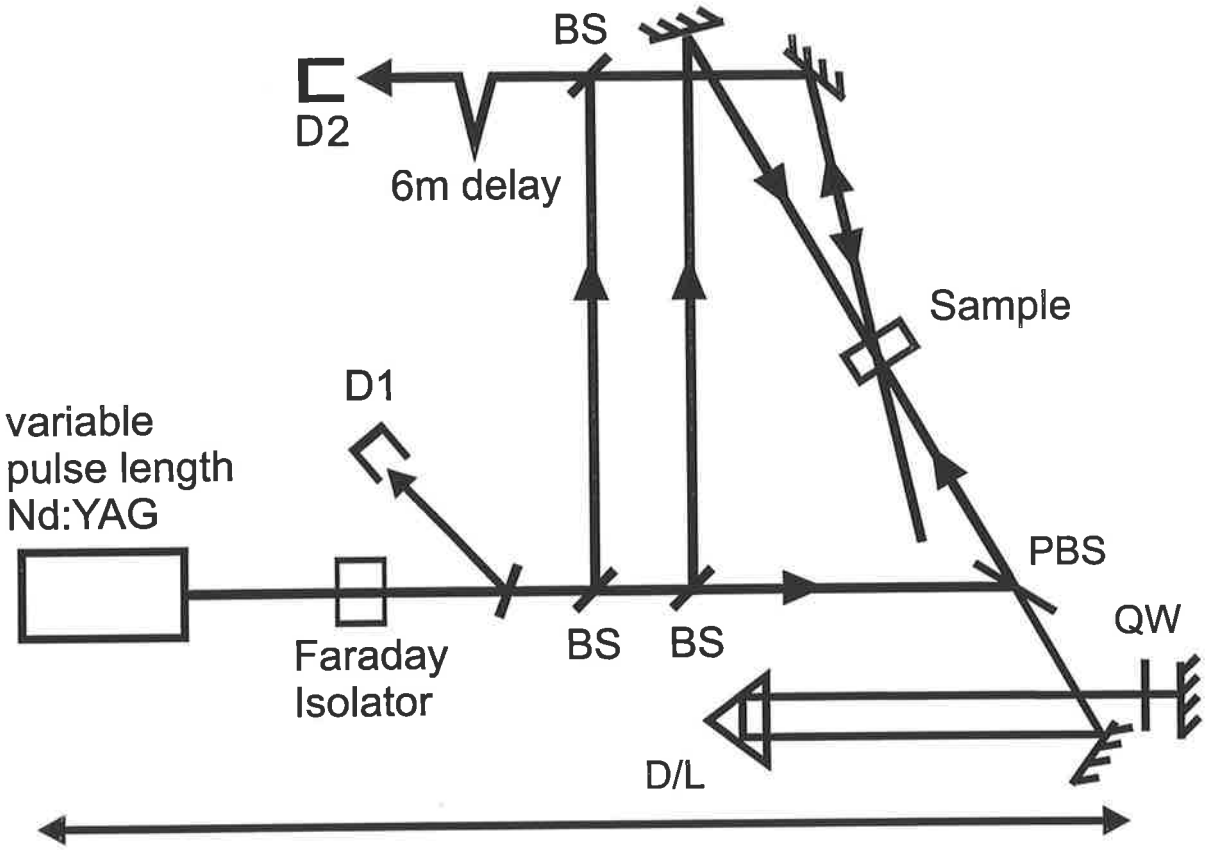

Figure 6: Experimental setup showing laser system and four-wave mixing details: HWP Halfwave plate, PBS polarizing beamsplitter, D/L delay line, QW quarter wave plate, D1 & D2 InGaAs photodetectors

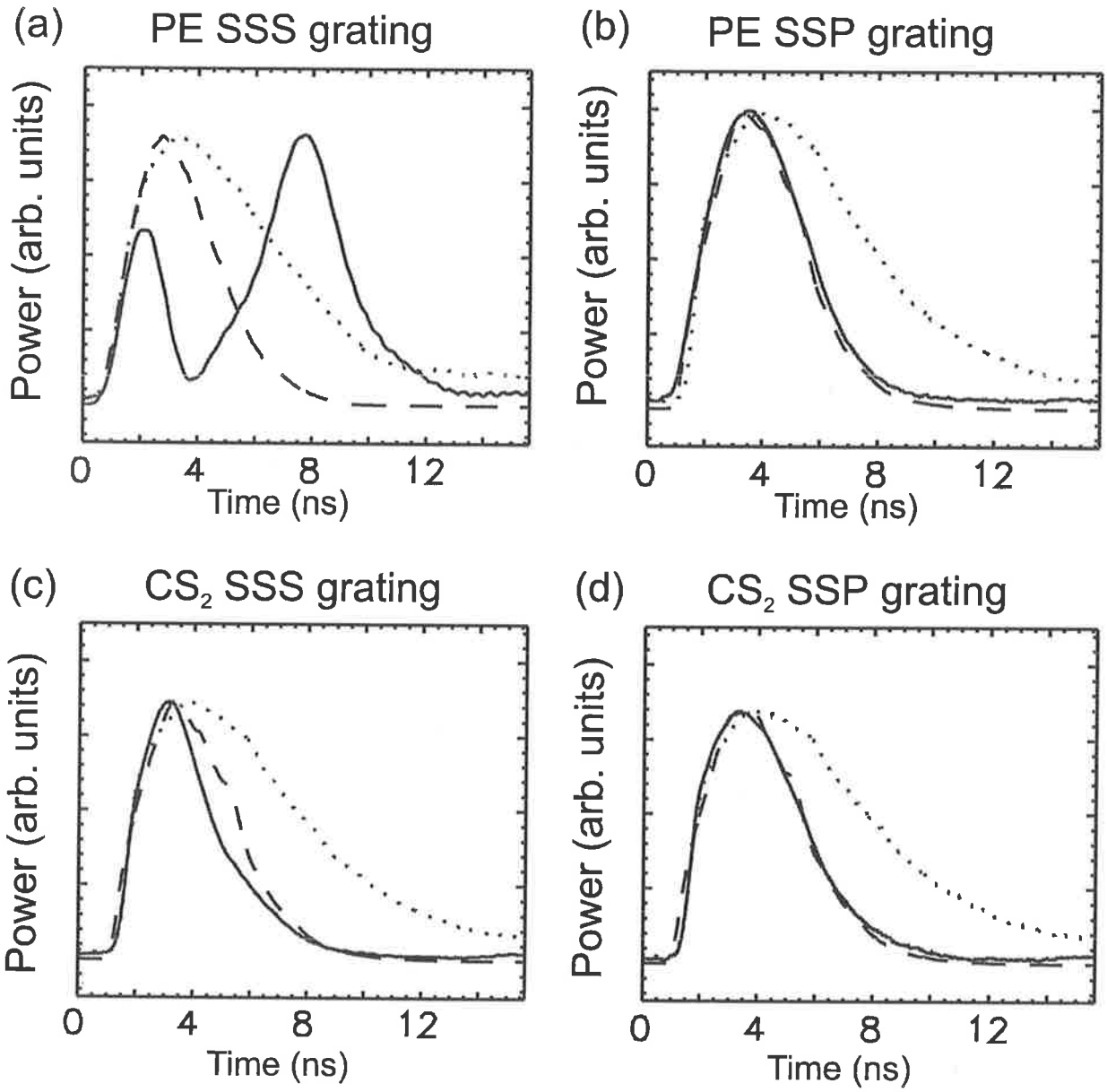

Figure 7: DFWM returns for the long pulse input. Dotted line: input pulse; broken line: cubic of input pulse; solid line: DFWM return;

(a) PE, intensity grating (b) PE, polarization grating (c) carbon disulphide, intensity grating.

(d) carbon disulphide, polarization grating.

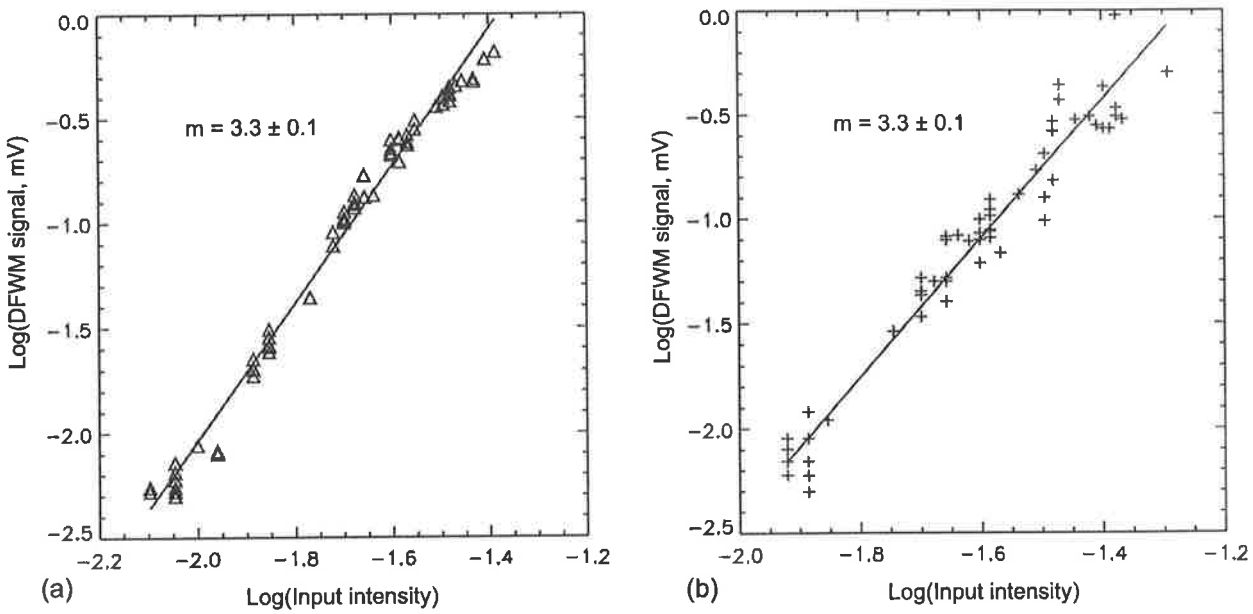

Figure 8: DFWM signal strength vs laser output power for both CS_2 and PE

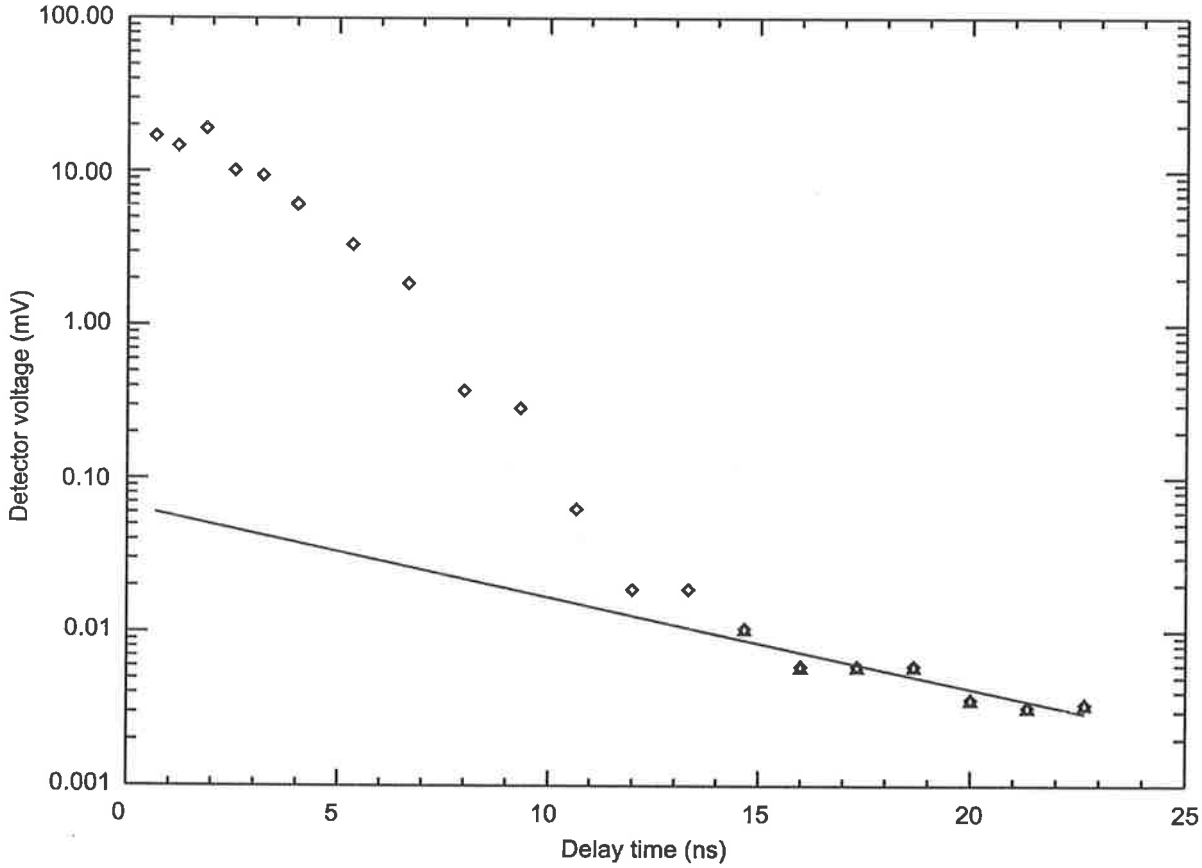

Figure 9: DFWM signal vs delay of backward pump in CS_2 using 7.5 ns pulses. Note the large signal exhibited by the material while all three beams overlap, as well as the residual, exponentially decaying signal for delays in excess of the pulse length.

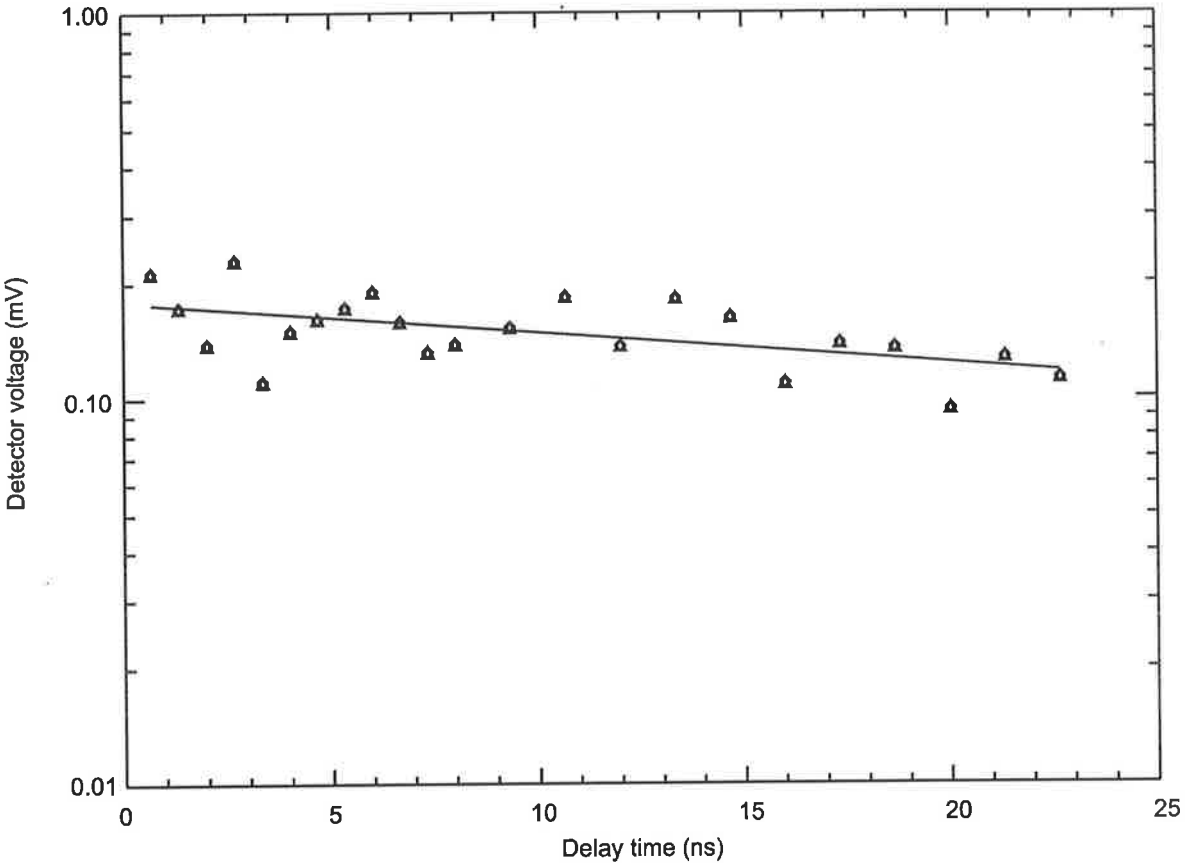

Figure 10: DFWM signal vs delay of backward pump in PE using 7.5 ns pulses

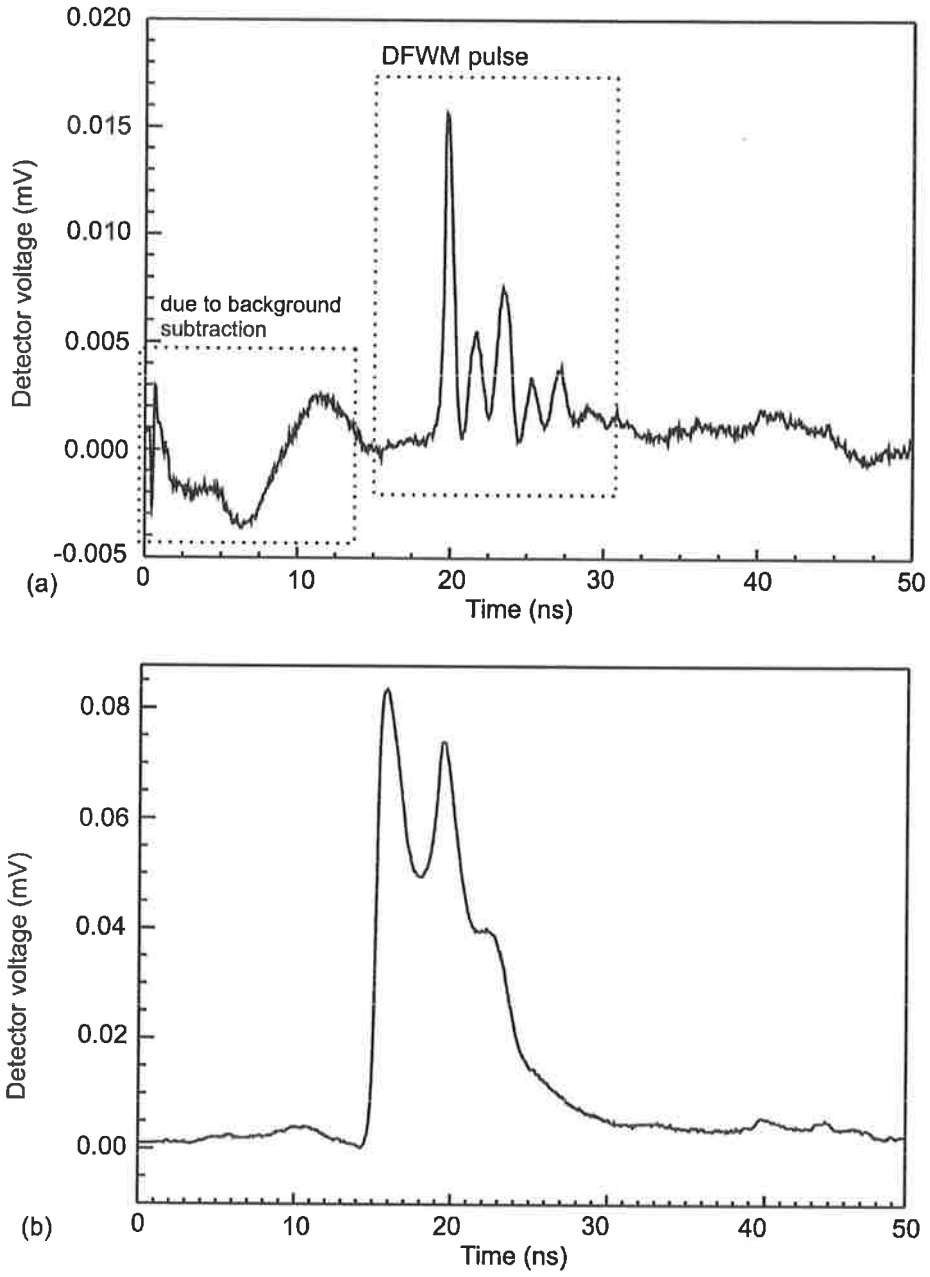

Figure 11: DFWM signal pulse shapes for delays greater than the pulse length, (a) CS_2 at 18.6 ns (b) PE at 14.6 ns.

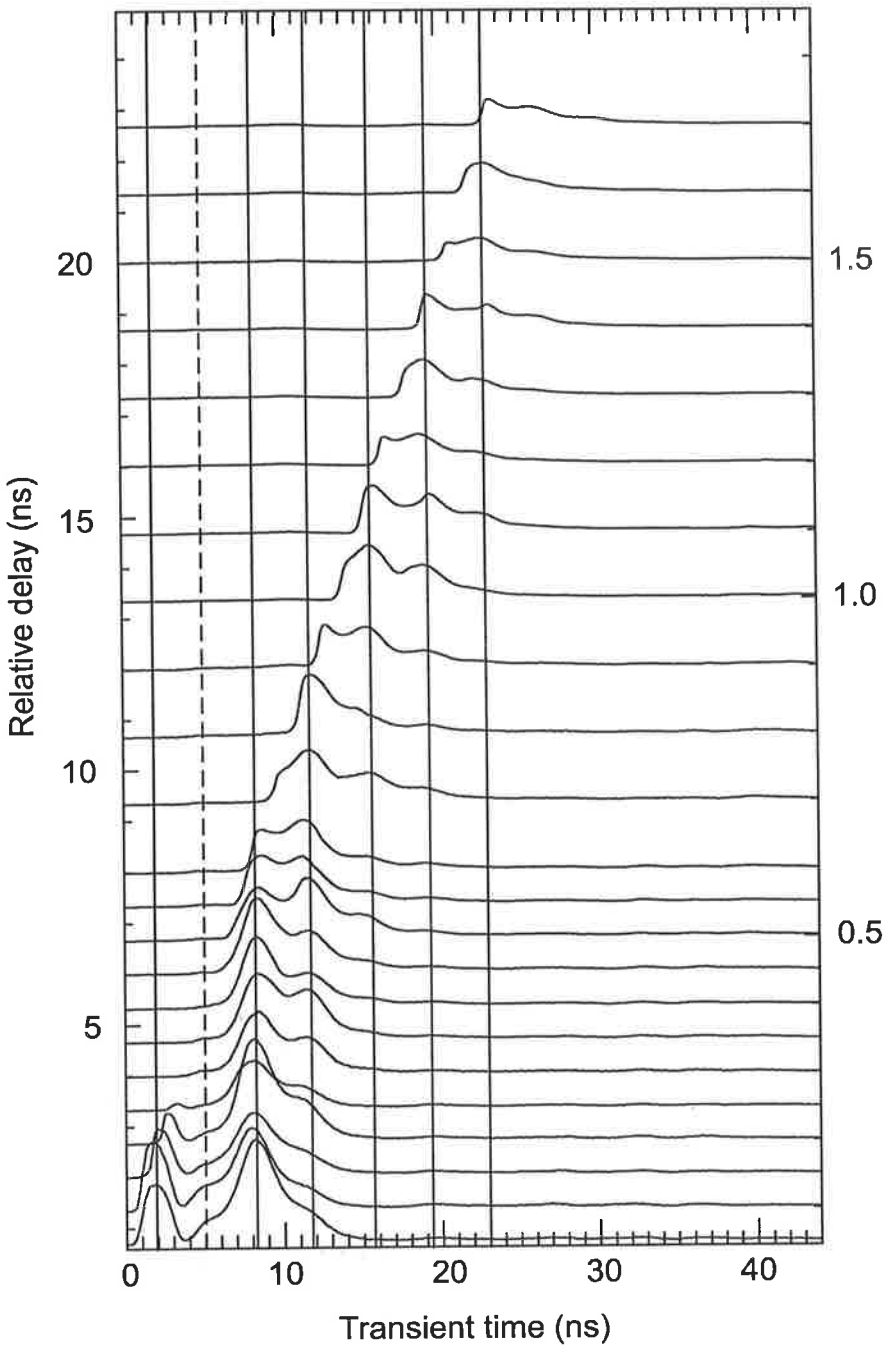

Figure 12: Pulse shape of DFWM return in PE as a function of delay of backward pump. The horizontal axis is the transient time evolution and the vertical axis shows the delay in nanoseconds of the backward pump.

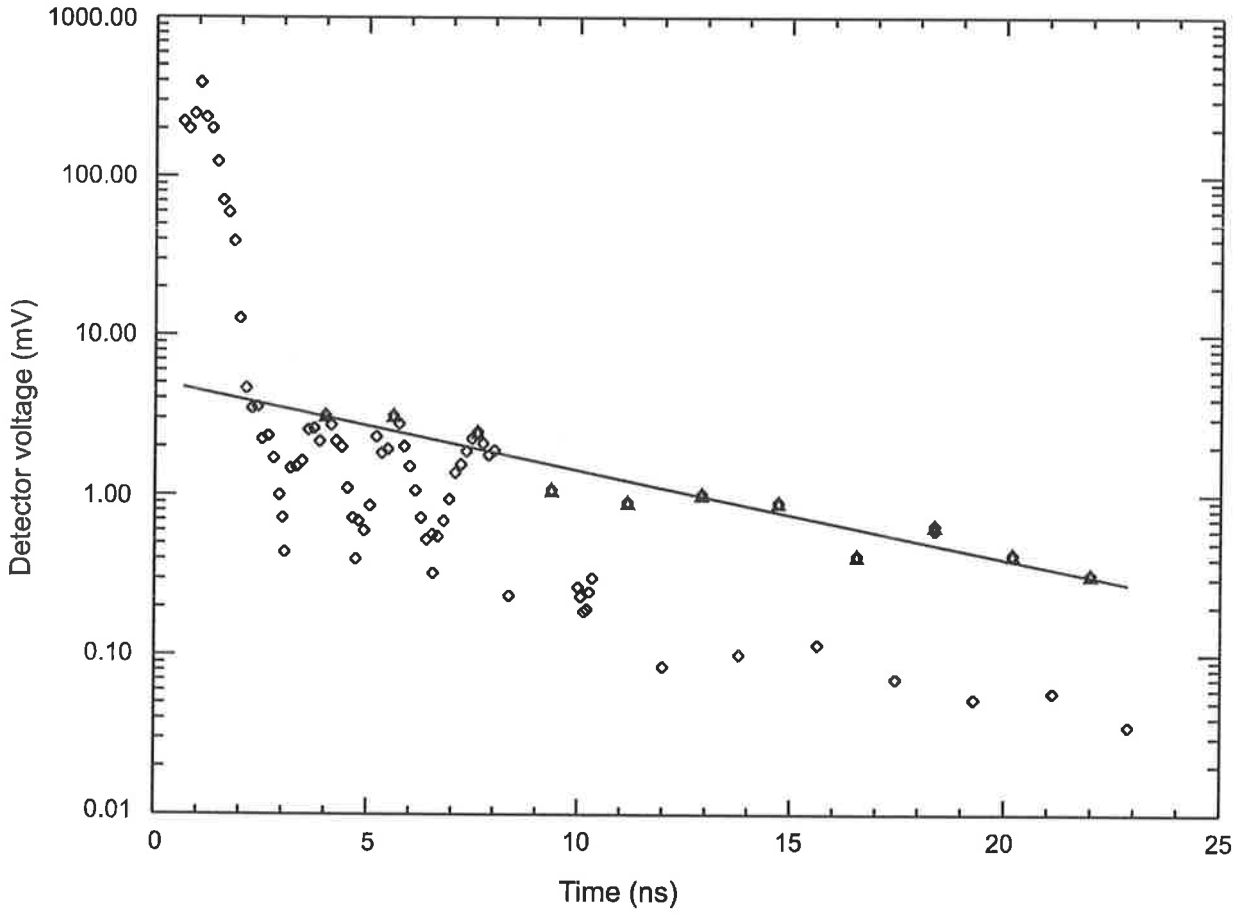

Figure 13: DFWM signal vs delay of backward pump in CS_2 using 0.7 ns pulses. Note the large signal while all beams are temporally coincident. For delays in excess of the pulse length we observe oscillations with exponentially decaying maxima.

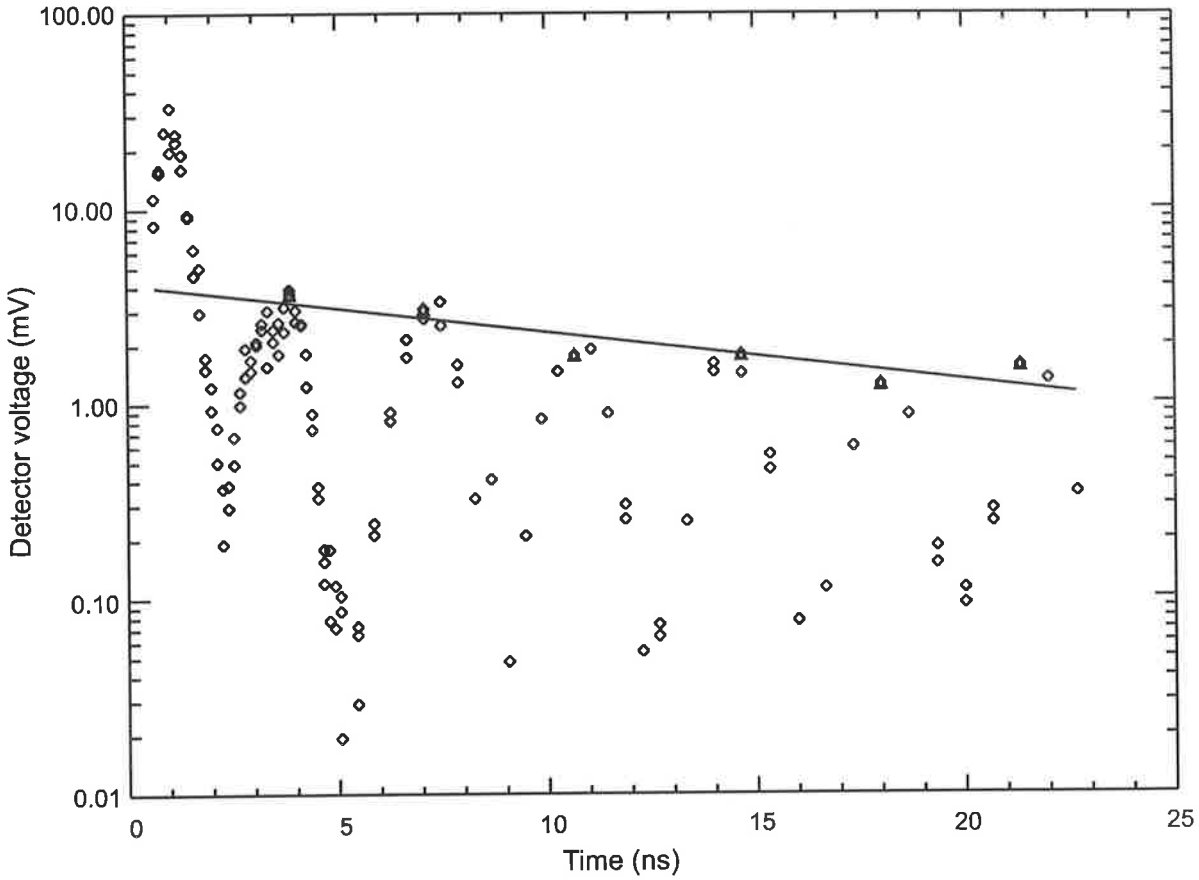

Figure 14: DFWM signal vs delay of backward pump in PE using 0.7 ns pulses. Note the large signal while all beams are temporally coincident. For delays in excess of the pulse length we observe oscillations with exponentially decaying maxima.

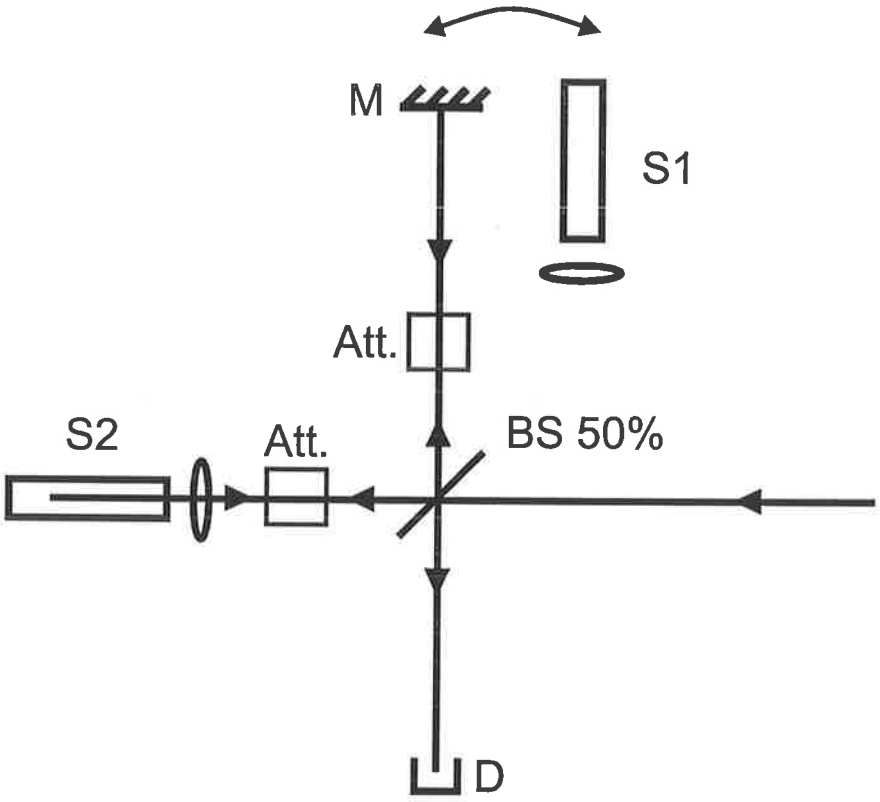

Figure 15: Heterodyne experiment to measure Doppler shift of SBS return. S1, S2: SBS samples; Att.: attenuators to achieve equal return intensities; BS: 50% nonpolarizing beam splitter; M: mirror used as non frequency shifting reference; D: photo detector (bandwidth 1GHz)

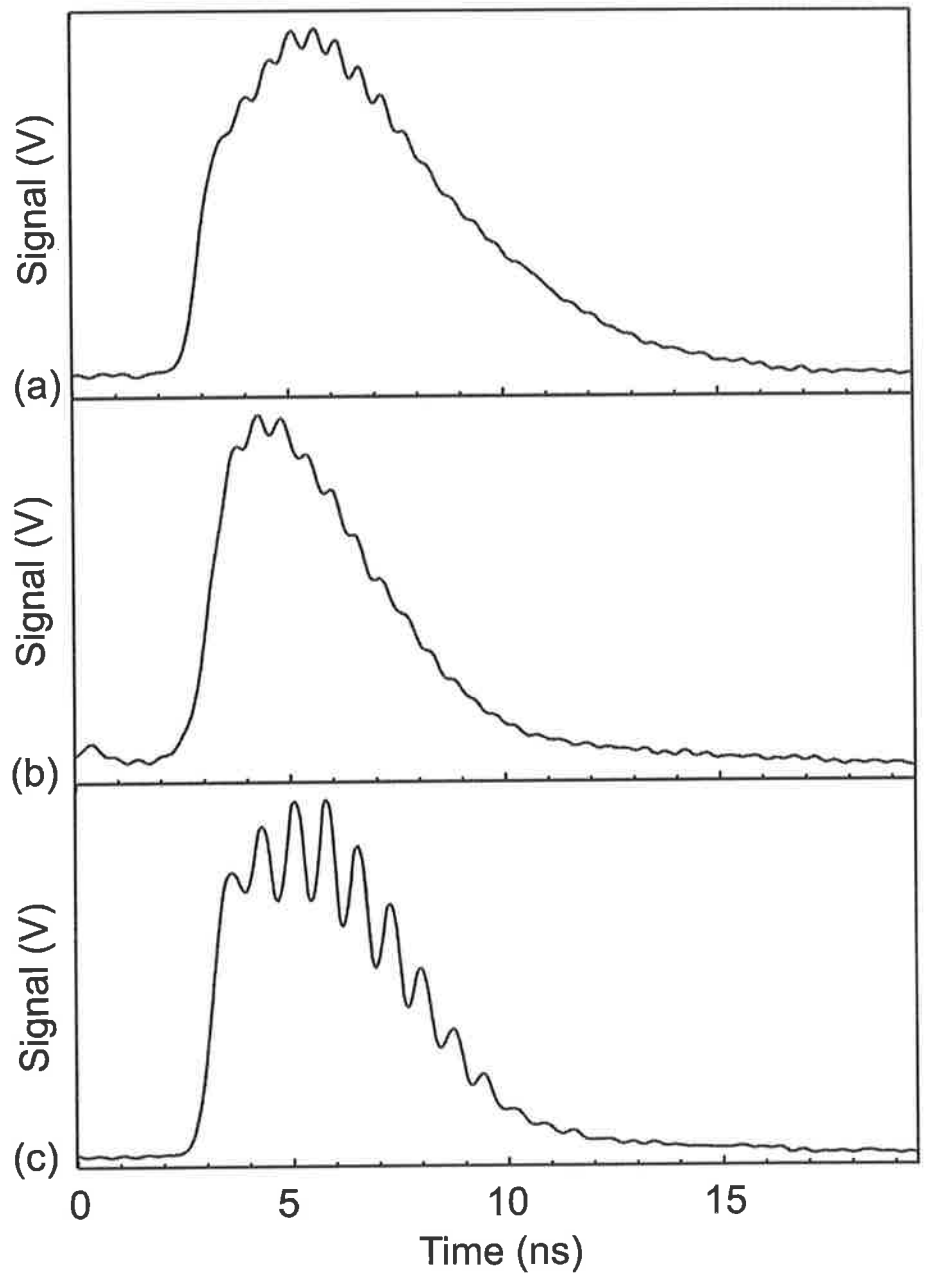

Figure 16: Heterodyne frequency beats between SBS returns of various materials. (a) Freon-plain mirror (b) CS_2-Freon (c) PE-Freon

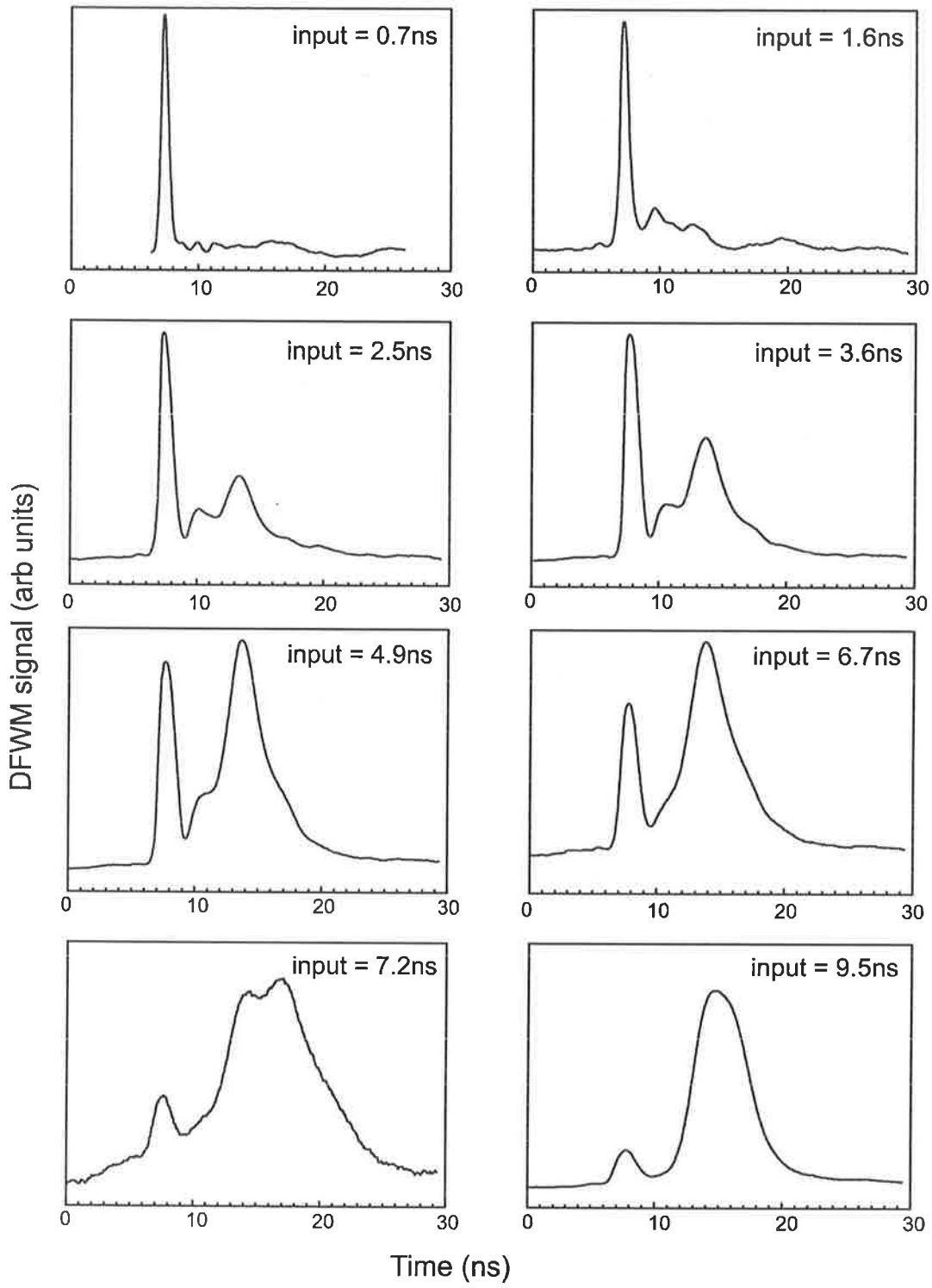

Figure 17: DFWM signal for the transition regime between intrinsic and opto-mechanical nonlinearities.

material	grating spacing μm	grating lifetime ns
CS_2	3.9	7.3
PE	4.1	53

Table 1: Results for dynamic grating decay using 7.5 ns pulses.

material	period ns	grating spacing μm	speed of sound $\times 10^3$ m/s	grating lifetime ns	phonon lifetime ns
CS_2	1.8	3.9	1.1 [1.15]	7.5	7.5 [6.5]
PE	3.8	4.1	0.54 (1.1)*	17	6.4

Table 2: Results for dynamic grating decay using 0.7 ns pulses. Literature values (in square bracketts) were taken from [46]. (*) Speed of sound values for PE were calculated for SEBS(STBS)

materials	period ns	frequency shift GHz	speed of sound $\times 10^3$ m/s
Freon-mirror	0.507	1.97 [1.86]	0.77
CS_2-Freon	0.523	1.91	1.29
PE-Freon	0.731	1.37	1.18

Table 3: Heterodyne frequency shifts: relative beat frequencies. Literature values (in square bracketts) from [46]

Appendix G

AOS Poster

Presented at the Australian Optical Society Conference in Adelaide, 12.12.1997

Variable Pulsewidth Laser to Access Nonlinear Optical Dynamics

Patrick Klövekorn
Jesper Munch

Lasers and Optics Group
University of Adelaide

Problem

- Pulse duration determines nonlinear optical (NLO) dynamics
- Commercial lasers: limited capability due to fixed pulse duration
- Need well defined beam quality for accurate determination of electric field inside material

Solution

Phase conjugated laser with:

- continuously variable pulse length
- Gaussian beam profile, beam quality ≈ 1

Features

- TAILOR input pulse duration to nonlinear material nonlinear mechanism
- SCAN through mechanisms
- OBSERVE transition between them

Benefits

- Better understanding of NLO dynamics
- Exact determination of nonlinear susceptibility

Overview of Experiment

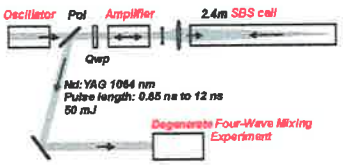

Laser Oscillator Desgin

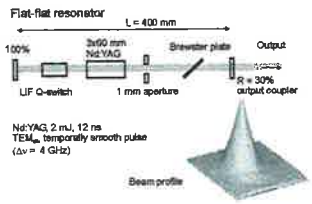

SBS Compression System

SBS material: Freon 113
phonon lifetime: 0.8 ns
singly distilled

Stimulated Brillouin Scattering

Stimulated scattering process

- Random scattering of acoustic phonons
- Backscatter interferes with forward beam, creating intensity grating
- Intensity threshold for stimulated scattering => reflectivity ~ 100%

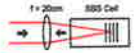

Phase conjugation process

- Lens converts phase information into intensity information
- electrostriction is an intensity process
- grating is produced with spatial phase info of beam
- gain is greatest for phase conjugate wave

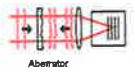

Power Amplifier

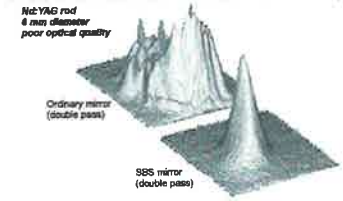

Variable Pulse Duration Output

Oscillator pulse 12ns
Shortest SBS pulse 0.6ns

Continuously variable pulses
0.6 ns,1.6ns, 3.3ns, 4.9ns, 6.7ns, 8.0ns, 9.5ns

Energy:
(long pulse) 53 mJ
(short pulse) 40 mJ

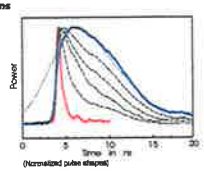

SBS Pulse Compression

- Intensity for SBS threshold is exceeded only at focus
- SBS return is generated at focus and travels back toward entry window
- As it travels back, it interferes with the incoming part of the pulse, thereby creating a moving, dynamically generated grating
- Center of reflection moves toward entrance window compressing the pulse

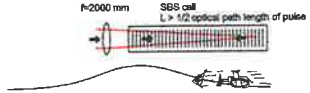

Degenerate Four-Wave Mixing

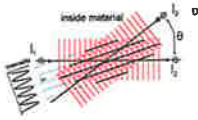

Dynamic laser-induced grating

Steady state case

$$I_{DFWM} \propto \left|\chi^{(3)}\right|^2 I_{in}^{\ 3}$$

Transient case

$$I_{DFWM}(t) \propto I_{in}(t) F \otimes I_{in}(t)^2$$

$$= I(t) \left| \int_{-\infty}^{t} F(t-\tau) I_{in}(\tau) d\tau \right|^2$$

F = response function nonlinear material

F(t) = δ(t) => temporal structure in FWM return

=> $I_4(t) \propto I^{(3)}(t)$

Experimental Setup

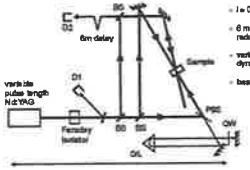

- I ≈ 0.1 to 1 GW/cm²
- 6 m delay to detector (to reduce stray scatter)
- variable delay line to probe dynamics of induced grating
- beam alignment to 10⁻⁴ rad

DFWM Mechanism selection

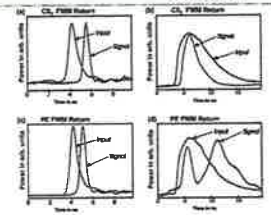

Transition Dynamics

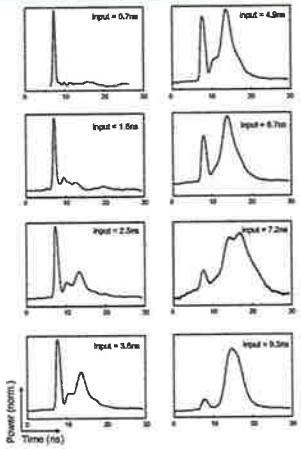

Nonlinear Optical Materials

Platinum Ethynyl	Carbon Disulfide
- Optical limiter in visible - nonlinear absorption & nonlinear scattering shown at 1064 nm - made by J.R. Davy (Defence Science and Technology Organization, South Australia)	- large $\chi^{(3)}$ - nonresonant at 1064 nm - standard nonlinear optical reference material S=C=S

Dynamic grating evolution, scattering parameters

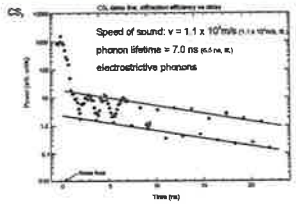

Future

- Further compress pulse down to 120 ps
- Include more nonlinear effects
- Transient model of transition regime

Appendix H

AOS Oral

Presented at the Australian Optical Society Conference in Adelaide, 11.12.1997

Time Dependent Characterization of Nonlinear Optical Materials

Patrick Klövekorn and Jesper Munch
Lasers and Optics Group
Department of Physics and Mathematical Physics
University of Adelaide

Motivation

DSTO, SA: need of Optical Limiter, Platinum ethynyl complex (PE)

good optical limiter in visible via *excited state absorption*

Major Optical Limiting mechanisms:

excited state absorption
nonlinear scattering

Nonlinear scattering shown to exist in PE

=> need to investigate nonlinear scattering in PE
=> in nonresonant regime to eliminate nonlinear absorption effects

Variable Pulse Length Laser

Continuously variable
0.7 ns to 9.5 ns pulses

POSTER:
Friday 3 pm Session

THIS TALK:
Demonstration of utility

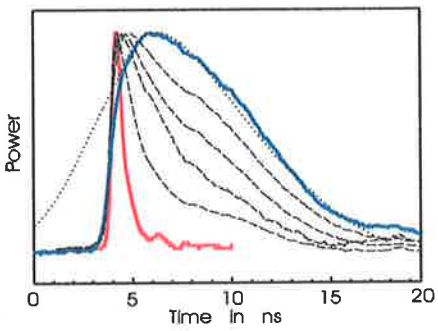

Transient Degenerate Four-Wave Mixing

Laser induced dynamic grating (LIDG)

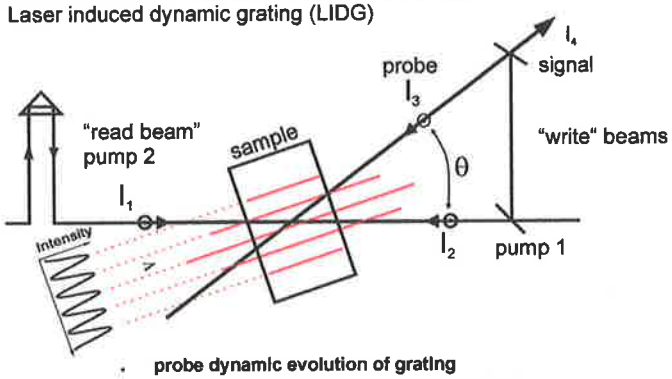

- probe dynamic evolution of grating
- can force stimulated acoustic grating (NLS)
- different time scales access different physical mechanisms
- compare PE to CS2 (standard nonlinear material)

Transient Nanosecond DFWM Response

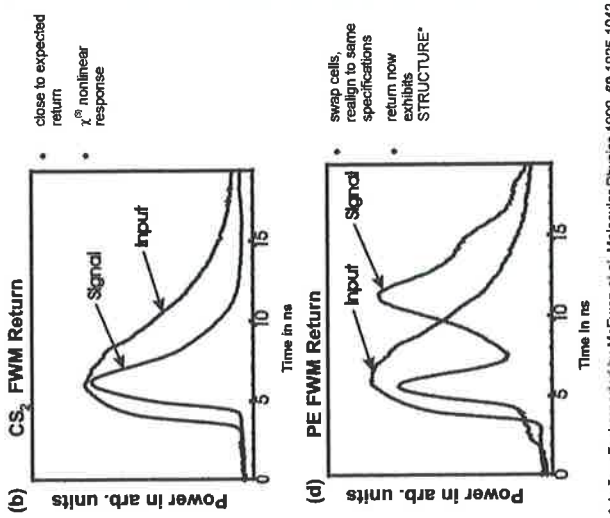

*similar effect reported by McEwan et al, Molecular Physics 1990, 69 1025-1042 modelled as fast reorientational nly. followed by slow thermal nly.

Experimental Objective

Resolve Nature of Competing Mechanisms
- one FAST
- one SLOW

Use Continuously Variable Pulse Length to Excite Transition Regime

Probe Dynamic Evolution of Grating

Use Sub-nanosecond Pulses to Determine Mechanism

Excite Transition Regime

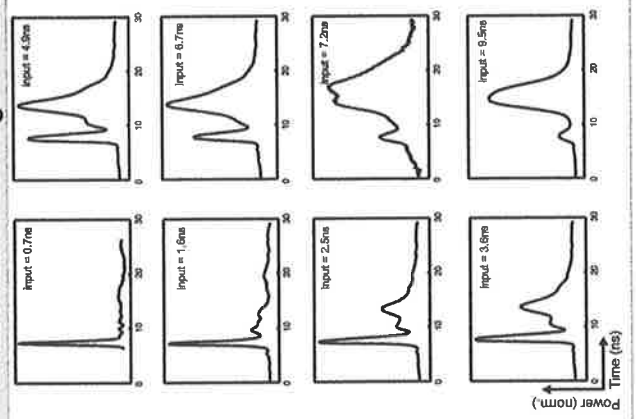

Nanosecond Dynamic Evolution

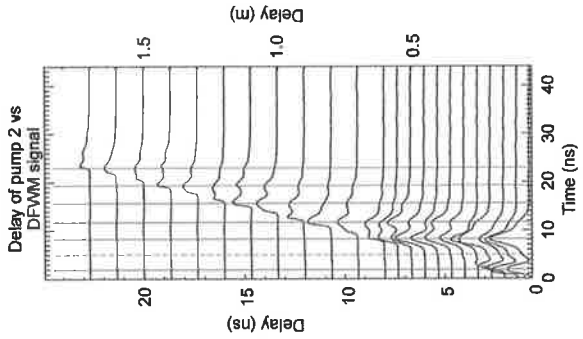

Acoustic Phonons

Thermal and electrostrictive forces create phonons giving rise to a standing wave

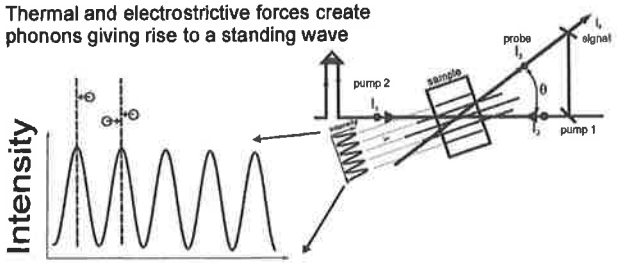

Electrostrictive phonons - molecules contract toward high intensity regions

$$T = \frac{\Lambda}{2v}$$

Thermal phonons - thermal expansion forces molecules away from high intensity regions

$$T = \frac{\Lambda}{v}$$

Sub-Nanosecond Dynamic Evolution

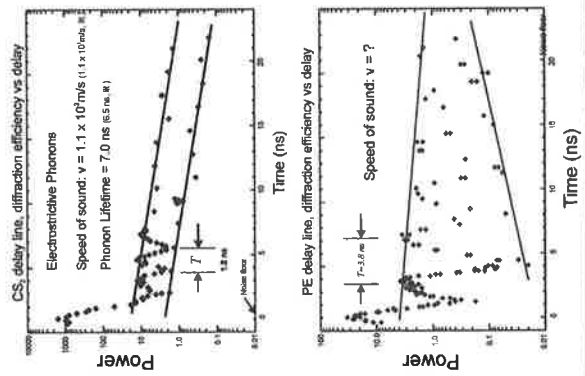

Heterodyne Speed of Sound Measurement

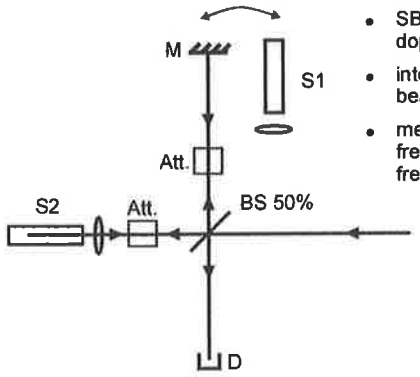

- SBS return induces doppler frequency shift
- interference to get beating effect
- measure doppler frequency against known frequency

$$v_s = \frac{\lambda f_{dop}}{2n}$$

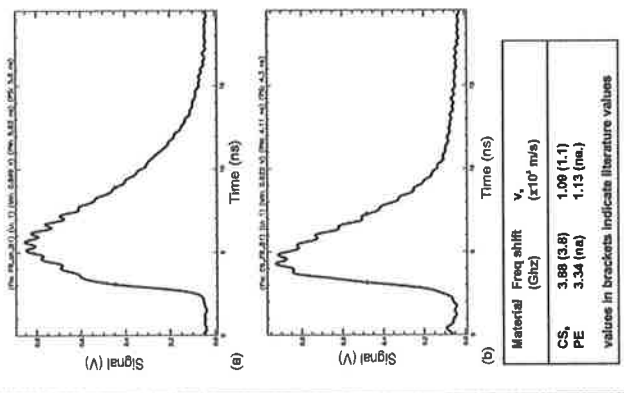

Material	Freq shift (Ghz)	v_s ($x10^5$ m/s)
CS_2	3.88 (3.8)	1.06 (1.1)
PE	3.34 (na)	1.13 (na)

values in brackets indicate literature values

Conclusion

Determined unambiguously the mechanism responsible for the transient structure in the DFWM return, as well as its origin

Determined nonlinear scattering parameters such as phonon lifetime, speed of sound, $\chi^{(3)}_{SBS}$, $\chi^{(3)}_{reorientation}$

Demonstrated the use of a variable pulse laser to scan through the transient regime between two nonlinear optical mechanisms.

Future

Further reduce pulse length down to 120 ps to
to give greater dynamic range
include more nonlinear effects

Bibliography

[1] J. Staromlynska, P. B. Chapple, J. R. Davy, and T. J. McKay, "A platinum ethynyl compound for optical limiting," *Proc. SPIE*, vol. 2229, pp. 59–66, 1994.

[2] S. Guha, K. Kang, P. Porter, J. F. Roach, D. E. Remy, F. J. Aranda, and D. V. G. L. N. Rao, "Third-order optical nonlinearities of metallotetrabenzoporphyrins and a platinum poly-yne," *Opt. Lett.*, vol. 17, pp. 264–266, 1992.

[3] S. Guha, C. C. Frazier, W. P. Chen, P. Porter, K. Kang, and S. E. Finberg, "Nonlinear devices using organometallic polymers," *SPIE*, vol. 1105, pp. 14–19, 1989.

[4] L. W. Tutt and T. F. Bogess, "A review of optical limiting mechanisms and devices using organics, fullerenes, semiconductors and other materials," *Prog. Quant. Electr.*, vol. 17, pp. 299–338, 1993.

[5] H. Fei, Y. Yang, Z. Wei, L. Han, Y. Che, P. Wu, and G. Sun, "Degenerate four-wave mixing based on excited-state absorption in azo-dye-doped polymer films," *Appl. Phys. B*, vol. 62, pp. 299–302, 1996.

[6] T. Steffen and K. Duppen, "Time resolved four- and six-wave mixing in liquids. ii. experiments," *J. Chem. Phys.*, vol. 106, pp. 3854–3864, 1997.

[7] A. M. Scott and M. S. Hazell, "High-efficiency scattering in transient Brillouin-enhanced four-wave mixing," *IEEE J. Quantum Electron.*, vol. 22, pp. 1248–1257, 1986.

[8] H. J. Eichler and P. Günter, *Laser-Induced Dynamic Gratings.* Springer-Verlag, 1986.

[9] M. Samoc and P. Prasad, "Dynamics of resonant third-order optical nonlinearity in perylene tetracarboxylic dianhydride studied by monitoring first and second order diffractions in subpicosecond degenerate four-wave mixing," *J. Chem. Phys.*, vol. 91, pp. 6643–6649, 1989.

[10] S. Guha and P. Conner, "Degenerate four-wave mixing in Kerr media in the presence of nonlinear refraction, pump depletion and linear absorption," *Optics Comm.*, vol. 89, pp. 107–118, 1992.

[11] W. M. Dennis and W. Blau, "Thermal effects in picosecond optical phase conjugation in soluble polydiacetylene," *Opt. Comm.*, vol. 57, pp. 371–374, 1986.

[12] D. J. McGraw, A. E. Siegman, G. M. Wallraff, and R. D. Miller, "Resolution of the nuclear and electronic contributions to the optical nonlinearity in polysilanes," *Appl. Phys. Lett.*, vol. 54, pp. 1713–1715, 1989.

[13] T. H. Maiman *Nature*, vol. 187, p. 493, 1960.

[14] A. L. Schawlow and C. H. Townes *Phys.Rev.*, vol. 112, p. 1940, 1958.

[15] P. A. Franken, A. E. Hill, C. W. Peters, and G. Weinreich *Phys.Rev.Lett*, vol. 7, p. 118, 1961.

[16] M. Bass, P. A. Franken, A. E. Hill, C. W. Peters, and G. Weinreich *Phys. Rev. Lett.*, vol. 8, p. 18, 1962.

[17] E. J. Woodbury and W. K. Ng *Proc. IRE*, vol. 50, p. 2347, 1962.

[18] G. M. Zerev, E. K. Malduties, and V. Pashkov *JETP Lett.*, vol. 9, p. 61, 1969.

[19] R. Y. Chiao, C. H. Townes, and B. P. Stoicheff, "Stimulated Brillouin scattering and coherent generation of intense hypersonic waves," *Phys. Rev. Lett.*, vol. 12, pp. 592–XX, 1964.

[20] R. L. Carman, R. Y. Chiao, and P. L. Kelley, "Observation of degenerate stimulated four-photon interaction and four-wave parametric amplification," *Physical Review Letters*, vol. 17, pp. 1281–1283, 1966.

[21] B. Y. Zel'dovich, N. F. Pilipetsky, and V. V. Shkunov, *Principles of Phase Conjugation.* Berlin: Springer-Verlag, 1985.

[22] R. A. Fisher, *Optical Phase Conjugation.* New York: Academic Press, 1983.

[23] R. W. Hellwarth, "Generation of time-reversed wave fronts by nonlinear refraction," *J.Opt.Soc.Am*, vol. 67, pp. 1–3, 1977.

[24] D. M. Bloom and G. C. Bjorklund, "Conjugate wave-front generation and image reconstruction by four wave mixing," *Appl. Phys. Lett*, vol. 31, pp. 592–594, 1977.

[25] P. D. Maker and R. W. Terhune, "Study of optical effects due to an induced polarization third order in the electric field strength," *Phys. Rev. A*, vol. 137, p. 801, 1965.

[26] A. Yariv, "Phase conjugate optics and real-time holography," *IEEE J. Quantum Electron.*, vol. 14, pp. 650–656, 1978.

[27] A. Yariv and D. M. Pepper, "Amplified reflection, phase conjugation, and oscillation in degenerate four-wave mixing," *Optics Letters*, vol. 1, pp. 16–18, 1977.

[28] D. M. Bloom, P. F. Liao, and N. P. Economou, "Observation of amplified reflection by degenerate four-wave mixing in atomic sodium vapor," *Opt. Lett.*, vol. 2, pp. 58–60, 1978.

[29] R. L. Abrams and R. C. Lind, "Degenerate four wave mixing in absorbing media," *Opt. Lett.*, vol. 2, pp. 94–96, 1978.

[30] G. P. Agrawal, "Phaseconjugation and degenerate four-wave mixing in three level systems," *IEEE J. Quantum Electron.*, vol. 17, pp. 2335–2340, 1981.

[31] P. F. Liao and D. M. Bloom, "Continuous-wave backward-wave generation by degenerate four-wave mixing in ruby," *Opt. Lett.*, vol. 3, pp. 4–6, 1978.

[32] M. Motzkus, G. Pichler, M. Dillmann, K. L. Kompa, and P. Hering, "Degenerate four-wave mixing spectroscopy in NaH," *Appl. Phys. B.*, vol. 57, pp. 261–265, 1993.

[33] N. Georgiev and M. Alden, "Two-photon degenerate four-wave mixing for the detection of ammonia: Applications to flames," *Appl. Phys. B.*, vol. 56, pp. 281–286, 1993.

[34] D. M. Pepper, J. AuYeung, D. Fekete, and A. Yariv, "Spatial convolution and correlation of optical fields via degenerate four-wave mixing," *Opt. Lett.*, vol. 3, pp. 7–9, 1978.

[35] G. Martin and R. W. Hellwarth, "Infrared to optical image conversion by Bragg reflection from thermally induced index gratings," *Appl. Phys. Lett.*, vol. 6, pp. 371–373, 1979.

[36] F. T. S. Yu, S. Wu, S. Rajan, and A. Mayers, "Optical novelty filter with phase carrier," *Opt. Comm.*, vol. 92, pp. 205–208, 1992.

[37] L. P. Schelonka and M. A. Kramer, "Theory of thermal blooming correction by phase conjugation," *Opt. Lett.*, vol. 14, pp. 949–951, 1989.

[38] P. Kürz and T. Mukai, "Frequency stabilization of a semiconductor laser by external phase conjugate feedback," *Opt. Lett.*, vol. 21, pp. 1369–1371, 1996.

[39] D. M. Pepper and R. L. Abrams, "Narrow optical bandpass filter via nearly degenerate four-wave mixing," *Opt. Lett.*, vol. 3, pp. 212–214, 1978.

[40] J. Nilsen and A. Yariv, "Nearly degenerate four-wave mixing applied to optical filters," *Appl. Opt.*, vol. 18, pp. 143–145, 1979.

[41] V. N. Blashchuk, F. F. Pilipetskii, and V. V. Shkunov, "Four-wave interaction as a controllable frequency filter," *Sov. Phys. Dokl.*, vol. 25, pp. 185–187, 1980.

[42] H. G. Winful and J. H. Marburger, "Hysteresis and optical bistability in degenerate four-wave mixing," *Appl. Phys. Lett.*, vol. 8, pp. 613–614, 1980.

[43] J. Buchert, R. Dorsinville, P. Delfyett, S. Krimchansky, and R. R. Alfano, "Determination of temporal correlation of ultrafast laser pulses using phase conjugation," *Opt. Comm.*, vol. 52, pp. 433–437, 1985.

[44] S. F.L. Pedrotti and L. Pedrotti, *Introduction to Optics.* Prentice Hall, Englewood Cliffs, New Jersey 07632, 1993.

[45] B. Sahraoui, R. Chevalier, G. Rivoire, J. Zaremba, and M. Sallé, "Nonlinear optical properties of new hyper-tetrathiafulvalene derivatives: Saturable absorption and degenerate four-wave mixing," *Opt. Comm.*, vol. 135, pp. 109–115, 1997.

[46] A. Agnesi, G. P. Banfi, M. Ghigliazza, and G. C. Reali, "Picosecond nonlinear optical characterization of GaAs," *Opt. Comm.*, vol. 92, pp. 300–306, 1992.

[47] N. P. Xuan, J. L. Ferrier, J. Gazengel, and G. Rivoire, "Picosecond measurement of the third-order susceptibility tensor in liquids," *Opt. Comm.*, vol. 51, pp. 433–437, 1984.

[48] L. Richard, J. Maurin, and J. P. Huignard, "Phase conjugation with gain at $CO_2 laserline \lambda = 10.6$ μ m from thermally induced gratings in nematic liquid crystals.," *Opt. Comm.*, vol. 57, pp. 365–370, 1986.

[49] K. J. McEwan, K. J. Harrison, and P. A. Madden, "Polarisation and material dependence of degenerate four-wave mixing transients in molecular fluids," *Molecular Physics*, vol. 69, pp. 1025–1042, 1990.

[50] K. J. McEwan and P. A. Madden, "Transient grating effects in absorbing colloidal suspensions," *J. Chem. Phys.*, vol. 97, pp. 8748–8759, 1992.

[51] I.-C. Khoo, *Liquid Crystals: Physical Properties and Nonlinear Optical Phenomena.* John Wiley and Sons, 1995.

[52] P. P. Ho and R. R. Alfano, "Optical Kerr effect in liquids," *Phys. Rev. A*, vol. 20, pp. 2170–2187, 1979.

[53] J. R. Lalanne, J. Buchert, and S. Kielich, "Fast molecular reorientation in liquid crystals probed by nonlinear optics," *Adv. Chem. Phys. Ser.*, vol. 85, pp. 159–215, 1993.

[54] A. M. Scott, "Four wave mixing due to the optical Kerr effect and Rayleigh-wing scattering," *Opt. Comm.*, vol. 45, pp. 207–210, 1983.

[55] H. J. Hoffman, "Thermally induced phase conjugation by transient real-time holography: A review," *J. Opt. Soc. Am. B*, vol. 3, pp. 253–273, 1986.

[56] J. A. Armstrong, N. Bloembergen, J. Ducuing, and P. S. Pershan *Phys. Rev.*, vol. 127, pp. 1918–???, 1962.

[57] H. Eichler, G. Enterlein, P. Glozbach, J. Munschau, and H. Stahl, "Power requirements and resolution of real-time holograms in saturable absorbers and absorbing liquids," *Applied Optics*, pp. 372–375, 1972.

[58] Y. R. Shen, *The Principles of Nonlinear Optics.* New York: John Wiley and Sons, 1984.

[59] R. W. Boyd, *Nonlinear Optics.* Academic Press, 1992.

[60] M. D. Levenson and S. S. Kano, *Introduction to Nonlinear Laser Spectroscopy, Revised Edition.* Academic Press, 1988.

[61] C. Maloney and W. Blau, "Resonant third-order hyperpolarizabilities of large molecules," *J.Opt.Soc.Am.B*, vol. 4, pp. 1035–1039, 1987.

[62] J. M. Nunzi and D. Grec, "Picosecond phase conjugation in polydiacetylene gels," *J. Appl. Phys.*, vol. 62, pp. 2198–2202, 1987.

[63] K. A. Nelson, D. R. Lutz, M. D. Fayer, and L. Madison, "Laser-induced phonon spectroscopy. optical generation of ultrasonic waves and investigation of elec-

tronic excited state interactions in solids," *Phys. Rev. B*, vol. 24, pp. 3261–3275, 1981.

[64] K. A. Nelson, R. Casalegno, R. J. D. Miller, and M. D. Fayer, "Laser-induced excited state and ultrasonic wave gratings: Amplitude and phase grating contributions to diffraction," *J. Chem. Phys.*, vol. 77, pp. 1144–1152, 1982.

[65] K. A. Nelson, R. J. D. Miller, D. R. Lutz, and M. D. Fayer, "Optical generation of tunable ultrasonic waves," *J. Appl. Phys.*, vol. 53, pp. 1144–1149, 1982.

[66] S. Takahashi, Y. Takai, H. Morimoto, K. Sonogashira, and N. Hagihara, "Direct N.M.R. observation of lyotropic liquid crystals formed by transition metal poly-yne polymers," *Molec. Cryst. Liq. Cryst.*, vol. 82, pp. 139–143, 1982.

[67] C. C. Frazier, S. Guha, P. L. Porter, and P. M. Cockerham, "Nonlinear optical properties of transition metal poly-ynes," *SPIE*, vol. 971, pp. 186–195, 1988.

[68] M. Sittig, *Handbook of Toxic and Hazardous Chemicals and Carcinogens*, pp. 346–348.

[69] K. J. Witte, M. Galanti, and R. Volk *Opt. Comm.*, vol. 34, p. 278, 1980.

[70] G. Eckhardt, R. W. Hellwarth, F. J. McClung, S. E. Schwarz, D. Weiner, and E. J. Woodbury, "Stimulated Raman scattering from organic liquids," *Phys. Rev. Lett.*, vol. 9, pp. 455–XX, 1962.

[71] B. Y. Zeldowich, V. I. Popovich, V. V. Ragulskii, and F. S. Faizullov, "Connection between the wave fronts of the reflected and exciting light in stimulated Mandel'shtam-Brillouin scattering," *Sov. Phys. JETP*, vol. 15, pp. 109–XX, 1972.

[72] J. Munch, R. F. Wuerker, and M. J. LeFebvre, "Interaction length for optical phase conjugation by stimulated Brillouin scattering: An experimental investigation," *Appl. Opt.*, vol. 28, pp. 3099–3105, 1989.

[73] D. Y. Nosach, V. I. Popovich, V. V. Ragul'skii, and F. S. Faizullov, "Cancellation of phase distrotions in an amplifying medium with a Brillouin mirror," *Sov. Phys. JETP*, vol. 16, pp. 435–442, 1972.

[74] D. A. Rockwell, "A review of phase conjugate solid state lasers," *IEEE J. Quantum Electron.*, vol. 24, pp. 1124–1140, 1988.

[75] T. D. Hon, "Pulse compression by stimulated Brillouin scattering," *Opt. Lett.*, vol. 5, pp. 516–518, 1980.

[76] M. J. Damzen and M. H. R. Hutchinson, "High efficiency laser-pulse compression by stimulated Brillouin scattering," *Opt. Lett.*, vol. 8, pp. 313–315, 1983.

[77] C. B. Dane, W. A. Neuman, and L. A. Hackel, "High-energy SBS pulse compression," *IEEE J. Quantum. Electron*, vol. 30, pp. 1907–1915, 1994.

[78] R. Fedosejevs and A. A. Offenberger, "Subnanosecond pulses from a KrF laser pumped $SF_6 Brillouin amplifier," IEEE J. Quantum Electron., vol. 21, pp. 1558--1562, 1985.$

[79] M. C. Gower, "The physics of phase conjugate mirrors," *Prog. Quantum Electr*, vol. 9, pp. 101–147, 1984.

[80] M. C. Gower, "Phase conjugation," *J. Mod. Opt.*, vol. 35, pp. 449–472, 1988.

[81] M. J. Damzen and H. Hutchinson, "Laser pulse compression by stimulated Brillouin scattering in tapered wave guides," *IEEE Quantum Electron.*, vol. 19, pp. 7–14, 1983.

[82] N. F. Andreev, E. Khazanov, and G. A. Pasmanik, "Application of Brillouin cells to high repetition rate solid state lasers," *IEEE J. Quantum Electron.*, vol. 28, pp. 330–341, 1992.

[83] D. V. G. L. N. Rao and D. K. Agrawal, "Stimulated Raman scattering in a nematic liquid crystal," *Physics Letters*, vol. 37A, pp. 383–384, 1971.

[84] P. Klövekorn and J. Munch, "Variable optical delay line with diffraction-limited autoalignment," *App. Opt.*, vol. 37, pp. 1903–1904, 1998.

[85] C. K. Wu, P. Agostini, G. Petite, and F. Fabre, "Time character of phase-conjugate reconstructed waves," *Opt. Lett.*, vol. 8, pp. 67–69, 1983.

[86] P. Klövekorn and J. Munch, "Variable SBS pulsecompressor for nonlinear optical measurements" *App. Opt.*, vol. 36, pp. 5913–5917, 1997.

[87] D. J. Brink and T. N. Kock, "A simple effective pulse compressor for pulsed dye lasers," *J. Phys. D*, vol. 20, pp. 1584–1589, 1987.

[88] M. J. Weber, *CRC Handbook of Laser Science and Technology, Supplement 2: Optical Materials*, ch. 8, p. 358. CRC Press, 1995.

[89] L. Genberg, Q. Bao, S. Gracewski, and R. J. D. Miller, "Picosecond transient thermal phase grating spectroscopy: A new approach to the study of vibrational energy relaxation processes in proteins," *Chem. Phys.*, vol. 131, pp. 81–97, 1989.

[90] M. J. Weber, *CRC Handbook of Laser Science and Technology, Supplement 2: Optical Materials*, ch. 12, p. 471. CRC Press, 1995.

[91] V. Kubecek, K. Hamal, I. Prochazka, and P. Valach, "Compression of the Nd:YAP laser pulse by two-stage stimulated backward scattering," *Opt. Comm.*, vol. 73, pp. 251–256, 1989.

[92] Y. Nizienko, A. Mamin, P. Nielsen, and B. Brown, "300 ps ruby laser using stimulated Brillouin scattering pulse compression," *Rev. Sci. Instrum.*, vol. 65, pp. 2460–2463, 1994.

[93] S. Schiemann, W. Ubachs, and W. Hogervorst, "Efficient temporal compression of coherent nano-second pulses in a compact SBS generator-amplifier setup," *IEEE J. Quantum. Electron.*, vol. 33, pp. 358–366, 1997.